Quantum feedback for quantum technology

Lewis Alexander Clark

School of Physics and Astronomy

University of Leeds

Submitted in accordance with the requirements for the degree of

Doctor of Philosophy

July 2017

Declaration

The candidate confirms that the work submitted is his/her own, except where work which has formed part of jointly authored publications has been included. The contribution of the candidate and the other authors to this work has been explicitly indicated below. The candidate confirms that appropriate credit has been given within the thesis where reference has been made to the work of others.

Some of the work in Chapter 3 of the thesis has appeared in publication as follows:

L. A. Clark, F. Torzewska, B. Maybee and A. Beige, *Non-ergodicity with quantum feedback*, submitted (arXiv:1611.03716).

I was the lead investigator of the research and the contribution of other authors was in discussion with me.

Some of the work in Chapter 4 of the thesis has appeared in publication as follows:

L. A. Clark, W. Huang, T. M. Barlow and A. Beige, *Hidden Quantum Markov Models and Open Quantum Systems with Instantaneous Feedback*, Emergence, Complexity and Computation, Vol. **14** 143 (Springer International Publishing Switzerland).

I was the lead investigator of the research and the contribution of other authors was in discussion with me.

Some of the work in Chapter 5 of the thesis has appeared in publication as follows:

L. A. Clark, A. Stokes and A. Beige, *Quantum-enhanced metrology through the single mode coherent states of optical cavities with quantum feedback*, Phys. Rev. A **94** 023840 (2016).

L. A. Clark, A. Stokes, M. Mubashir Khan, G. Wang and A. Beige, *Quantum-enhanced metrology without entanglement based on optical cavities with feedback*, PHOTOPTICS conference proceedings, p. 223 (2017).

I was the lead investigator of the research and the contribution of other authors was in discussion with me.

You only live forever in the lights you make.

Acknowledgements

I would like to thank all the people who have supported me throughout my time working towards this thesis. In particular, I thank my supervisor, Almut Beige, for providing great support and knowledge to me during my studies. I would also like to thank all my other co-authors on my publications, who listed in alphabetical order are Tom Barlow, Nicholas Furtak-Wells, Wei Huang, Mubashir Khan, Ben Maybee, Robert Purdy, Adam Stokes, Fiona Torzewska and Gangcheng "Sanguine" Wang.

Finally, I would like to thank all my friends, family and co-workers who have supported me over the past four years, whether through scientific discussion and/or a £2 pint of Fenton Bitter in The Fenton.

Cheers!

List of publications

[1] L. A. Clark, W. Huang, T. M. Barlow and A. Beige, *Hidden Quantum Markov Models and Open Quantum Systems with Instantaneous Feedback*, Emergence, Complexity and Computation, Vol. **14** 143 (Springer International Publishing Switzerland).

[2] L. A. Clark, A. Stokes and A. Beige, *Quantum-enhanced metrology through the single mode coherent states of optical cavities with quantum feedback*, Phys. Rev. A **94** 023840 (2016).

[3] L. A. Clark, A. Stokes, M. Mubashir Khan, G. Wang and A. Beige, *Quantum-enhanced metrology without entanglement based on optical*

cavities with feedback, PHOTOPTICS conference proceedings, p. 223 (2017).

[4] L. A. Clark, F. Torzewska, B. Maybee and A. Beige, *Non-ergodicity with quantum feedback*, submitted (arXiv:1611.03716).

[5] N. Furtak-Wells. L. A. Clark, R. Purdy and A. Beige *Quantising the electromagnetic field near a semi-transparent mirror*, submitted (arXiv:1704.02898).

Abstract

It is widely believed that quantum physics is a fundamental theory describing the Universe. As such, one would expect to be able to see how classical physics that is observed in the macroscopic world emerges from quantum theory. This has so far largely eluded physicists, due to the inherent linear nature of quantum physics and the non-linear behaviour of classical physics. One of the principle differences between classical and quantum physics is the statistical, probabilistic nature of quantum theory. It is from this property that non-classical states can arise, such as entangled states. These states possess maximal correlations. However, they are not the only way in which correlations are created in quantum systems. This thesis aims to show how open quantum systems naturally contain correlations from their quantum nature. Moreover, even seemingly simple open quantum systems can behave far more complexly than expected upon the introduction of quantum feedback. Using this effect, the dynamics may become non-linear and as such behave non-trivially. Furthermore, it is shown how these effects may be exploited for a variety of tasks, including a computational application in hidden quantum Markov models and a quantum metrology scheme that does not require the use of exotic quantum states. This results in the design of systems that benefit from the use of quantum mechanics, but are not constrained by the use of experimentally difficulties such as entanglement.

Abbreviations

HMM	Hidden Markov model
HQMM	Hidden quantum Markov model
LON	Linear optics network
MC	Markov chain
RWA	Rotating Wave Approximation

Contents

List of Figures

Chapter 1

Introduction

The proceeding work analyses open quantum systems with quantum feedback for quantum technological applications. In this chapter, we shall provide some general background and motivation to the following chapters.

1.1 Motivation

The emergence of quantum physics in the early 1900s initiated one of the biggest scientific revolutions in history. Many of the fundamental aspects of nature were now able to be explained with this new physics. Moreover, as well as better explaining the observed world, new phenomena were discovered. In particular, this includes the introduction of quantum information. One such development of quantum physics is the quantum theory of light. The focus of this thesis is all around the quantum behaviour of light, in particular by manipulating light at the quantum level. In doing so, there is a wide range of technological applications. Most successfully, quantum optical systems have found uses in quantum metrology [1] and quantum communication [2], as well as having potential for quantum computing [3].

However, most implementations of the above mentioned applications rely on difficult experimental procedures. For example, controlled entanglement for information processing tasks is difficult to efficiently generate on a large scale, particularly in optical systems, which is required for gaining a useful enhancement on classical systems. Particularly in optical systems, large-scale entanglement is

hard to achieve due to the difficulties involved in creating interactions between photons. As such, entanglement is often made only probabilistically. This is the main limitation of implementing quantum technologies. Fortunately, there are other ways to create quantum effects. One such way of generating quantum effects is by manipulating open quantum systems and analysing the photon statistics emitted from the system. In particular, this thesis will analyse how an optical cavity can be manipulated and monitored in order to produce novel quantum effects amongst other results.

As an example, quantum metrology is an area that has been studied extensively recently. A typical example of how a parameter can be measured is with an interferometer to measure a phase shift φ, as shown in Fig. 1.1. Classically, this is straightforward, as light can be sent into the input ports and measured at the outputs. Depending on the intensity measured at the outputs, information can be gained about φ. At a quantum level, the same can be done. If a single photon is inserted into the interferometer, the same procedure can be conducted. This can be repeated with many photons and reproduces the classical results. However, if an entangled state is used as an input, the non-classical correlations present can result in more information obtained per-photon than in a single photon case.

A typical state used for this purpose is the $N00N$ state, which is defined as

$$|N00N\rangle = \frac{1}{\sqrt{2}} \left(|N_{\mathrm{a}}\, 0_{\mathrm{b}}\rangle + |0_{\mathrm{a}}\, N_{\mathrm{b}}\rangle \right) , \tag{1.1}$$

where the subscripts a and b describe the photons in path a and b respectively. As with many entangled states like this, it is hard to produce for large N. This is similar for a large number of implementations of quantum metrology schemes, as can be seen in Ref. [1]. This problem is analysed in more detail later in Ch. 5, but for now we consider this as motivation for the development of simpler novel techniques.

1.2 Open quantum systems

The main focus of this thesis is on the behaviour of light trapped within an optical cavity. Like most quantum optical systems, this must be treated as open in order

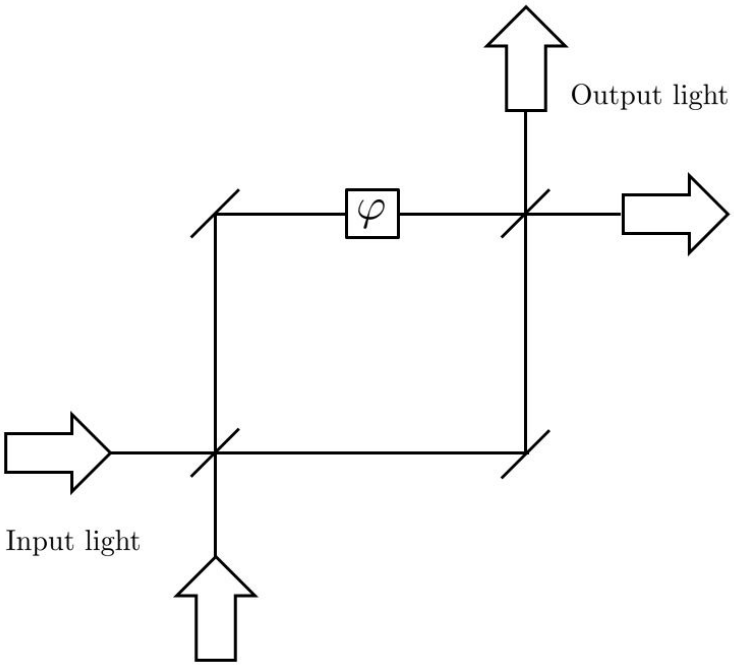

Figure 1.1: Typical Mach-Zehnder interferometric setup for a metrology scheme. Light is input into the interferometer and allowed to experience a phase shift in one arm. Then, upon measurement at the end, the interference of the two pathways of light reveals information about the phase shift parameter φ.

to be accurately modelled and to track photon emissions. By this, we mean that the system to be analysed should be allowed to interact with its environment. A closed quantum system is one that simply evolves in time according to the Schrödinger equation. Specifically, this means a state $|\psi\rangle$ evolves according to

$$|\dot{\psi}\rangle \;=\; -\frac{\mathrm{i}}{\hbar} H\,|\psi\rangle\ , \tag{1.2}$$

where H is the Hamiltonian operator describing the system. However, the evolution of an open quantum system is more complex. Suppose a system interacts with some other external system that has infinitely many degrees of freedom, which is essentially a classical system. This system is known as a bath or environment. In this case, as we shall see in Chapter 2, the system no longer evolves according to a Schrödinger equation. Instead, we now use a density matrix ρ to

describe the system and its evolution is given by a master equation. Assuming Markovianity, the master equation is Lindbladian [4] and is of the form

$$\dot{\rho} = -\frac{\mathrm{i}}{\hbar}[H,\rho] + \sum_{m,n=1}^{N^2-1} \Gamma_{m,n}\left(L_m \rho L_n^\dagger - \frac{1}{2}\left[L_m^\dagger L_n, \rho\right]_+\right). \tag{1.3}$$

In Chapter 2 we shall derive this equation for an open quantum system with a single decay channel. This means all $\Gamma_{m,n} = 0$ except one. An important feature of open quantum systems is the ability to alter these decay channels with feedback. This will be used extensively in this work and is introduced in Chapter 2.

1.3 Background

Despite theoretical success in developing a variety of schemes for quantum metrological applications, experimental implementations are still difficult to achieve. This is largely due to requirement of entanglement in most proposed schemes. For example, there is a wealth of literature on quantum metrology, where a variety of schemes are proposed [1]. Unfortunately, most have not been implemented due to experimental difficulty in generating the quantum features required such as large scale entanglement.

Recent work has been conducted on investigating how open quantum systems can be used for quantum metrology applications [5, 6, 7]. These methods provide a novel technique in achieving enhanced measurements without the need to build large-scale entanglement. The results of these papers shows that quantum metrology can be achieved by using time as a resource. This is not possible in interferometric setups, as there the system is closed and ends upon measuring the output light; it cannot be left to run for an arbitrary time. These new methods of using time as a resource in open quantum systems therefore offer a potential advantage over standard interferometric methods.

Furthermore, there has been recent interest in the use of open quantum systems for computer science applications. In particular, quantum neural networks and quantum machine learning systems are being investigated [8, 9]. Open quantum systems may find applications within this field also. As a stepping stone to

this, part of the work in this thesis will investigate a computer science application in the form of Hidden Quantum Markov Models (HQMMs). These machines were recently introduced [10] and have found interest in some adaptations [11, 12]. However, there is still little work conducted on alternative computer science applications for quantum systems.

The theory behind open quantum systems has been studied extensively already in the literature [13]. In particular, quantum optical systems are well understood in a variety of scenarios. Typical quantum optical systems, such as optical cavities and two-level atoms can be modelled with relative ease due to their simple Markovian dynamics and hence their dynamics are well known. A way of making these systems more complex is to introduce quantum feedback. This process has been used for a variety of tasks [14]. Most notably in the literature, feedback is used for the stabilisation [15, 16] and control [17] of quantum systems, usually for quantum information purposes. In this work, we shall see feedback used for a different purpose. In effect, the feedback used in the work in this thesis acts to destabilise the system, inducing far more complex behaviour in previously simple quantum optical systems.

1.4 Outline

This thesis can effectively be split into three parts. The first part in Chapter 2 provides a theoretical background on the modelling of open quantum systems. The first step here is deriving a master equation for a general Markovian open quantum system. After this, we look at two concrete systems that will be of interest in the proceeding chapters. Specifically, we derive the master equation for an optical cavity and a two level atom. We also consider the unravelling of these master equations, allowing for the study of individual quantum trajectories.

The second part consists of Chapter 3. In this chapter, we present a study of the effect of quantum feedback on open quantum systems in the form of strong laser pulses upon photon emission. In particular, we shall compare and analyse the ergodicity of an optical cavity that is subject to continuous laser driving and one that is inside a quantum feedback loop. This provides an insight into the

complex dynamics that can be achieved by introducing quantum feedback into an open quantum system.

Finally, in the third part of the thesis, we look at quantum technological applications of the behaviour studied in Chapter 3. Firstly, in Chapter 4, we look at a computer science application in the form of Hidden Quantum Markov Models. We first provide a mathematical model for describing both classical Hidden Markov Models and their quantum analogue, Hidden Quantum Markov Models. We then provide an example of how such a scheme may be implemented and compare classical and quantum machines statistical properties with a simple example.

We then consider a further quantum technological application in Chapter 5. Here, we study quantum metrology. We begin by reviewing the Fisher information and parameter estimation theory, before the applying it to a simple two-level system. By introducing feedback appropriately, we find we may make a quantum-enhanced measurement. We then apply similar ideas to an optical cavity inside a quantum feedback loop. Finally, in Chapter 6, we summarise the work presented and consider potential future work and its applications.

Part I

Theoretical Background

Chapter 2

Open quantum systems with quantum feedback

The aim of this chapter is to give a brief introduction to the modelling of open quantum systems [13, 18], thereby providing a theoretical background to the proceeding chapters. To do so, we first consider a general quantum system that interacts with a surrounding bath. This bath is assumed to also interact with an external environment, which causes it to thermalise continuously. More concretely, the environment constantly resets the bath into its environmentally preferred state – its so-called pointer state [19]. Hence, the resulting effective time evolution of the open quantum system is approximately Markovian and its density matrix ρ_S obeys a master equation in Lindblad form [4]. When the bath surrounding the quantum system is continuously monitored by the environment for the detection of spontaneously emitted photons [20, 21, 22], this master equation can be unravelled into an infinite set of physically-meaningful quantum trajectories. An unravelling involves splitting the overall average evolution into its individual components and looking at a possible evolution along such a path. Considering such an unravelling and assuming that any instantaneous quantum feedback is triggered by sudden changes of the state of the quantum system, it becomes clear how to incorporate instantaneous feedback into the master equation [7, 11, 14]. This shall be seen more precisely later in this chapter.

In this chapter we first review what is meant by an open quantum system, before deriving the master equation governing a general Markovian open quantum

system's time evolution evolution with quantum feedback. We then derive this equation for an optical cavity inside an instantaneous quantum feedback loop, which is extensively studied in the rest of this thesis. Finally, we present an analysis of a two-level atom with instantaneous quantum feedback and provide a simple example of how feedback can alter the dynamics of such a system.

2.1 General derivation of the master equation

To describe the evolution of a closed quantum system, the Schrödinger equation is used. This means that a closed quantum system $|\psi\rangle$ evolves according to

$$|\dot{\psi}\rangle \;=\; -\frac{\mathrm{i}}{\hbar}H\,|\psi\rangle\;, \tag{2.1}$$

where H is the Hamiltonian describing the system of interest. This equation applies when there is no loss of energy or correlations to an external environment. However, realistically this is never the case, as a system will always couple to its surroundings in some form. If this is to be incorporated into the dynamics, the system must be considered open. To analyse the behaviour of such systems, we must introduce the quantum master equation [4, 18]. The standard quantum optical master equation is given by

$$\dot{\rho} \;=\; \mathcal{L}\rho\,, \tag{2.2}$$

where ρ is the density matrix describing the system and $\mathcal{L}$ is a superoperator of the general form

$$\begin{aligned}\mathcal{L}\rho \;=\; & -\frac{\mathrm{i}}{\hbar}\left[H,\rho\right] \\ & +\frac{1}{2}\sum_{m=0}^{N}\sum_{n=0}^{N}\Gamma_{m,n}\left(2L_n\rho L_m^{\dagger}-\left[L_m^{\dagger}L_n,\rho\right]_{+}\right)\,.\end{aligned} \tag{2.3}$$

Here, $\Gamma_{m,n}$ describes the decay rate of the channel m,n and L_n is known as a Lindblad operator. Most quantum optical systems have a master equation of the form

$$\dot{\rho}=-\frac{\mathrm{i}}{\hbar}\left[H,\rho\right]+\frac{1}{2}\Gamma\left(2L\rho L^{\dagger}-\left[L^{\dagger}L,\rho\right]_{+}\right)\,, \tag{2.4}$$

where there is just a single decay channel. Solving Eq. (2.3), it is found that

$$\rho(t+\Delta t) \;=\; \exp\left(\mathcal{L}\Delta t\right)\rho(t) \tag{2.5}$$

is always the solution. Although the time evolution of an open quantum system is more complex than that of a closed system, they are both characterised by linear differential equations. In the next subsection, we will present a derivation of the general quantum optical master equation and show how feedback can be incorporated.

2.1.1 Master equations without feedback

Let us first have a closer look at an open quantum system without feedback. The Hamiltonian H of such a system and its surrounding bath can be split into two parts,

$$H \;=\; H_0 + H_1\,, \tag{2.6}$$

with H_0 denoting the free energy of the quantum system H_{S} and its bath or environment H_{B}, meaning

$$H_0 \;=\; H_{\mathrm{S}} + H_{\mathrm{B}}\,, \tag{2.7}$$

and with H_1 consisting of two terms,

$$H_1 \;=\; H_{\mathrm{int}} + H_{\mathrm{SB}}\,. \tag{2.8}$$

Here H_{SB} describes system-environment interactions and H_{int} describes the internal system interactions. Typically for quantum optical systems, H_{SB} describes a linear coupling between the system and bath. Moving into the interaction picture with respect to H_0, the Hamiltonian simplifies to the interaction Hamiltonian

$$H_{\mathrm{I}}(t) \;=\; U_0^{\dagger}(t,0)\,H_1\,U_0(t,0)\,, \tag{2.9}$$

which is of the general form

$$H_{\mathrm{I}}(t) \;=\; H_{\mathrm{int\,I}} + H_{\mathrm{SB\,I}}\,, \tag{2.10}$$

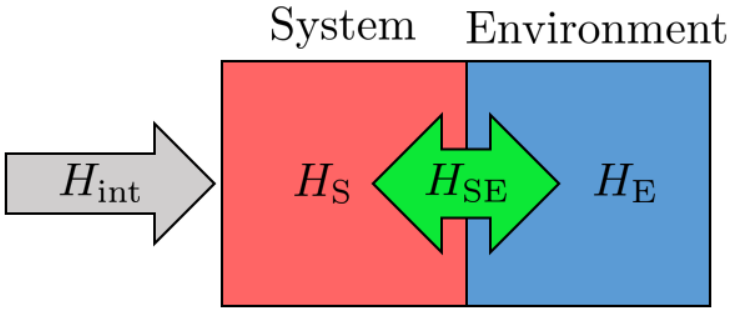

Figure 2.1: Overview of total system with corresponding Hamiltonians.

and where U_0 is the time evolution operator with respect to the Hamiltonian H_0,

$$U_0(t+\Delta t, t) \;=\; \mathrm{e}^{-\frac{\mathrm{i}}{\hbar}\int_t^{t+\Delta t} \mathrm{d}t' H_0(t')}\,, \tag{2.11}$$

which can be found by solving Eq. (2.1). Typically, H_0 is time independent and the calculation of the time evolution operator is determined trivially.

Now, suppose the state of the quantum system at time t is given by the density matrix $\rho_{\mathrm{S}}(t)$. Moreover, adopting the ideas of Refs. [18, 19, 20, 21, 22], we assume in the following that the bath surrounding the quantum system is in general in its environmentally preferred state – the so-called einselected state or pointer state – which we denote by $|0\rangle$. Hence the general density matrix of system and bath at some time t can be written as

$$\rho_{\mathrm{SB}}(t) \;=\; |0\rangle\, \rho_{\mathrm{S}}(t)\, \langle 0|\,. \tag{2.12}$$

As argued in Ref. [19], the pointer state $|0\rangle$ is environmentally preferred because it minimises the entropy of the bath. Hence, the bath only evolves due to system-bath interactions, but is invariant with respect to its own internal dynamics.

Next, we assume that system-bath interactions perturb the state of the bath on a time scale Δt, which is short compared to the time scale given by the effective internal dynamics of the quantum system. During this time interval, the density matrix $\rho_{\mathrm{SB}}(t)$ evolves via the time evolution operator $U_{\mathrm{I}}(t+\Delta t, t)$ into a new density matrix $\rho_{\mathrm{SB}}(t+\Delta t)$ given by

$$\rho_{\mathrm{SB}}(t+\Delta t) \;=\; U_{\mathrm{I}}(t+\Delta t, t)\, |0\rangle\, \rho_{\mathrm{S}}(t)\, \langle 0|\, U_{\mathrm{I}}^{\dagger}(t+\Delta t, t)\,. \tag{2.13}$$

Following the discussion in Refs. [18, 19, 20], we now assume that environmental interactions subsequently relax the reservoir very rapidly back into its environmentally preferred state. If the environment acts only locally and does not affect the expectation values of the quantum system, the result of this thermalisation is a new system-bath density matrix

$$\rho_{\mathrm{SB}}(t+\Delta t) \;=\; |0\rangle\,\rho_{\mathrm{S}}(t+\Delta t)\,\langle 0|\;, \tag{2.14}$$

with the state of the system given by

$$\rho_{\mathrm{S}}(t+\Delta t) \;=\; \mathrm{Tr}_{\mathrm{B}}\left(\rho_{\mathrm{SB}}(t+\Delta t)\right)\;, \tag{2.15}$$

where we have performed a trace over the environmental modes. Importantly, the trace is a local operation, meaning that acting it upon the environment does not (non-locally) alter any of the system's expectation values. Effectively, only $\rho_{\mathrm{S}}(t)$ has evolved over the interval Δt, and its dynamics can be summarised by the master equation

$$\dot{\rho}_{\mathrm{S}}(t) \;=\; \frac{1}{\Delta t}\left[\rho_{\mathrm{S}}\left(t+\Delta t\right)-\rho_{\mathrm{S}}\left(t\right)\right]\,. \tag{2.16}$$

Given a clear time scale separation between the effective inner dynamics of the quantum system and the relevant system-bath interactions, the right-hand-side of Eq. (2.16) can be evaluated using second-order perturbation theory. To do so, we write the time evolution operator $U_{\mathrm{I}}(t+\Delta t,t)$ as

$$U_{\mathrm{I}}(t+\Delta t,t) \;\simeq\; 1-\frac{i}{\hbar}\int_t^{t+\Delta t}\mathrm{d}t'\,H_{\mathrm{I}}(t')-\frac{1}{\hbar^2}\int_t^{t+\Delta t}\mathrm{d}t'\int_t^{t'}\mathrm{d}t''\,H_{\mathrm{I}}(t')H_{\mathrm{I}}(t'')\,. \tag{2.17}$$

Substituting this equation into Eq. (2.13) and combining the result with Eqs. (2.15) and (2.16), we find that

$$\begin{aligned}\dot{\rho}_{\mathrm{S}}(t) \;=\;& -\frac{\mathrm{i}}{\hbar}\big[\,H_{\mathrm{int\,I}}(t),\rho_{\mathrm{S}}(t)\,\big]\\ &-\frac{1}{\Delta t}\,\frac{1}{\hbar^2}\int_t^{t+\Delta t}\mathrm{d}t'\int_t^{t'}\mathrm{d}t''\left(\langle 0|H_{\mathrm{SB\,I}}(t')H_{\mathrm{SB\,I}}(t'')|0\rangle\,\rho_{\mathrm{S}}(t)+\mathrm{H.c.}\right)\\ &+\frac{1}{\Delta t}\,\frac{1}{\hbar^2}\,\mathrm{Tr}_{\mathrm{B}}\left(\int_t^{t+\Delta t}\mathrm{d}t'\int_t^{t+\Delta t}\mathrm{d}t''\,H_{\mathrm{SB\,I}}(t')\,|0\rangle\,\rho_{\mathrm{S}}(t)\,\langle 0|\,H_{\mathrm{SB\,I}}\,(t'')\right)\end{aligned} \tag{2.18}$$

up to zeroth order in Δt. When deriving this equation, it has been taken into account that Δt is relatively small and that a typical bath has infinitely many degrees of freedom. Therefore, the double integrals in Eq. (2.18) scale in general as Δt and not as Δt^2, due to the Markov approximation that will be introduced shortly. This will become clearer when a real system is considered later in this chapter and is in fact a consequence of the Markov approximation.

2.1.2 Unravelling into quantum trajectories

To incorporate instantaneous quantum feedback [11, 14] into the above master equation, we notice that the application of feedback requires monitoring the bath for triggering signals. Assuming the presence of such measurements on the above introduced time scale Δt allows us to unravel the above master equation into physically meaningful quantum trajectories [20, 21, 22]. The master equation describes the evolution of the ensemble average of the system. This means it tells us how a system will behave on average. However, an actual individual quantum system may evolve differently to this. Such an evolution is what is known as a quantum trajectory. A quantum trajectory is a stochastic process and must be analysed accordingly. One such way of modelling a quantum trajectory is with the quantum jump approach, which shall be introduced later in this chapter and used throughout this thesis. Quantum trajectories may be obtained by stochastically evolving a state through a set of possible evolutionary paths. These paths may be obtained by looking at the unravelled form of the master equation, where the evolution is split into (phyiscally meaningful) parts. These individual evolutions may then be stochastically applied to a state in order to obtain a quantum trajectory.

Denoting the (unnormalised) density matrix of the subensemble of quantum systems for which the bath remains in its environmentally preferred state $|0\rangle$ by $\rho_{\mathrm{S}}^{0}(t)$, and the (unnormalised) density matrix of the subensemble for which the bath changes due to non-zero (photon) excitations in the environment by $\rho_{\mathrm{S}}^{\neq}(t)$, one can show that

$$\dot{\rho}_{\mathrm{S}}(t) \;=\; \dot{\rho}_{\mathrm{S}}^{0}(t) + \dot{\rho}_{\mathrm{S}}^{\neq}(t)\,, \tag{2.19}$$

with

$$\begin{aligned}\dot{\rho}_{\mathrm{S}}^{0}(t) &= -\frac{\mathrm{i}}{\hbar}\left[\, H_{\mathrm{int\,I}}(t'), \rho_{\mathrm{S}}(t)\,\right] \\ &\quad -\frac{1}{\Delta t}\frac{1}{\hbar^2}\int_t^{t+\Delta t}\mathrm{d}t'\int_t^{t'}\mathrm{d}t''\Big(\langle 0|H_{\mathrm{SB\,I}}(t')H_{\mathrm{SB\,I}}(t'')|0\rangle\,\rho_{\mathrm{S}}(t)+\mathrm{H.c.}\Big)\end{aligned} \tag{2.20}$$

and

$$\dot{\rho}_{\mathrm{S}}^{\neq}(t) = \frac{1}{\Delta t}\frac{1}{\hbar^2}\,\mathrm{Tr_B}\left(\int_t^{t+\Delta t}\mathrm{d}t'\int_t^{t+\Delta t}\mathrm{d}t''H_{\mathrm{SB\,I}}(t')\,|0\rangle\,\rho_{\mathrm{S}}(t)\,\langle 0|\,H_{\mathrm{SB\,I}}\,(t'')\right). \tag{2.21}$$

Notice that the trace operation in Eq. (2.15) is independent of the basis in which it is performed. Consequently, the dynamics of ρ_{S} does not depend on how the bath is actually measured. Comparing to the master equation in Eq. (2.2), we in fact see that

$$\begin{aligned}\dot{\rho}_{\mathrm{S}}^{0}(t) &= -\frac{\mathrm{i}}{\hbar}\left[H_{\mathrm{int\,I}},\rho_{\mathrm{S}}\right]-\frac{1}{2}\Gamma\left[L^{\dagger}L,\rho_{\mathrm{S}}\right]_{+} \\ \dot{\rho}^{\neq} &= \Gamma L\rho_{\mathrm{S}}L^{\dagger}\end{aligned} \tag{2.22}$$

For very small Δt, Eq. (2.20) can be written in the more compact form of

$$\dot{\rho}_{\mathrm{S}}^{0}(t) = -\frac{\mathrm{i}}{\hbar}\left[H_{\mathrm{cond\,I}}(t)\,\rho_{\mathrm{S}}(t)-\rho_{\mathrm{S}}(t)\,H_{\mathrm{cond\,I}}^{\dagger}(t)\right], \tag{2.23}$$

with $H_{\mathrm{cond\,I}}(t)$ being the (non-Hermitian) conditional Hamiltonian of the open quantum system defined as

$$H_{\mathrm{cond\,I}} = H_{\mathrm{int\,I}}-\frac{1}{\Delta t}\frac{1}{\hbar^2}\int_t^{t+\Delta t}\mathrm{d}t'\int_t^{t'}\mathrm{d}t''\langle 0|H_{\mathrm{SB\,I}}(t')H_{\mathrm{SB\,I}}(t'')|0\rangle\,. \tag{2.24}$$

This means, $\rho_{\mathrm{S}}^{0}(t)$ evolves effectively according to a Schrödinger equation. If the quantum system is initially in a pure state $|\psi_{\mathrm{S}}(t)\rangle$, it remains pure as long as the state of the bath does not change due to system-bath interactions [18, 20]. The probability for the bath to remain in its preferred state $|0\rangle$ for a time Δt equals

$$\begin{aligned}P_0(\Delta t) &= \|\,U_{\mathrm{cond}}(t+\Delta t,t)\,|\psi_{\mathrm{S}}(t)\rangle\,\|^2 \\ &= \mathrm{Tr}\left(\rho_{\mathrm{S}}^{0}(t+\Delta t)\right),\end{aligned} \tag{2.25}$$

where $U_{\text{cond}}(t+\Delta t, t)$ denotes the time evolution operator corresponding to $H_{\text{cond}}(t)$.

Finally, it should be noted that this unravelling provides the Kraus operators describing the system's evolution [23]. Kraus operators are generalised measurements that describe how the system evolves given a certain measurement. The set of Kraus operators describing a system provides a completely positive trace preserving map (CPTP map). In this case, we have seen that the system can be decomposed into two subensembles. Hence, there are two Kraus operators that describe the evolution of our system. Over a short time interval $(t, t+\Delta t)$, the Kraus operators describing the system's evolution may be defined as

$$K_0(\Delta t) \;=\; U_{\text{cond}}(t+\Delta t, t) \quad K_1(\Delta t) = \sqrt{\Gamma \Delta t} L\,, \tag{2.26}$$

where $K_0(\Delta t)$ describes the no-photon evolution, while $K_1(\Delta t)$ describes the evolution under photon emission. Applying these operators to a quantum state returns the unnormalised state describing the system at a later time, the size of which corresponds to the probability of the transition. Using these equations, identifying the relevant Kraus operators for a specific open quantum system is now straightforward. The Kraus operators should form a complete set to ensure probabilities are properly defined, meaning

$$\sum_i K_i^\dagger K_i \;=\; 1\,. \tag{2.27}$$

This condition is approximately fulfilled so long as Δt is sufficiently small.

2.1.3 Master equations with instantaneous feedback

Repeating the above derivation of Eq. (2.18) while assuming that the quantum system experiences a unitary feedback operation, R_m, with probability η_m whenever the state of the bath is found in $|m\rangle$ and $m \neq 0$, we arrive again at Eqs. (2.20)

and (2.23) but with Eq. (2.21) replaced by

$$\begin{aligned}\dot{\rho_{\mathrm{S}}}^{\neq}(t) &= \frac{1}{\Delta t}\frac{1}{\hbar^2}\sum_{m\neq 0}(1-\eta_m)\int_t^{t+\Delta t}\mathrm{d}t'\int_t^{t+\Delta t}\mathrm{d}t'' \\ &\quad\times\langle m|\,H_{\mathrm{SB\,I}}(t')\,|0\rangle\,\rho_{\mathrm{S}}(t)\,\langle 0|\,H_{\mathrm{SB\,I}}\,(t'')\,|m\rangle \\ &\quad+\frac{1}{\Delta t}\frac{1}{\hbar^2}\sum_{m\neq 0}\eta_m\int_t^{t+\Delta t}\mathrm{d}t'\int_t^{t+\Delta t}\mathrm{d}t'' \\ &\quad\times R_m\,\langle m|\,H_{\mathrm{SB\,I}}(t')\,|0\rangle\,\rho_{\mathrm{S}}(t)\,\langle 0|\,H_{\mathrm{SB\,I}}\,(t'')\,|m\rangle\,R_m^{\dagger}\,. \end{aligned} \tag{2.28}$$

The kind of feedback described in this work is often referred to as *instantaneous feedback*, since it acts on the time scale Δt that is much shorter than the time scale given by the internal system dynamics [14]. If the feedback was not considered to be instantaneous, it would make the evolution non-Markovian. An alternate way to introduce feedback is to consider the change in the Hamiltonian H_{SB}. As the introduction of the feedback described above only alters the dissipation terms it must be present in H_{SB} and not in H_{int}. We will now look at a general quantum optical system to see how the above can be applied to derive a master equation.

2.1.4 General derivation of master equations for quantum optical system

In the following, we show how master equations can be used to model the time evolution of open quantum systems with linear couplings between the quantum system and its surrounding bath. In this section, we shall consider a very general quantum optical system that will be required later in Chapter 4.

Our starting point is the Hamiltonian H for system and bath, which can be split into four parts as usual. These are

$$H = H_{\mathrm{S}} + H_{\mathrm{int}} + H_{\mathrm{B}} + H_{\mathrm{SB}}\,, \tag{2.29}$$

where the Hamiltonians represent the same as described above. When denoting the energy eigenstates of system and bath by $|n\rangle_{\mathrm{S}}$ and $|m\rangle_{\mathrm{B}}$, respectively, and assuming a linear coupling between system and environment, H_{S}, H_{B}, and H_{SB}

can be written as

$$\begin{aligned} H_{\mathrm{S}} &= \sum_{n=1}^{N} \hbar\omega_n |n\rangle_{\mathrm{SS}}\langle n| \,, \\ H_{\mathrm{B}} &= \sum_{m=0}^{\infty} \hbar\omega_m |m\rangle_{\mathrm{BB}}\langle m| \,, \\ H_{\mathrm{SB}} &= \sum_{m,m'=0}^{\infty} \sum_{n,n'=1}^{N} \hbar g_{nm,n'm'} |n'm'\rangle_{\mathrm{SB\,SB}}\langle nm| + \mathrm{H.c.} \,, \end{aligned} \tag{2.30}$$

without loss of generality. Because of being a bath, an infinite number of highly degenerate energy levels $\hbar\omega_m$ may occur. Finally, the g's are system-bath coupling constants. Here, we assume for simplicity that these are time independent, though this is not always the case.

Since we are interested in identifying the relatively slow, effective internal dynamics of the open quantum system, we now move into the interaction picture with respect to the free system $H_0 = H_{\mathrm{B}} + H_{\mathrm{S}}$, giving the interaction Hamiltonian

$$\begin{aligned} H_{\mathrm{I}}(t) &= \sum_{m,m'=0}^{\infty} \sum_{n,n'=1}^{N} \hbar g_{nm,n'm'} |n'm'\rangle_{\mathrm{SB\,SB}}\langle nm| \, \mathrm{e}^{-\mathrm{i}(\omega_m - \omega_{m'} + \omega_n - \omega_{n'})t} \\ &\quad + \mathrm{H.c.} + H_{\mathrm{int\,I}}(t) \,, \end{aligned} \tag{2.31}$$

with $H_{\mathrm{int\,I}}(t)$ describing the internal dynamics of the system in the interaction picture.

Next, if we assume the environment is now a continuum of modes, we may use the arguments presented in above to derive the master equation of this system. Hence, we find that the master equation is given by

$$\begin{aligned} \dot{\rho}_{\mathrm{S}} &= -\frac{i}{\hbar}\left[H_{\mathrm{int\,I}}, \rho_{\mathrm{S}}\right] - \frac{1}{2} \sum_{n,n',n'',n'''=1}^{N} \xi_{nn'} \xi^*_{n''n'''} \left[L^\dagger_{n''n'''} L_{nn'}, \rho_{\mathrm{S}}\right]_+ \\ &\quad + \sum_{n,n',n'',n'''=1}^{N} \xi_{nn'} \xi^*_{n''n'''} \, L_{nn'} \, \rho_{\mathrm{S}} \, L^\dagger_{n''n'''} \,. \end{aligned} \tag{2.32}$$

The L's in this equation are operators that act on the internal states of the open quantum system and the ξ's are constants. In addition, one can show that the above equation is of Lindblad form [4].

Eq. (2.32) describes open quantum systems without feedback. These are quantum systems where the environment does nothing else but reset the bath that surrounds the system back into its pointer state. However, this does not necessarily have to be the case. As we have already seen in previous chapters, open quantum systems can be designed such that the transfer of energy into the environment triggers a back action, which changes the density matrix $\rho_{\rm S}(t)$ by a unitary operation. This is achieved by introducing feedback. Using the same arguments as above, one can show that the open quantum system evolves in this case according to a master equation of the general form

$$\begin{aligned}\dot{\rho}_{\rm S} &= -\frac{i}{\hbar}\left[H_{\rm int\,I},\rho_{\rm S}\right] \\ &\quad -\frac{1}{2}\sum_{m=1}^{\infty}\sum_{n,n',n'',n'''=1}^{N}\xi_{nn',m}\xi^{*}_{n''n''',m}\left[L^{\dagger}_{n''n''',m}L_{nn',m},\rho_{\rm S}\right]_{+} \\ &\quad +\sum_{m=1}^{\infty}\sum_{n,n',n'',n'''=1}^{N}\xi_{nn',m}\xi^{*}_{n''n''',m}\,L_{nn',m}\,\rho_{\rm S}\,L^{\dagger}_{n''n''',m}\,, \end{aligned} \tag{2.33}$$

with the $L_{nn',m}$ operators defined such that

$$L_{nn',m} = R_m\,L_{nn'}\,. \tag{2.34}$$

Here, the $L_{nn'}$ operators are the standard Lindblad operators for the system and the R_m are unitary operations applied depending on the measured state of the environment $|m\rangle$. This equation is of exactly the same form as the master equation for open quantum systems with instantaneous feedback in Eq. (2.28) and others already encountered. Here, $|m\rangle_{\rm B}$ is the state that became excited by the system-bath interaction and the R_m is a unitary operator, which acts conditionally on the internal state of the quantum system and describes the respectively applied feedback operation.

2.2 Optical cavity in a quantum feedback loop

We shall now consider a more specific example. An open quantum system that we will analyse more thoroughly later in this work is that of an optical cavity inside an instantaneous quantum feedback loop. In this section, we shall discuss the

theoretical background needed to study this system. Applying the ideas introduced in Section 2.1 to a specific Hamiltonian is now straightforward. Here, we derive the master equation of a laser-driven optical cavity inside an instantaneous quantum feedback loop in its most basic form. In later sections, this derivation will be recalled and adapted to highlight specific additional features.

2.2.1 Master equation for an optical cavity without feedback

Using the notation introduced in Section 2.1 and in Refs. [7, 11, 13, 18], we split our Hamiltonian into four parts as shown in Eqs. (2.6)-(2.10). For this system, these terms are given by

$$\begin{aligned} H_{\mathrm{S}} &= \hbar\omega_{\mathrm{cav}} c^{\dagger} c \\ H_{\mathrm{B}} &= \sum_{\lambda=1,2} \int_0^{\infty} \mathrm{d}\omega\, \hbar\omega a_{\lambda}^{\dagger}(\omega) a_{\lambda}(\omega) \\ H_{\mathrm{int}} &= \frac{1}{2}\hbar\Omega \left(\mathrm{e}^{\mathrm{i}\omega_{\mathrm{L}} t} c + \mathrm{H.c.}\right) \\ H_{\mathrm{SB}} &= \sum_{\lambda=1,2} \int_0^{\infty} \mathrm{d}\omega\, \hbar g(\omega) a_{\lambda}(\omega) c^{\dagger} + \mathrm{H.c.}\,, \end{aligned} \tag{2.35}$$

where $a_{\lambda}(\omega)(a_{\lambda}^{\dagger}(\omega))/c(c^{\dagger})$ are the annihilation (creation) operators for the field/cavity and obey bosonic commutation rules of $\left[a_{\lambda}(\omega), a_{\lambda'}^{\dagger}(\omega')\right] = \delta_{\lambda\lambda'}\delta(\omega - \omega')$ and $\left[c, c^{\dagger}\right] = 1$. Furthermore, the ω terms are frequencies and Ω is the laser Rabi frequency. From here on, only one polarisation is considered, which remains constant throughout all work here and we shall set $\omega_{\mathrm{L}} = \omega_{\mathrm{cav}}$ for simplicity. As in Eq. (2.8), we can split the Hamiltonian H into two parts, H_0 and H_1. In doing so and moving into an interaction Hamiltonian with respect to $H_0 = H_{\mathrm{S}} + H_{\mathrm{B}}$, we obtain a Hamiltonian $H_{\mathrm{I}}(t)$ as in Eq. (2.10). Explicitly, this Hamiltonian is now given by

$$H_{\mathrm{I}}(t) = \frac{\hbar\Omega}{2}\left(c + c^{\dagger}\right) + \int_0^{\infty} \mathrm{d}\omega\, \left(\hbar g(\omega) \mathrm{e}^{-\mathrm{i}(\omega - \omega_{\mathrm{cav}})t} a(\omega) c^{\dagger} + \mathrm{H.c.}\right). \tag{2.36}$$

Perturbative expansion

As highlighted in Section 2.1, we now perform second order perturbation theory in order to generate the master equation. The ultimate aim of this process is to find the coarse-grained time evolution between two close time intervals. Up to second order, the time evolution operator describing the evolution between t and $t+\Delta t$ is given by Eq. (2.17). When considering the first term of Eq. (2.36), we notice that it is time-independent. As such, moving to higher orders of perturbation theory increases the scaling in Δt. For example, the time evolution for this Hamiltonian is $U(t+\Delta t, t) = \exp\left(-\frac{\mathrm{i}}{\hbar} H_{\mathrm{int}} \Delta t\right)$. Applying perturbation theory to this time evolution operator up to second order in Δt, we find

$$U(t+\Delta t, t) \;=\; 1 - H_{\mathrm{int\,I}}\Delta t - \frac{1}{2} H_{\mathrm{int\,I}}^2 \Delta t^2 \,. \tag{2.37}$$

However, as Δt is required to be extremely small, higher order terms become negligible. When evaluating Eq. (2.16) we only consider terms linear in Δt. In fact, upon taking the limit $\Delta t \to 0$ when calculating the master equation and mapping onto the continuous time evolution, the terms of order Δt^2 and above naturally tend to zero. Hence, this term simply gives the von Neumann term in the master equation, as second order and above perturbations are vanishingly small. However, when evaluating the perturbative expansion for the system-environment Hamiltonian $H_{\mathrm{SE\,I}}$, it can be shown that the first order terms do not contribute. This is because of the trace over the environment, as first order terms will always create an imbalance in the environmental density matrix. As such, we must consider second order terms in order to get a contribution.

Hence, considering up to second order in perturbation theory, we can evaluate the time evolution of the density matrix describing the cavity. Following the procedure highlighted in Section 2.1, we may now evaluate the terms in perturbation theory by using the specific Hamiltonians. Using the properties of $H_{\mathrm{int\,I}}$ and $H_{\mathrm{SE\,I}}$

described above, we may write $\rho(t+\Delta t)$ as

$$\begin{aligned}\rho_{\mathrm{I}}(t+\Delta t) &= \rho_{\mathrm{I}}(t) - \frac{\mathrm{i}}{\hbar}\int_{t}^{t+\Delta t}\mathrm{d}t'\,[H_{\mathrm{int\,I}},\rho_{\mathrm{I}}(t')] \\ &\quad + \frac{1}{\hbar^2}\langle 0_{\mathrm{E}}|\int_{t}^{t+\Delta t}\mathrm{d}t'\int_{t}^{t+\Delta t}\mathrm{d}t'' H_{\mathrm{SE\,I}}(t')\,|0_{\mathrm{E}}\rangle\,\rho_{\mathrm{I}}\,\langle 0_{\mathrm{E}}|\,H_{\mathrm{SE\,I}}(t'')\,|0_{\mathrm{E}}\rangle \\ &\quad - \frac{1}{\hbar^2}\langle 0_{\mathrm{E}}|\int_{t}^{t+\Delta t}\mathrm{d}t'\int_{t}^{t'}\mathrm{d}t''\,[H_{\mathrm{SE\,I}}(t'')H_{\mathrm{SE\,I}}(t'),\rho_{\mathrm{I}}(t)]_{+}\,|0_{\mathrm{E}}\rangle\ . \end{aligned} \tag{2.38}$$

We shall begin by reviewing Eq. (2.37) and seeing that the first line of Eq. (2.38) simplifies to

$$\rho_{\mathrm{I}}(t) - \frac{\mathrm{i}}{\hbar}\int_{t}^{t+\Delta t}[H_{\mathrm{int\,I}},\rho_{\mathrm{I}}(t)] = \rho_{\mathrm{I}}(t) - \frac{\mathrm{i}}{\hbar}[H_{\mathrm{int\,I}},\rho_{\mathrm{I}}(t)]\,\Delta t\,. \tag{2.39}$$

Next, we shall consider the second and third lines of Eq. (2.38). For ease of writing, we shall label the co-efficient of the second line A and of the third line B for this section. In the second term, A, the application of the trace creates a delta-function. Specifically, when substituting in the expression H_{SE}, we find that

$$\begin{aligned} A &= \mathrm{Tr}_{\mathrm{E}}\Bigg(\int_{0}^{\infty}\mathrm{d}\omega\int_{0}^{\infty}\mathrm{d}\omega'\int_{t}^{t+\Delta t}\mathrm{d}t'\int_{t}^{t+\Delta t}\mathrm{d}t''\mathrm{e}^{-\mathrm{i}[(\omega-\omega_{\mathrm{cav}})t'-(\omega'-\omega_{\mathrm{cav}})t'']} \\ &\qquad \times g^{*}(\omega)g(\omega')a^{\dagger}(\omega)c\,|0_{\mathrm{E}}\rangle\,\rho_{\mathrm{I}}(t)\,\langle 0_{\mathrm{E}}|\,a(\omega')c^{\dagger}\Bigg) \\ &= \mathrm{Tr}_{\mathrm{E}}\Bigg(\int_{0}^{\infty}\mathrm{d}\omega\int_{0}^{\infty}\mathrm{d}\omega'\int_{t}^{t+\Delta t}\mathrm{d}t'\int_{t}^{t+\Delta t}\mathrm{d}t''\mathrm{e}^{-\mathrm{i}[(\omega-\omega_{\mathrm{cav}})t'-(\omega'-\omega_{\mathrm{cav}})t'']} \\ &\qquad \times g^{*}(\omega)g(\omega')c\,|1_{\mathrm{E}}(\omega)\rangle\,\rho_{\mathrm{I}}(t)\,\langle 1_{\mathrm{E}}(\omega')|\,c^{\dagger}\Bigg)\,. \end{aligned} \tag{2.40}$$

We now evaluate the trace, giving

$$\begin{aligned} A &= \int_0^\infty \mathrm{d}\omega \int_0^\infty \mathrm{d}\omega' \int_t^{t+\Delta t} \mathrm{d}t' \int_t^{t+\Delta t} \mathrm{d}t'' \mathrm{e}^{-\mathrm{i}[(\omega-\omega_{\mathrm{cav}})t'-(\omega'-\omega_{\mathrm{cav}})t'']} \\ &\quad \times g^*(\omega) g(\omega') c \rho_{\mathrm{I}}(t) c^\dagger \delta\left(\omega-\omega'\right) . \end{aligned} \tag{2.41}$$

Finally, performing the integral over ω', we find that

$$A = \int_0^\infty \mathrm{d}\omega \int_t^{t+\Delta t} \mathrm{d}t' \int_t^{t+\Delta t} \mathrm{d}t'' \mathrm{e}^{-\mathrm{i}(\omega-\omega_{\mathrm{cav}})(t'-t'')} \left|g(\omega')\right|^2 c \rho_{\mathrm{I}}(t) c^\dagger . \tag{2.42}$$

Similarly for B, we have

$$\begin{aligned} B &= \mathrm{Tr}_{\mathrm{E}}\Bigg(\int_0^\infty \mathrm{d}\omega \int_0^\infty \mathrm{d}\omega' \int_t^{t+\Delta t} \mathrm{d}t' \int_t^{t+\Delta t} \mathrm{d}t'' \mathrm{e}^{-\mathrm{i}[(\omega-\omega_{\mathrm{cav}})t'-(\omega'-\omega_{\mathrm{cav}})t'']} \\ &\quad \times g^*(\omega) g(\omega') \left[a(\omega) c^\dagger a^\dagger(\omega) c, \left|0_{\mathrm{E}}\right\rangle \rho_{\mathrm{S}}(t) \left\langle 0_{\mathrm{E}}\right|\right]_+ \\ &= \mathrm{Tr}_{\mathrm{E}}\Bigg(\int_0^\infty \mathrm{d}\omega \int_0^\infty \mathrm{d}\omega' \int_t^{t+\Delta t} \mathrm{d}t' \int_t^{t+\Delta t} \mathrm{d}t'' \mathrm{e}^{-\mathrm{i}[(\omega-\omega_{\mathrm{cav}})t'-(\omega'-\omega_{\mathrm{cav}})t'']} \\ &\quad \times g^*(\omega) g(\omega') \left[\delta\left(\omega-\omega'\right) c^\dagger c, \left|0_{\mathrm{E}}\right\rangle \rho_{\mathrm{I}}(t) \left\langle 0_{\mathrm{E}}\right|\right]_+ \Bigg) \\ &= \int_0^\infty \mathrm{d}\omega \int_t^{t+\Delta t} \mathrm{d}t' \int_t^{t+\Delta t} \mathrm{d}t'' \mathrm{e}^{-\mathrm{i}(\omega-\omega_{\mathrm{cav}})(t'-t'')} \left|g(\omega)\right|^2 \left[c^\dagger c, \rho_{\mathrm{I}}(t)\right]_+ . \end{aligned} \tag{2.43}$$

The trace enforces frequency matching on the photons emitted by the cavity field and those detected in the environment. This takes care of one of the integrals in a straightforward way. Now, we shall consider how to further simplify these expressions by evaluating the remaining integrals. Let us consider B initially. The first step in simplifying this expression is to impose Markovianity. In doing so, we make the so-called Markov approximation. This means in effect we replace the lower limit of the t'' integral with $-\infty$, meaning

$$\int_t^{t'} \mathrm{d}t'' \to \int_{-\infty}^{t'} \mathrm{d}t'' . \tag{2.44}$$

This applies very well when $t \ll t + \Delta t$. We next notice that this integral has a singularity for $\omega = \omega_{\text{cav}}$ that we must be careful of when evaluating it. To do so, we shall use a form of the Cauchy principle value theorem. Firstly, we introduce an infinitesimal term η to the exponential to help us evaluate it. Starting from Eq. (2.43), considering only the t'' initially and using Eq. (2.44), we have

$$\begin{aligned}
&\int_{-\infty}^{t'} \mathrm{d}t'' \, |g(\omega)|^2 \, \mathrm{e}^{-\mathrm{i}(\omega-\omega_{\text{cav}})(t'-t'')} \\
&\qquad = \lim_{\eta\to 0^+} \int_{-\infty}^{t'} \mathrm{d}t'' \, |g(\omega)|^2 \, \mathrm{e}^{-\mathrm{i}(\omega-\omega_{\text{cav}})(t'-t'')+\eta t''} \\
&\qquad = \lim_{\eta\to 0^+} |g(\omega)|^2 \, \frac{\mathrm{e}^{\eta t'}}{\eta + \mathrm{i}\,(\omega-\omega_{\text{cav}})} \\
&\qquad = \lim_{\eta\to 0^+} |g(\omega)|^2 \, \mathrm{e}^{\eta t'} \left(\frac{\eta}{\eta^2 + (\omega-\omega_{\text{cav}})^2} - \frac{\mathrm{i}\,(\omega-\omega_{\text{cav}})}{\eta^2 + (\omega-\omega_{\text{cav}})^2} \right) \\
&\qquad = \lim_{\eta\to 0^+} |g(\omega)|^2 \, \frac{\eta \, \mathrm{e}^{\eta t'}}{\eta^2 + (\omega-\omega_{\text{cav}})^2} - \frac{\mathrm{i}}{\omega-\omega_{\text{cav}}} \, . \qquad (2.45)
\end{aligned}$$

The limit in the first term can be evaluated by noticing it is of the form of a Lorentzian or Cauchy-distribution, $L(x)$, which is defined as

$$L(x) \;=\; \frac{1}{\pi} \frac{\gamma}{x^2+\gamma^2} \, . \qquad (2.46)$$

This function is normalised such that

$$\int_{-\infty}^{\infty} L(x)\mathrm{d}x \;=\; 1 \, . \qquad (2.47)$$

It can also be used as a way of defining the δ-function due to its unit area. By taking the limit of $\gamma \to 0$, the curve becomes infinitely narrow and tall but maintains its normalisation and is hence a δ-function. Thus,

$$\lim_{\gamma\to 0} \frac{1}{\pi} \frac{\gamma}{x^2+\gamma^2} \;=\; \delta\,(x) \, . \qquad (2.48)$$

Hence, using Eq. (2.48), we can evaluate the limit in Eq. (2.45) and thus find

$$\int_{-\infty}^{t'} \mathrm{d}t'' \, |g(\omega)|^2 \, \mathrm{e}^{-\mathrm{i}(\omega-\omega_{\text{cav}})(t'-t'')} \;=\; |g(\omega)|^2 \, \pi\delta\,(\omega-\omega_{\text{cav}}) - \mathrm{i}\,|g(\omega)|^2 \, \frac{1}{(\omega-\omega_{\text{cav}})} \, . \qquad (2.49)$$

The first term of this equation is the decay rate of the cavity, while the second represents a level shift. The level shift has the effect of modifying the energy of a mode. Its exact form is not important for the work presented here, as it can be absorbed into the free energy of the system. Hence, it shall be ignored from here on. Now, without considering the level shift, substituting the result of Eq. (2.49) into Eq. (2.43), we now have

$$B = \int_0^\infty \mathrm{d}\omega \int_t^{t+\Delta t} \mathrm{d}t' \kappa \delta\left(\omega - \omega_{\mathrm{cav}}\right) , \tag{2.50}$$

where $\kappa = 2\pi \left|g(\omega)\right|^2$ and is the cavity decay rate. Applying the final two integrals, we finally arrive at

$$B = \kappa \Delta t \, . \tag{2.51}$$

By using the properties of integrals, one can show that $A = 2\,\mathrm{Re}(B)$ (and is hence independent of the level shift). Alternatively, it the integral in A transforms as

$$\int_t^{t+\Delta t} \mathrm{d}t'' \to \int_{-\infty}^{\infty} \mathrm{d}t'' \, , \tag{2.52}$$

by the Markov approximation. Using this property with Eq. (2.51) and recalling Eq. (2.39), we can substitute back into Eq. (2.38) to find

$$\rho_{\mathrm{I}}(t+\Delta t) = \rho_{\mathrm{I}}(t) - \frac{\mathrm{i}}{\hbar}\left[H_{\mathrm{int\,I}}, \rho_{\mathrm{I}}(t)\right]\Delta t + \kappa\left(c\rho_{\mathrm{I}}(t)c^\dagger - \frac{1}{2}\left[c^\dagger c, \rho_{\mathrm{I}}(t)\right]_+\right)\Delta t \, . \tag{2.53}$$

Substituting this into Eq. (2.16), we finally arrive at

$$\dot{\rho}_{\mathrm{I}} = -\frac{\mathrm{i}}{\hbar}\left[H_{\mathrm{int\,I}}, \rho_{\mathrm{I}}\right] + \kappa\left(c\rho_{\mathrm{I}}c^\dagger - \frac{1}{2}\left[c^\dagger c, \rho_{\mathrm{I}}\right]_+\right) , \tag{2.54}$$

which is the master equation in Lindblad form. Here, the time argument of the density matrix ρ_{I} has been dropped for simplicity.

2.2.2 Master equation for an optical cavity with instantaneous quantum feedback

As highlighted in Section 2.1.3, incorporating instantaneous feedback into the master equation is straightforward. Effectively, we transform the Lindblad terms. The feedback that we wish to consider here is in the form of a displacement operator. Details on displacement operators and coherent states can be found in Appendix A. In order to do this, we simply make the change

$$c \rightarrow D(\beta)c\,. \tag{2.55}$$

This means Eq. (2.54) is transformed into

$$\dot{\rho}_{\mathrm{I}} = -\frac{\mathrm{i}}{\hbar}\left[H_{\mathrm{int\,I}},\rho_{\mathrm{I}}\right] + \kappa\left(D(\beta)c\rho_{\mathrm{I}}c^{\dagger}D^{\dagger}(\beta) - \frac{1}{2}\left[c^{\dagger}c,\rho_{\mathrm{I}}\right]_{+}\right). \tag{2.56}$$

Notice the final term $\left[c^{\dagger}c,\rho_{\mathrm{I}}\right]_{+}$ is unchanged, as $c^{\dagger}D^{\dagger}(\beta)D(\beta)c = c^{\dagger}c$ due to the unitarity of $D(\beta)$. This equation is still of Lindblad form, as we could introduce a new operator $L = D(\beta)c$, meaning we can write the master equation as

$$\dot{\rho}_{\mathrm{I}} = -\frac{\mathrm{i}}{\hbar}\left[H_{\mathrm{int\,I}},\rho_{\mathrm{I}}\right] + \kappa\left(L\rho_{\mathrm{I}}L^{\dagger} - \frac{1}{2}\left[L^{\dagger}L,\rho_{\mathrm{I}}\right]_{+}\right). \tag{2.57}$$

This equation is of the same form as Eq. (2.54).

2.2.3 Unravelling of the master equation for an optical cavity inside a quantum feedback loop

We will now introduce the theoretical tools needed to analyse the dynamics of an optical cavity with continuous laser driving and an optical cavity inside an instantaneous quantum feedback loop. The master equation that we have derived here describes the evolution of an ensemble of quantum systems. However, we shall later need to consider individual quantum trajectories of this system. Hence, in order to effectively study these systems, particularly in the case of feedback, we need to consider the unravelled dynamics. We will now introduce this for the specific example of an optical cavity inside an instantaneous quantum feedback loop. This shall follow the ideas introduced in Section 2.1.2

The no-photon time evolution of the cavity field

Following the ideas of Refs. [20, 21, 22], Section 2.1.2 and the above calculations from this section, we assume in the following that the free radiation field surrounding the cavity is in general in its so-called environmentally preferred state, the vacuum state. Denoting the vacuum state by $|0\rangle$ and the state of the cavity at time t by $|\psi_{\mathrm{S}}(t)\rangle$, the total state of the system equals

$$|\psi_{\mathrm{SB}}(t)\rangle \;=\; |0\rangle\,|\psi_{\mathrm{S}}(t)\rangle\,. \tag{2.58}$$

Using the results of Section 2.1.2 and the preceeding work in this section we find that the state $|\psi_{\mathrm{S}}^{0}(t)\rangle$ evolves effectively with the non-Hermitian conditional Hamiltonian

$$H_{\mathrm{cond\,I}} \;=\; H_{\mathrm{int\,I}} - \frac{\mathrm{i}}{2}\hbar\kappa\, c^{\dagger}c\,, \tag{2.59}$$

under the condition of no photon emission in $(t, t+\Delta t)$ and in the interaction picture. As it should, this Hamiltonian is of the same form as the conditional Hamiltonian in Eq. (2.24). Comparing both equations with the master equation, we see that the Lindblad operator L of an optical cavity is given by $L = c$, while the spontaneous decay rate $\Gamma = \kappa$. Finally, using Eq. (2.25), we may calculate the probability of the cavity not emitting a photon in a time interval $(t, t+\Delta t)$, i.e. $P_0(\Delta t)$. Trivially, this also tells us the probability of the cavity emitting a photon in this time period ($P_1(\Delta t) = 1 - P_0(\Delta t)$). This is important for simulating the dynamics of an open quantum system, as we will see later.

Spontaneous photon emission and quantum feedback

Analogously, proceeding as suggested in Refs. [20, 21, 22] and evaluating the density matrix $\rho^{\neq}(t+\Delta t)$ of an optical cavity under the condition of a photon detection in $(t, t+\Delta t)$ using second order perturbation theory, we find that the state of the resonator immediately after an emission equals [7]

$$|\psi_{\mathrm{S}}^{\neq}(t+\Delta t)\rangle \;=\; \sqrt{\kappa\,\Delta t}\,c\,|\psi_{\mathrm{S}}(t)\rangle\,, \tag{2.60}$$

up to normalisation. The absolute value of the normalisation constant of this state squared equals the probability for the emission of a photon in $(t, t + \Delta t)$. Hence

$$I(t) \quad = \quad \kappa \langle c^\dagger c \rangle_t \tag{2.61}$$

is the probability density for the emission of a photon at time t. Here $\langle c^\dagger c \rangle_t = \langle \psi_{\rm S}(t) | c^\dagger c \, | \psi_{\rm S}(t) \rangle$ denotes the mean number of photons inside the resonator at a time t, when prepared in the state $|\psi_{\rm S}(t)\rangle$.

If the emission of a photon successfully triggers a feedback pulse, up to normalisation, the state $|\psi_{\rm S}^{\neq}(t + \Delta t)\rangle$ of the cavity becomes [7, 14]

$$|\psi_{\rm S}^{\neq}(t + \Delta t)\rangle \quad = \quad \sqrt{\kappa}\, Rc \, |\psi_{\rm S}(t)\rangle \tag{2.62}$$

in case of an emission, where R is the unitary operator that describes the effect of the feedback on the resonator field.

The relevant master equations

To obtain the density matrix $\rho(t)$ of the cavity field, we need to add the density matrix $\rho_{\rm S}^0(t)$ of the subensemble of cavities with no photon emission in $(t, t + \Delta t)$ and the density matrix $\rho_{\rm S}^{\neq}(t)$ of the subensemble of cavities with a photon emission in $(t, t+\Delta t)$. If Δt is sufficiently small, contributions with more than one emission remain negligible and

$$\dot\rho_{\rm S}(t) \quad = \quad \dot\rho_{\rm S}^0(t) + \dot\rho_{\rm S}^{\neq}(t) \, . \tag{2.63}$$

For this equation to apply, both density matrices $\rho_{\rm S}^0(t)$ and $\rho_{\rm S}^{\neq}(t)$ need to be normalised such that their relative size coincides with the probability density for an emission or no emission at time t. Taking this into account and using the results of the previous two subsections, we obtain the time derivative $\dot\rho_{\rm S}$ of an optical cavity with continuous laser driving. It equals

$$\dot\rho_{\rm I} \quad = \quad -\frac{\rm i}{2}\Omega \, \left[c + c^\dagger, \rho_{\rm I}\right] + \frac{1}{2}\kappa \left(2c\rho_{\rm I}c^\dagger - \left[c^\dagger c, \rho_{\rm I}\right]_+\right) \tag{2.64}$$

in the interaction picture with respect to the free energy of the resonator field.

Now suppose the continuous laser driving is turned off and a detector monitors the spontaneous leakage of photons through one of its mirrors, as illustrated in Fig. 3.4. Moreover suppose an instantaneous quantum feedback loop is activated whenever a photon is detected. Proceeding as described above, we find that the master equation of the resonator equals

$$\dot{\rho}_{\mathrm{I}} = \frac{1}{2}\eta\kappa\left(2R_{\mathrm{I}}c\rho_{\mathrm{I}}c^{\dagger}R_{\mathrm{I}}^{\dagger} - \left[c^{\dagger}c,\rho_{\mathrm{I}}\right]_{+}\right) + \frac{1}{2}\left(1-\eta\right)\kappa\left(2c\rho_{\mathrm{I}}c^{\dagger} - \left[c^{\dagger}c,\rho_{\mathrm{I}}\right]_{+}\right) \tag{2.65}$$

in this case, where H_{cond} is now of the form

$$H_{\mathrm{cond}} = -\mathrm{i}\hbar\kappa c^{\dagger}c\,. \tag{2.66}$$

The first term in Eq. (2.65) effectively describes resonators that experience feedback, while the second term takes undetected photon emission events into account. As usual, η denotes the detector efficiency. Moreover, R_{I} denotes the unitary operator R in Eq. (2.62) after transformation into the interaction picture with respect to $H_0 = H_{\mathrm{S}}$. In this section, we consider quantum feedback in the form of very short and strong resonant laser pulses. This means that R_{I} is the unitary time evolution operator associated with a laser Hamiltonian with a time-independent Rabi frequency. Hence R_{I} too is time-independent and is chosen to be equal to a displacement operator as before. Simplifying Eq. (2.65) eventually yields

$$\dot{\rho}_{\mathrm{I}} = \frac{1}{2}\kappa\left(2c\rho_{\mathrm{I}}c^{\dagger} - \left[c^{\dagger}c,\rho_{\mathrm{I}}\right]_{+}\right) + \eta\kappa\left(R_{\mathrm{I}}c\rho_{\mathrm{I}}c^{\dagger}R_{\mathrm{I}}^{\dagger} - c\rho_{\mathrm{I}}c^{\dagger}\right). \tag{2.67}$$

As a final step, we may now consider the general case of an optical cavity subject to continuous laser driving and also quantum feedback. In this case we add the complete solutions from Eq. (2.62) and Eq. (2.59) with the appropriate choices for $H_{\mathrm{int\,I}}$ and R into Eq. (2.63), which gives exactly Eq. (2.56). Hence, this gives the same master equaiton that was previously obtained in Section 2.2. However, the unravelled dynamics will be important in future chapters when the system needs to be analysed in more detail.

Numerical simulation of master equation

In some cases, solving the master equation analytically is difficult. In such a case, a useful way of studying the dynamics of an open quantum system is by use of the quantum jump approach. This utilises the unravelling of the master equation. This method can be summarised as follows:

1. Apply the no-photon time evolution operator $U_{\text{cond}}(t+\Delta t, t)$. It is important Δt is chosen to be small compared to the emission rate of the cavity $\left(\Delta t \ll \left(\Gamma \left\langle c^\dagger c \right\rangle\right)^{-1}\right)$, so as to insure photon emissions are not overlooked.
2. Calculate the probability of emission P_1 using Eq. (2.25).
3. Call a random number. If the random number is less than or equal to P_1, record a photon emission. Reset the system accordingly (apply the Lindblad operator L to the system and renormalise).
4. Repeat for desired amount of time.

For coherent states $|\alpha\rangle$ this is particularly straightforward, as only the parameter α describing the coherent state needs to be kept track of in terms of the state of the system.

2.3 Two-level atom with feedback

We shall now consider another specific simple example of a system that is subject to quantum feedback. Specifically, we will examine the behaviour of a two-level atom subject to a rotation on the Bloch sphere (corresponding to some excitaiton put into the system) upon emission and resonant laser driving. The basic Hamiltonian of this system is given by $H = H_0 + H_1$, where similarly to the previous case we have

$$\begin{aligned} H_0 &= H_{\text{atom}} + H_{\text{field}} \\ &= \hbar\omega_0 \sigma^+\sigma^- + \sum_{\lambda=1,2} \int_0^\infty \mathrm{d}\omega\, \hbar\omega a_\lambda^\dagger(\omega) a_\lambda(\omega) \\ H_1 &= H_{\text{atom-field}} + H_{\text{laser}}\,, \end{aligned} \tag{2.68}$$

where ω is the frequency of the field modes described by the bosonic annihilation/creation operators $a_\lambda(\omega)/a_\lambda^\dagger(\omega)$ obeying the same bosonic commutation rules as before and the λ are the two respective polarisations of light. Furthermore, ω_0 is the frequency of the atomic system described by the raising/lowering operators σ^+/σ^-. The interaction terms in H_1 are of similar form to those in the previous subsection. The atom-field coupling can be calculated in the exact same way as in the previous case. Once again, the polarisation may be neglected from here on as it will not affect the dynamics of our system. The laser-driving term in H_{laser} now comes from the coupling of the applied laser field to the atom. As is standard for such quantum optical systems, we assume dipole coupling of the form

$$H_{\text{laser}} \;=\; e\,\mathbf{d}\cdot\mathbf{E}\,, \tag{2.69}$$

where $\mathbf{d}$ is the atomic dipole moment and $\mathbf{E}$ is the electric field being applied by the laser. As is standard, we shall use a semi-classical approximation here. Specifically, we take the definitions of $\mathbf{D}$ and $\mathbf{E}$ to be

$$\begin{aligned} \mathbf{d} &= e\,\mathbf{x} = \mathbf{D}\sigma^- + \mathbf{D}^*\sigma^+ \\ \mathbf{E} &= \mathbf{E}_0 \mathrm{e}^{-\mathrm{i}\omega_0 t} + \text{c.c.}\,, \end{aligned} \tag{2.70}$$

where $\mathbf{x}$ is the position operator and we have chosen the laser field to be resonant with the atom, meaning it too has frequency ω_0. The expression for $\mathbf{d}$ comes from expanding it in terms of the identity and then simplifying. Specifically,

$$\begin{aligned} \mathbf{d} &= \mathbb{1}\,\mathbf{x}\,\mathbb{1} \\ &= \langle 0|\,\mathbf{x}\,|0\rangle\,|0\rangle\langle 0| + \langle 0|\,\mathbf{x}\,|1\rangle\,|0\rangle\langle 1| + \langle 1|\,\mathbf{x}\,|0\rangle\,|1\rangle\langle 0| + \langle 1|\,\mathbf{x}\,|1\rangle\,|1\rangle\langle 1|\,. \end{aligned} \tag{2.71}$$

Now, we notice that the diagonal elements $\langle 0|\,\mathbf{x}\,|0\rangle$ and $\langle 1|\,\mathbf{x}\,|1\rangle$ must equal zero due to the symmetric/anti-symmetric properties of the wavefunction. Furthermore, we identify $\mathbf{D} = e\,\langle 0|\,\mathbf{x}\,|1\rangle$, leaving us with the expression for $\mathbf{d}$ in Eq. (2.70). Now, combining these equations, we can evaluate H_{laser}, giving

$$H_{\text{laser}} \;=\; e\left(\mathrm{e}^{-\mathrm{i}\omega_0 t}\mathbf{E}_0\cdot\mathbf{D}\sigma^- + \mathrm{e}^{\mathrm{i}\omega_0 t}\mathbf{E}_0^*\cdot\mathbf{D}\sigma^- + \mathrm{e}^{-\mathrm{i}\omega_0 t}\mathbf{E}_0\cdot\mathbf{D}^*\sigma^+ + \mathrm{e}^{\mathrm{i}\omega_0 t}\mathbf{E}_0^*\cdot\mathbf{D}^*\sigma^+\right). \tag{2.72}$$

The final step is to move into an interaction picture with respect to the free energy Hamiltonian H_0. In doing so, we find that

$$H_{\text{laser I}} = e\left(\mathrm{e}^{-2\mathrm{i}\omega_0 t}\mathbf{E}_0\cdot\mathbf{D}\sigma^- + \mathbf{E}_0^*\cdot\mathbf{D}\sigma^- + \mathbf{E}_0\cdot\mathbf{D}^*\sigma^+ + \mathrm{e}^{2\mathrm{i}\omega_0 t}\mathbf{E}_0^*\cdot\mathbf{D}^*\sigma^+\right). \tag{2.73}$$

We now apply what is known as the rotating wave approximation (RWA), where terms involving fast oscillating complex exponential terms are removed from the dynamics. This is well known to be a valid approximation in the weak coupling regime that we are concerned with here, as these terms contribute little to the evolution of the system. In removing these terms, and identifying the Rabi frequency Ω as

$$\Omega = \frac{2e\mathbf{E}_0\cdot\mathbf{D}^*}{\hbar}, \tag{2.74}$$

we arrive at the final form of $H_{\text{laser I}}$, given by

$$\begin{aligned} H_{\text{laser I}} &= \frac{\hbar}{2}\left(\Omega^*\sigma^- + \Omega\sigma^+\right) \\ &= \frac{\hbar\Omega}{2}\left(\mathrm{e}^{\mathrm{i}\varphi}\sigma^- + \mathrm{e}^{-\mathrm{i}\varphi}\sigma^+\right), \end{aligned} \tag{2.75}$$

where in the last line we have now taken Ω to be real and expressed any complex phase in terms of φ. Without loss of generality, we may absorb this complex phase into the definition of the excited state, for example. However, in Chapter 5 we will choose to explicitly consider this phase and hence keep it within the dynamics.

Following the derivation in Section 2.1 and Section 2.2 and proceeding in the exact same way, one can show that the master equation describing this system is given by

$$\dot{\rho}_{\text{I}} = -\frac{\mathrm{i}}{\hbar}\left[H_{\text{laser I}}, \rho_{\text{I}}\right] + \Gamma\left(\sigma^-\rho_{\text{I}}\sigma^+ - \frac{1}{2}\left[\sigma^+\sigma^-, \rho_{\text{I}}\right]_+\right), \tag{2.76}$$

with the dynamics being in an interaction picture with respect to the free energy Hamiltonian H_0. The Hamiltonian $H_{\text{atom-field}}$ behaves exactly as H_{SB} and $H_{\text{laser I}}$ replaces $H_{\text{int I}}$. Here, Γ is the atom's spontaneous decay rate. Incorporating

quantum feedback as outlined above, this master equation is modified to be of the form

$$\begin{aligned}\dot{\rho}_{\rm I} &= -\frac{\mathrm{i}}{\hbar}\left[H_{\rm int,I},\rho_{\rm I}\right] \\ &\quad +\Gamma\left(\eta R(\theta)\sigma^{-}\rho_{\rm I}\sigma^{+}R^{\dagger}(\theta)+(1-\eta)\sigma^{-}\rho_{\rm I}\sigma^{+}-\frac{1}{2}\left[\sigma^{+}\sigma^{-},\rho_{\rm I}\right]_{+}\right),\end{aligned} \tag{2.77}$$

with $R(\theta)$ being chosen to be a rotation operator here defined as

$$R(\theta) = \begin{pmatrix} \cos(\theta) & -\mathrm{i}\sin(\theta) \\ -\mathrm{i}\sin(\theta) & \cos(\theta) \end{pmatrix}, \tag{2.78}$$

for $\theta \in [0,\pi]$. Such an operation could be achieved by applying a strong laser pulse over a short time period (consider a strong Rabi oscillation over a short time period). Using this master equation, we may obtain a set of rate equations describing the dynamics of the system. Using the properties of a density matrix, we notice that there are only three real parameters needed to describe all the dynamics of a two level system. If we introduce the notation

$$\begin{aligned} x &= \mathrm{Re}\left(\rho_{01}\right) \\ y &= \mathrm{Im}\left(\rho_{01}\right) \\ z &= \rho_{11}\,, \end{aligned} \tag{2.79}$$

we may write the density matrix describing the system as

$$\rho = \begin{pmatrix} \rho_{00} & \rho_{01} \\ \rho_{10} & \rho_{11} \end{pmatrix} = \begin{pmatrix} 1-z & x+\mathrm{i}y \\ x-\mathrm{i}y & z \end{pmatrix}. \tag{2.80}$$

Using this notation and Eq. (2.77), we find that

$$\begin{aligned} \dot{x} &= -\frac{\Gamma}{2}x \\ \dot{y} &= \frac{1}{2}\left(\Omega\left(1-2z\right)-\Gamma y+\Gamma\eta\sin(2\theta)z\right) \\ \dot{z} &= \Omega y+\Gamma z\left(\eta\sin^{2}(\theta)-1\right). \end{aligned} \tag{2.81}$$

This set of differential equations can be solved in order to analyse the behaviour of the system. This can be used to plot the population of the excited state of the atom as a function of time ($z(t)$). The results for a variety of parameters are shown in Fig. 2.2.

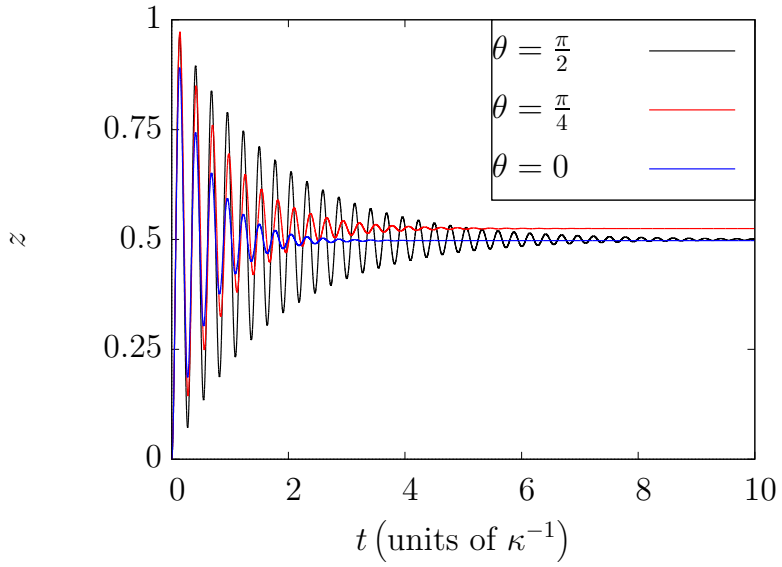

Figure 2.2: Plots of the population of the excited state of a two-level system subject to laser driving and instantaneous quantum feedback, where the feedback parameter is varied for each plot. These plots are created with $\eta = 1$ and $\Omega = 10\Gamma$.

When looking at Fig. 2.2, we see that the dynamics tend towards a stationary state. However, this stationary state changes depending on the value of θ. Explicitly, the stationary state values are given by

$$\begin{aligned} x_{\text{ss}} &= 0 \\ y_{\text{ss}} &= \frac{\Gamma\Omega\left(1-\eta\sin^2(\theta)\right)}{\Gamma^2+2\Omega^2-\Gamma\eta\left(\Gamma\sin^2(\theta)-\Omega\sin(2\theta)\right)} \\ z_{\text{ss}} &= \frac{\Omega^2}{\Gamma^2+2\Omega^2-\Gamma\eta\left(\Gamma\sin^2(\theta)-\Omega\sin(2\theta)\right)}\,. \end{aligned} \tag{2.82}$$

By plotting z_{ss} as a function of θ for a variety of values of Ω, we find that we may drive the atom into a desired stationary state by controlling the feedback and laser parameters, as shown in Fig. 2.3. This shows a simple example of how feedback can be used to control the dynamics of a system. However, there are more exotic uses that shall be explored in more detail later. This example is simply used to present how instantaneous quantum feedback can be implemented in an open quantum system.

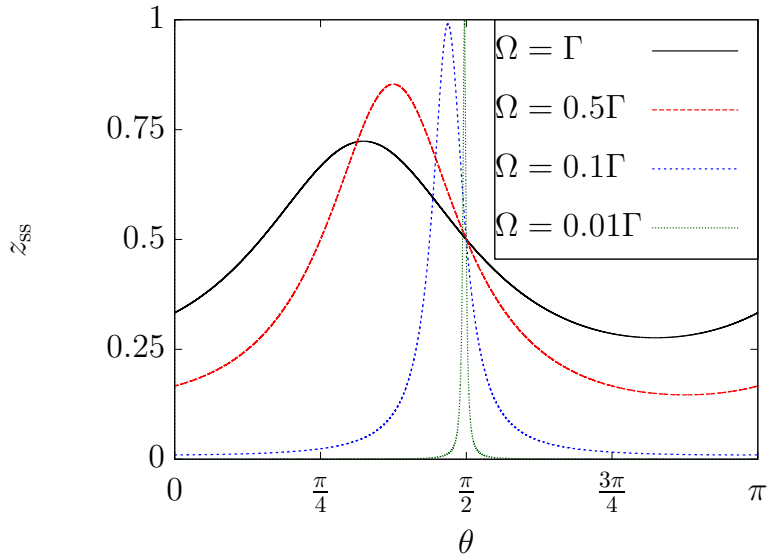

Figure 2.3: Plots of z_{ss} as a function of θ and for a variety of values of Ω. The stationary state value can be manipulated by changing the parameters. These plots are created by setting $\eta = 1$.

2.4 Summary

In this chapter, we have introduced the theoretical background needed to study open quantum systems with instantaneous quantum feedback. In particular, we have derived the Lindbladian master equation for an optical cavity with instantaneous feedback in the form of a displacement operator. As we shall see in Chapter 3, the introduction of quantum feedback in this form can vastly alter the dynamics of the system. This enhanced behaviour will then be studied for applications in the proceeding chapters.

Furthermore, we then introduced a two-level atom that is subject to quantum feedback in the form of a rotation on the Bloch sphere. As this is a relatively simple system, we showed how this system evolves in time and how altering the feedback parameters changes its evolution. For example, by choosing appropriate parameters for the feedback and laser-driving, a desired stationary state can be chosen. This is in line with many traditional uses of feedback, which focus on applications such as stabilisation [14]. However, as we shall see in Chapter 5,

even a relatively simple system like this can have uses for quantum technological applications.

Part II

Physical Behaviour

Chapter 3

Non-ergodic dynamics in an open quantum system with quantum feedback

Open quantum systems usually reach a unique stationary state with ergodic dynamics. In other words, the ensemble averages and the time averages of the expectation values of open quantum systems are usually the same for most quantum trajectories. Although open quantum systems are in general ergodic, many classical stochastic processes are not. Hence if classical physics emerges from microscopic quantum models, there have to be mechanisms which induce non-ergodicity in open quantum systems. In this chapter, we identify such a mechanism by showing that quantum feedback dramatically alters the dynamics of open quantum systems, thereby possibly inducing non-ergodicity and a persistent dependence of ensemble averages on initial conditions. As a concrete example we study an optical cavity inside an instantaneous quantum feedback loop.

Suppose a large number of identical physical systems generate time-dependent stochastic signals. The dynamics of these systems is called ergodic when any single, sufficiently long sample of the process has the same statistical properties as the entire process. By this, we mean that a single sample may yield the same information as a large number of repeats of the same process. More concretely, suppose we consider N identical systems with stochastic dynamics, where N is

large, and

$$E(A) \quad = \quad \lim_{T\to\infty} \lim_{N\to\infty} \frac{1}{N} \sum_{n=1}^{N} E_n(A,T) \tag{3.1}$$

denotes the ensemble average of the expectation values $E_n(A,T)$ of an observable A after a long time T. Then the system dynamics are ergodic when also

$$E(A) \quad = \quad \lim_{T\to\infty} \frac{1}{T} \int_0^T \mathrm{d}t\, E_n(A,t) \tag{3.2}$$

for all observables A and for all systems n. In other words, the system dynamics are ergodic when ensemble averages and time averages are the same for all observables and for all possible realisations of the process [24].

A completely generalised definition of ergodicity does not exist currently and can vary depending on the type of system being considered. In statistical processes, the definition provided here is often used. However, in other types of systems/processes alternatives may be used. For example, in condensed matter physics in particular, a phase space representation is considered [25]. Here, we shall adopt the definition given above for the purposes of this study, though it should be noted that there is equivalence amongst definitions. They differ only in representations.

Standard examples of physical systems with ergodic dynamics are systems that eventually lose any information about their initial state. This applies, for example, to systems whose dynamics result in a unique stationary state [24]. In this case, the right hand sides of Eqs. (3.1) and (3.2) both sum over stationary state expectation values and are hence equal. In statistical physics, systems usually reach a unique thermal equilibrium that is independent of their initial state. Ergodic systems therefore lie at the heart of statistical physics [26, 27]. Nevertheless, an ergodic hypothesis remains hard to deduce from microscopic equations of motion [28, 29, 30]. Moreover, physical systems whose dynamics depend forever on their initial state are in general non-ergodic. A particular class of non-ergodic systems that receive a lot of attention in the literature are physical systems with chaotic trajectories (see e.g. Refs. [31, 32]). For these, the right hand sides of Eqs. (3.1) and (3.2) are in general different.

In this chapter, we are especially interested in the ergodicity of open quantum systems with Markovian dynamics [33]. The ensemble averages of the expectation values of these systems can be deduced from their density matrix ρ, which evolves according to a master equation in Lindblad form [4, 18] as we saw in Chapter 2. However, to decide whether an open quantum system is ergodic or not, we also need to have a closer look at its individual quantum trajectories [20, 21, 22]. To do so, we need to unravel the above master equation in a physically meaningful way into equations that predict the dynamics of the individual quantum trajectories. In the case of spontaneous photon emission by a quantum optical system, a physically meaningful unravelling of Eq. (2.2) is obtained when writing $\mathcal{L}(\rho)$ in Eq. (2.3) as

$$\mathcal{L}(\rho) \;=\; -\frac{\mathrm{i}}{\hbar}\left[H_{\mathrm{cond}},\rho\right] + \Gamma\, L\rho L^{\dagger}\,, \tag{3.3}$$

with the non-Hermitian conditional Hamiltonian H_{cond} as given in Eq. (2.59). There are now two main terms contributing to the time evolution of ρ. The first term in Eq. (3.3) describes the dynamics of the open quantum system under the condition of no photon emission. In this case, it evolves according to a Schrödinger equation but with the system Hamiltonian H replaced by H_{cond}. This Hamiltonian no longer describes the total energy of the system but of only a subensemble. The second term describes the effect of a photon emission. Up to normalisation, the state vector changes from $|\psi_n(t)\rangle$ into $L\,|\psi_n(t)\rangle$ in this case. Furthermore, as we saw in Eq. (2.61), the probability density for an emission to occur equals $I(t) = \Gamma\,\langle L^{\dagger}L\rangle_t$, where $\langle L^{\dagger}L\rangle_t$ denotes a time-dependent expectation value. Knowing H, Γ and L of a quantum optical system with spontaneous photon emission allows us to generate all its possible quantum trajectories.

Although it is widely believed that open quantum systems with Markovian dynamics are almost always ergodic, a general proof of their ergodic dynamics cannot be found in the literature [34] and they must be tested individually. What has been shown, for example, is that the dynamics of an open Markovian quantum system are ergodic if the system reaches a steady state that is independent of its initial state [33]. Non-ergodicity seems to require the existence of multiple stationary states (see e.g. Refs. [6, 35, 36]), which occur only in specially designed circumstances, such as engineering supplementary decay channels or manipulating

them to behave differently. This is usually not the case in nature. However, many classical stochastic processes are non-ergodic and exhibit complex dynamics. Exactly how the complex dynamics of classical systems, including non-ergodicity and chaos, may arise in open quantum systems and in closed many-body quantum systems is the subject of extensive research [19, 29, 30, 31, 37, 38, 39]. While in the field of interacting systems this is being extensively studied, including for open quantum systems [40], it remains an open question for quantum optical systems.

In this chapter, we identify a mechanism with the ability to induce such complex dynamics in open quantum systems and thereby provide a counter-example to claims that open quantum systems with a single decay channel exhibit ergodic behaviour. It is shown that quantum feedback [11, 14, 41, 42] can induce non-ergodicity even when the quantum system possesses only a single unique stationary state. As we shall see below, the stationary state of an open quantum system inside a quantum feedback loop can become a repulsive fixed point of the system dynamics. When this applies, a system in its stationary state drifts away, even in the case of only tiny fluctuations. Instead of losing any information about the initial state, there can be a persistent dependence of the ensemble averages of expectation values on initial conditions. To show that this is indeed the case, we study a concrete example, namely the dynamics of an optical cavity with spontaneous photon emission inside an instantaneous quantum feedback loop. The quantum feedback-induced non-ergodicity of such cavities has already been shown to have applications in quantum-enhanced metrology [7].

There are three sections in this chapter. In Section 3.1, we review the dynamics of an optical cavity when subject to continuous laser driving to provide a reference point for later discussions. As we shall see below, the dynamics of the resonator is linear and ergodic in this case. Afterwards, in Section 3.2, we replace the continuous laser driving by instantaneous quantum feedback and show that this relatively simple change results in significant changes of the system's dynamics. Finally, in Section 3.3 we review our findings.

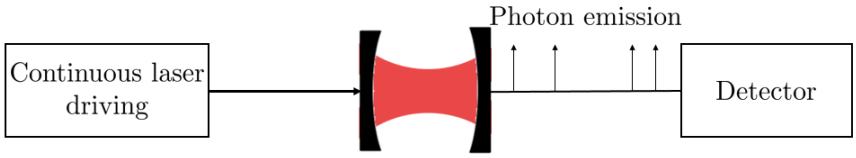

Figure 3.1: Schematic view of an optical cavity with continuous laser driving and spontaneous photon emission. A detector observes the field outside the resonator and registers the arrival of single photons at random times.

3.1 An optical cavity with continuous laser driving

For benchmarking and to later get a better feeling of how quantum feedback alters the dynamics of an open quantum system with spontaneous photon emission, this section analyses the dynamics of an optical cavity with continuous laser-driving from an open systems perspective. After looking at the individual quantum trajectories of the resonator, we derive its stationary state and show that its dynamics are indeed ergodic. We especially emphasise that if the cavity is initially in a coherent state, it remains always coherent.

3.1.1 Individual quantum trajectories

First, we have a closer look at the dynamics of the cavity field under the condition of no photon emission. In the interaction picture with respect to $H_0 = H_\mathrm{S}$, the resonator evolves with the conditional time evolution operator

$$U_{\mathrm{cond\,I}}\left(t+\Delta t, t\right) \;=\; \exp\left(-\frac{\mathrm{i}}{\hbar} H_{\mathrm{cond\,I}} \Delta t\right) \tag{3.4}$$

between photon emissions. Using Eq. (2.59) and applying the Baker-Campbell-Hausdorff formula, one can show that

$$U_{\mathrm{cond\,I}}\left(t+\Delta t, t\right) \;=\; \mathrm{e}^{-\frac{\mathrm{i}}{2}\Omega\left(c+c^\dagger\right)\Delta t}\, \mathrm{e}^{-\frac{1}{2}\kappa\, c^\dagger c\, \Delta t}\,, \tag{3.5}$$

up to terms of second order in Δt. Now suppose the cavity is initially in a coherent state $|\alpha_\mathrm{I}(t)\rangle$. In this case, calculating the effect of the second exponential on

$|\alpha_{\mathrm{I}}(t)\rangle$ is best done using the Fock basis. To apply the first exponential, we use the general properties of displacement operators with respect to coherent states. Doing so, we find that the state of the cavity at a time $t+\Delta t$ is again a coherent state, which we denote $|\alpha_{\mathrm{I}}(t+\Delta t)\rangle$. To a very good approximation, we find that

$$\alpha_{\mathrm{I}}(t+\Delta t) \;=\; \mathrm{e}^{-\frac{1}{2}\kappa\Delta t}\,\alpha_{\mathrm{I}}(t) - \frac{\mathrm{i}}{2}\Omega\,\Delta t\,. \tag{3.6}$$

This equation tells us that

$$\dot{\alpha}_{\mathrm{I}}(t) \;=\; -\frac{1}{2}\kappa\,\alpha_{\mathrm{I}}(t) - \frac{\mathrm{i}}{2}\Omega\,, \tag{3.7}$$

without any approximations. Solving this differential equation for an initial coherent state $|\alpha_{\mathrm{I}}(0)\rangle$, we obtain a general solution for the state $|\alpha_{\mathrm{I}}(t)\rangle$ of the cavity field under the condition of no photon emission in an arbitrarily long time interval $(0,t)$,

$$\alpha_{\mathrm{I}}(t) \;=\; \mathrm{e}^{-\frac{1}{2}\kappa t}\,\alpha_{\mathrm{I}}(0) - \frac{\mathrm{i}\Omega}{\kappa}\left(1-\mathrm{e}^{-\frac{1}{2}\kappa t}\right). \tag{3.8}$$

Returning to the Schrödinger picture, the state of the cavity becomes the coherent state $|\alpha_{\mathrm{S}}(t)\rangle$, with $\alpha_{\mathrm{S}}(t)$ given by

$$\alpha_{\mathrm{S}}(t) \;=\; \left[\mathrm{e}^{-\frac{1}{2}\kappa t}\,\alpha_{\mathrm{S}}(0) - \frac{\mathrm{i}\Omega}{\kappa}\left(1-\mathrm{e}^{-\frac{1}{2}\kappa t}\right)\right]\mathrm{e}^{-\mathrm{i}\omega_{\mathrm{cav}}t} \tag{3.9}$$

with $\alpha_{\mathrm{S}}(0) = \alpha_{\mathrm{I}}(0)$. Using Eq. (2.25), the calculation that lead to Eq. (3.6) moreover reveals that

$$P_0(\Delta t) \;=\; \exp\left[-|\alpha_{\mathrm{S}}(t)|^2\left(1-\mathrm{e}^{-\kappa\Delta t}\right)\right] \tag{3.10}$$

is the probability for no photon emission in a short time interval $(t, t+\Delta t)$.

Finally, we have a closer look at the effect of a photon emission on the state of the resonator field. Using Eq. (2.60), we immediately see that the spontaneous emission of a photon does not change the field inside the resonator, if the cavity is initially in a coherent state, since coherent states are the eigenstates of the photon annihilation operator c. Hence, Eq. (3.9) not only describes the state of the cavity field under the condition of no photon emission in the time interval $(0,t)$, but also describes the state of the resonator in case of emissions.

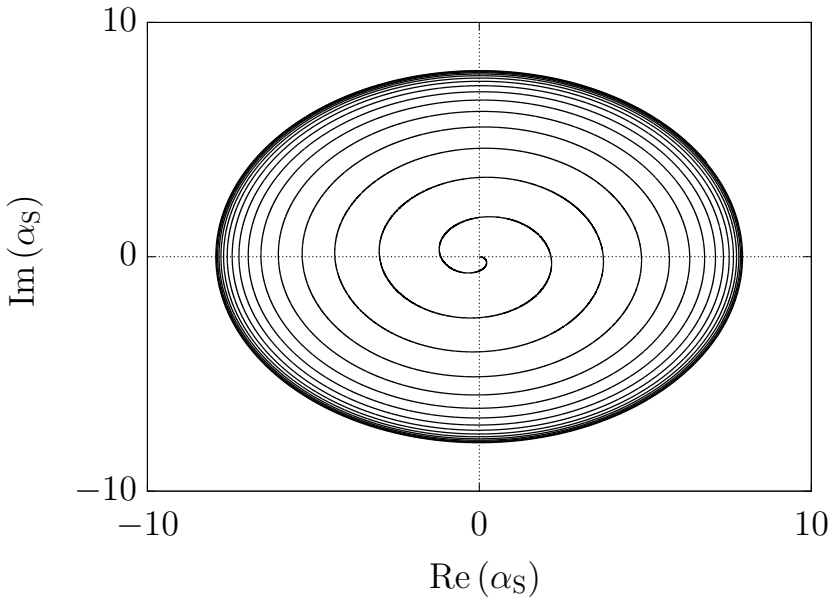

Figure 3.2: Phase space diagram illustrating the dynamics of a laser-driven optical cavity with spontaneous cavity decay in the Schrödinger picture. The cavity is initially in its vacuum state $|0\rangle$ and $\Omega = 8\kappa$. The field inside the resonator remains always in the coherent state $|\alpha_{\mathrm{S}}(t)\rangle$ given in Eq. (3.9). The state of the cavity follows an outwards spiral until it eventually reaches the stable circular orbit described by Eq. (3.11).

3.1.2 Long-term dynamics

Fig. 3.2 visualises the trajectory of an optical cavity with continuous laser driving with the help of a phase diagram. This is possible since the resonator remains always in a coherent state $|\alpha_{\mathrm{S}}\rangle$, which can be represented by a point in the complex plane. The x-co-ordinate of this point equals the real part of α_{S}, while the y-co-ordinate coincides with its imaginary part. Suppose the resonator is initially in its vacuum state with $\alpha_{\mathrm{S}}(0) = 0$. Then $\alpha_{\mathrm{S}}(t)$ in the Schrödinger picture describes an outwards spiral, which starts at the origin and eventually reaches a stable circular orbit. Eventually, the distance of the complex numbers $\alpha_{\mathrm{S}}(t)$ from the origin remains constant in time. Eq. (3.9) shows that

$$\alpha_{\mathrm{S}}(t) \quad = \quad -\frac{\mathrm{i}\Omega}{\kappa}\,\mathrm{e}^{-\mathrm{i}\omega_{\mathrm{cav}}t} \tag{3.11}$$

to a very good approximation, when t is sufficiently large. In the interaction picture (c.f. Eq. (3.8)), $\alpha_{\mathrm{I}}(t)$ assumes the stationary state value $\alpha_{\mathrm{ss\,I}}$,

$$\alpha_{\mathrm{ss\,I}} \;=\; -\frac{\mathrm{i}\Omega}{\kappa}\,. \tag{3.12}$$

This state is invariant under the no-photon time evolution of the system as well as being immune to the spontaneous emission of a photon.

Moreover, Eq. (2.61) in the previous chapter allows us to calculate the probability density $I(t)$ for the emission of a photon at any time t. If the system is initially prepared in a coherent state $|\alpha_{\mathrm{S}}(0)\rangle$, it remains coherent and $I(t)$ simply equals

$$I(t) \;=\; \kappa\,|\alpha_{\mathrm{S}}(t)|^2\,. \tag{3.13}$$

Substituting Eq. (3.9) into this equation yields

$$I(t) \;=\; \kappa\,\mathrm{e}^{-\kappa t}\,|\alpha_{\mathrm{S}}(0)|^2 + \frac{\Omega^2}{\kappa}\left(1-\mathrm{e}^{-\frac{1}{2}\kappa t}\right)^2 - 2\Omega\,\mathrm{e}^{-\frac{1}{2}\kappa t}\left(1-\mathrm{e}^{-\frac{1}{2}\kappa t}\right)\mathrm{Im}(\alpha_{\mathrm{S}}(0))\,. \tag{3.14}$$

Fig. 3.3 shows $I(t)$ for the case where the cavity is initially in its vacuum state and $I(0)=0$. Eventually, $I(t)$ assumes the constant value I_{ss},

$$I_{\mathrm{ss}} \;=\; \frac{\Omega^2}{\kappa}\,, \tag{3.15}$$

which is the stationary state photon emission rate of the laser-driven optical cavity. To obtain numerical results, we determine the mean number of photon emissions within short time intervals $(t, t+\Delta t)$ by averaging over a large number of quantum trajectories using the numerical method outlined in Section 2.2.3. We observe relatively good agreement between analytical and numerical results. This agreement increases when more individual quantum trajectories are taken into account as the statistical random noise is suppressed.

3.1.3 Ergodicity

To decide whether the dynamics of the cavity field are ergodic or non-ergodic, we need to check whether we can deduce all statistical properties of this physical

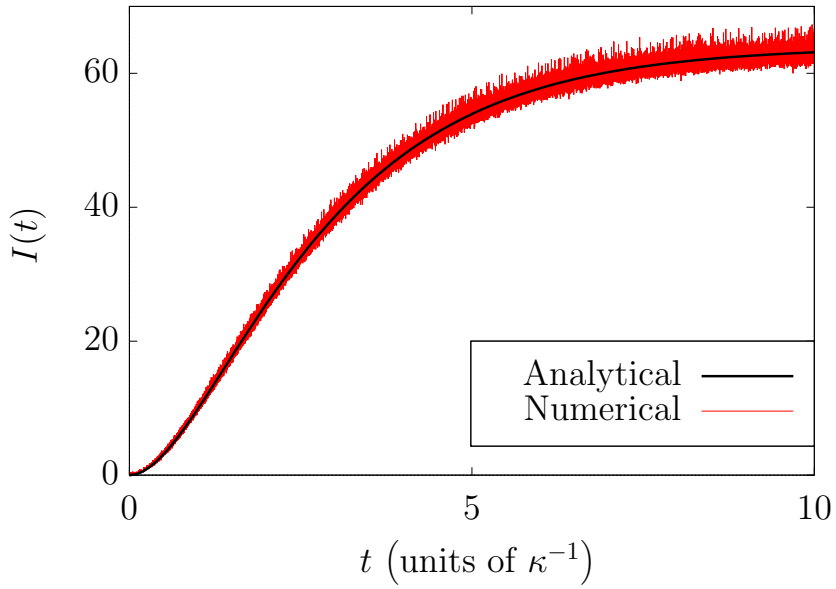

Figure 3.3: Time dependence of the photon emission rate $I(t)$ of a laser-driven optical cavity. As in Fig. 3.2, the resonator is initially in its vacuum state and $\Omega = 8\kappa$. The emission rate $I(t)$ soon reaches its stationary state value I_{ss} in Eq. (3.15). A comparison between the analytical result in Eq. (3.14) and a quantum jump simulation of $I(t)$, which averages over 10^6 individual quantum trajectories, shows relatively good agreement.

system from a single, sufficiently long quantum trajectory. In the previous two subsections, we have seen that the state of the resonator $|\alpha_{\text{I}}(t)\rangle$ at any time t is the same for all possible quantum trajectories with a fixed initial state, no matter when photon emissions occur. Moreover, we have seen that $\alpha_{\text{I}}(t)$ reaches its stationary state value α_{ss} in Eq. (3.12) relatively rapidly. It is therefore not surprising to find that the experimental setup in Fig. 3.1 is indeed ergodic. The time and ensemble averages of a laser driven optical cavity with spontaneous photon emission are the same. This is due to each individual quantum trajectory tending towards the same fixed point in the dynamics, leading them to equivalence in the large time limit, independent of their initial state. More precisely, the unique fixed point in the dyanmics is attractive for all values of α. Indeed, as is suggested in Ref. [33], a system like the one here with a unique stationary

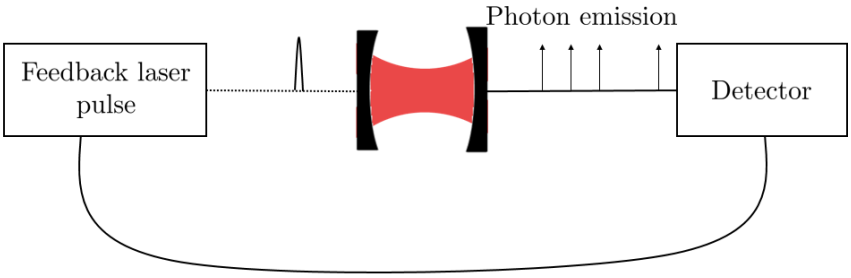

Figure 3.4: Schematic view of an optical cavity inside an instantaneous quantum feedback loop. Now the continuous laser driving is replaced by a random sequence of pulses. These are triggered by the detection of a single photon at the detector and displace the field inside the resonator in a well defined way.

state and a single decay channel should be ergodic. Hence in order to obtain non-ergodic dynamics we must add more complexity to the dynamics.

3.2 An optical cavity inside an instantaneous quantum feedback loop

In this section, we replace the continuous laser-driving of the resonator with instantaneous quantum feedback. As illustrated in Fig. 3.4, we assume that the spontaneous emission of a photon triggers a short, strong, resonant laser pulse, which can be modelled as a displacement operator. For simplicity, we assume that the effect of the laser is instantaneous, which applies to a very good approximation if its length is short compared to the inverse of the cavity decay rate κ. In the following, we see that changing the way in which energy is fed into the system alters the system dynamics dramatically.

3.2.1 Analytical solutions for an optical cavity inside an instantaneous quantum feedback loop

In this subsection, we look at finding a solution for the dynamics of the optical cavity inside a quantum feedback loop. In particular, we shall consider the case

highlighted in Fig. 3.4 where the continuous laser driving is removed and the only driving is of the form of instantaneous quantum feedback. The master equation for this system is given by Eq. (2.67).

Let us first take a closer look at the photon emission term of the unravelled quantum evolution of our system. Recalling Eq. (2.60), we know that the state of the system under photon-emission is given by $|\psi_{\mathrm{S}}^{\neq}(t+\Delta t)\rangle = \sqrt{\kappa\Delta t}\, L\, |\psi_{\mathrm{S}}(t)\rangle$. In the case of having continuous laser driving and no feedback, we have $L = c$ and $|\psi_{\mathrm{S}}(t)\rangle = |\alpha(t)\rangle$, meaning the unnormalised state after photon emission is

$$\begin{aligned} |\psi_{\mathrm{S}}^{\neq}(t+\Delta t)\rangle &= \sqrt{\kappa\Delta t}\, c\, |\psi_{\mathrm{S}}(t)\rangle \\ &= \sqrt{\kappa\Delta t}\, \alpha(t)\, |\alpha(t)\rangle \ . \end{aligned} \tag{3.16}$$

Hence, a photon emission does not alter the state of the optical cavity and there is no quantum jump in dynamics. However, in the case that we now wish to consider, the Lindblad operator is given by $L = D(\beta)c$. Therefore, we now have

$$\begin{aligned} |\psi_{\mathrm{S}}^{\neq}(t+\Delta t)\rangle &= \sqrt{\kappa\Delta t}\, D(\beta)c\, |\psi_{\mathrm{S}}(t)\rangle \\ &= \sqrt{\kappa\Delta t}\, \alpha(t)\, |\alpha(t)+\beta\rangle \ . \end{aligned} \tag{3.17}$$

It is no longer the case that $|\psi_{\mathrm{S}}^{\neq}(t+\Delta t)\rangle = |\psi_{\mathrm{S}}(t)\rangle$ anymore, meaning a quantum jump has occured in the system's dynamics. Because of this, it is no longer enough to merely track the system's no-photon evolution to give a complete analysis of the quantum system's evolution. The time of photon emissions is now significant.

However, if we want to consider ensemble averages, we should still be able to use the master equation to provide rate equations for expectation values, as the master equation still describes the ensemble average evolution of the system. Suppose we wish to consider the expectation value of some general operator A. Then, its time derivative is given by

$$\left\langle \dot{A} \right\rangle = -\frac{\mathrm{i}}{\hbar} \langle [A, H] \rangle + \kappa \left\langle \eta c^{\dagger} D^{\dagger}(\beta) A c D(\beta) c + (1-\eta)\, c^{\dagger} A c - \frac{1}{2} \left[A, c^{\dagger} c\right]_{+} \right\rangle , \tag{3.18}$$

for a master equation with instantaneous quantum feedback in the form of a strong laser pulse. Let us now look to find the time evolution of the photon

number operator $n = \langle c^\dagger c \rangle$. Furthermore, in our case here the continuous laser-driving has been turned off, meaning $H = 0$ here. Then we find that

$$\dot{n} = \kappa \left(\eta\beta \langle c^\dagger c^\dagger c \rangle + \eta\beta^* \langle c^\dagger c c \rangle + \left(\eta |\beta|^2 - 1 \right) \langle c^\dagger c \rangle \right) \tag{3.19}$$

The rate equations unfortunately do not form a closed set, as the displacement operator in the feedback always creates a new operator that is a function of c and $c^\dagger$ that had previously not been introduced. We therefore get an infinite set of linear differential equations, which is a characteristic of non-linear systems. This means that in order to study this system's behaviour we should use quantum jump simulations to obtain a numerical solution to the system's dynamics. Moreover, we can easily see that by removing the feedback (setting β or η to zero) returns the rate equation to the typically expected value, which is

$$\dot{n} = -\kappa n \,, \tag{3.20}$$

which describes an exponential decay in the population of photons inside the cavity. However, we see in Eq. (3.19) that this is suppressed by the feedback and may even become an exponential growth, as well as the introduction of the further new terms. Hence, we see a qualitatively difference between the cases with and without the feedback.

3.2.2 Non-linear dynamics of ensemble averages

In this subsection, we have a closer look at the time-dependence of expectation values averaged over a large ensemble of individual quantum trajectories. Since the cavity field remains always in a coherent state, the density matrix $\rho_{\mathrm{I}}(t)$, which allows us to calculate the expectation value $\langle A \rangle_t = \mathrm{Tr}\left(A \rho_{\mathrm{I}}(t) \right)$ of an observable A at any time t, needs to be a statistical mixture of coherent states. Hence, without restrictions we can assume that

$$\rho_{\mathrm{I}}(t) = \int_{\mathbb{C}} \mathrm{d}\alpha \, P(\alpha, t) \, |\alpha\rangle\langle\alpha| \,, \tag{3.21}$$

where the $P(\alpha, t)$ denote time-dependent probabilities. Taking this into account, using Eqs. (A.4) and (2.67) and calculating the density matrix ρ_{I} with $\dot{\rho}_{\mathrm{I}} = 0$, we

find that the cavity possesses a unique stationary state $\rho_{\rm ss}$. As one would expect, this state is the vacuum state of the resonator,

$$\rho_{\rm ss} \quad = \quad |0\rangle\langle 0| \,. \tag{3.22}$$

Clearly, when reaching this state the dynamics of the resonator come to a hold, as the only driving acting upon the system is the feedback, which is dependent on photon emissions. If the system is in the vacuum, it cannot emit photons and therefore cannot be driven away from the vacuum. However, Fig. 3.5 shows that often the cavity does not reach this state. For a wide range of initial states $|\alpha_{\rm S}(0)\rangle$, there is a significant probability for the mean number of photons inside the cavity to continue to grow in time. Moreover, Eq. (3.10) is now exact for all times Δt. Hence, we see that for all $|\alpha(t)| > 0$, there is always a finite probability for the cavity to emit a photon. Upon emission of a photon, the feedback may increase the size of $\alpha(t)$, thereby increasing the probability of emission.

To calculate the probability density $I(t)$ for the emission of a photon at time t averaged over a large ensemble of individual quantum trajectories, we now have a closer look at the dynamics of the photon number operator. Using Eq. (3.18) and setting $A = c^\dagger c$ and taking into account that $I(t) = \kappa \langle c^\dagger c \rangle_t$ and $[c, c^\dagger] = 1$, the differential equation yields

$$\dot{I}(t) \quad = \quad -\kappa^2 \int_{\mathbb{C}} {\rm d}\alpha \, \left[1 - \eta \left(|\alpha + \beta|^2 - |\alpha|^2\right)\right] P(\alpha, t) \, |\alpha|^2 \tag{3.23}$$

for the density matrix $\rho_{\rm I}(t)$ in Eq. (3.21). In the absence of any feedback, i.e. for $\eta = 0$, Eq. (3.23) simplifies to the simple linear differential equation $\dot{I}(t) = -\kappa \, I(t)$. However, in the presence of sufficiently strong feedback, the η-term dominates the dynamics of $I(t)$ and makes it non-linear. For relatively large values of η and β, $\dot{I}(t)$ even becomes positive and the mean number of photons inside the resonator grows in time. As we have seen in Ref. [7], the phase space volume occupied by the resonator grows in time in case of sufficiently strong instantaneous quantum feedback, which is often the case for non-ergodic systems.

3.2.3 Instability of the stationary state

The aforementioned dynamics are in stark contrast to other quantum optical systems with spontaneous photon emission. Like the experimental setup that

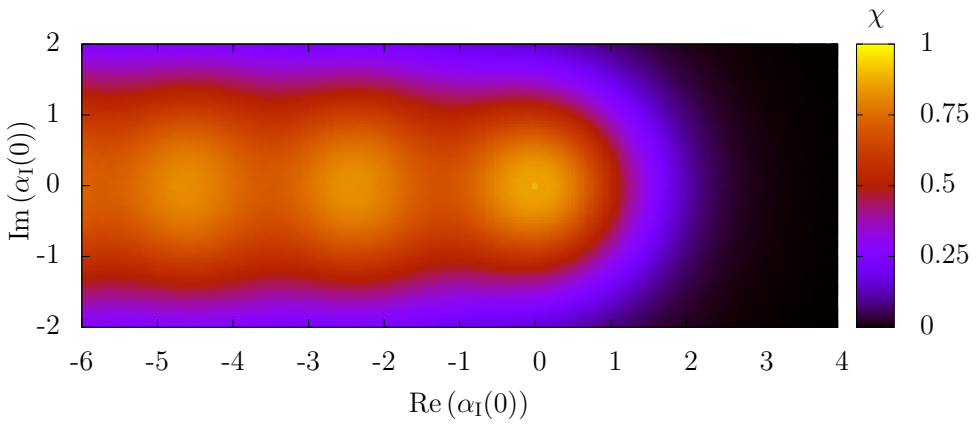

Figure 3.5: Heat-plot showing the dependence of the probability χ on the initial coherent state $|\alpha_{\rm I}(0)\rangle$ of the resonator. Here χ denotes the probability that coherent state $|\alpha_{\rm I}(t)\rangle$ of the cavity is such that $|\alpha_{\rm I}(t)| < 0.1$ after a time $t = 10\kappa^{-1}$. Hence it equals the probability that the cavity eventually reaches its vacuum state to a very good approximation. The plot is the result of a quantum jump simulation which averages over 10^4 quantum trajectories for 25000 different initial states uniformly separated. In this simulation we have set $\beta = 2$ and $\eta = 0.5$.

we studied in Section 3.1, quantum optical systems usually occupy a constantly shrinking or fixed phase space volume. Eventually they reach a stationary state that is independent of their initial state. In other words, the stationary state of a quantum optical system is usually an attractive fixed point of its dynamics. In contrast to this, as we shall see below, the stationary state of an optical cavity inside a quantum feedback loop becomes repulsive if the feedback is sufficiently strong.

Suppose the cavity is initially in its vacuum state and a small perturbation moves the resonator into a coherent state $|\alpha_{\rm I}(t)\rangle$ with $|\alpha_{\rm I}(t)|^2 \ll |\beta|^2$. When this applies, Eq. (3.23) simplifies to

$$\dot{I}(t) \;=\; -\kappa^2 \left(1 - \eta|\beta|^2\right) |\alpha_{\rm I}(t)|^2 \,. \tag{3.24}$$

The right hand side of this equations becomes positive when

$$\eta\,|\beta|^2 \;>\; 1\,. \tag{3.25}$$

This shows that the ensemble average of the mean number of photons inside the resonator increases further in time in case of sufficiently strong feedback. The stationary state of the resonator is no longer an attractor of the system dynamics but a repulsive fixed point. This behaviour is illustrated in Fig. 3.6, which shows the time dependence of the mean cavity photon emission rate $I(t)$ for quantum feedback pulses of different strength, i.e. for different values of β. As expected, the photon emission rate $I(t)$ only converges to zero when β is relatively small.

In fact, for any given initial state, we can determine $\dot{I}(0)$, as at this point the coherent state is unique and known. Following from the experimental setup shown in Fig. 3.4, if we take $\beta = |\alpha|$, we may re-write Eq. (3.23) as

$$\dot{I}(0) \quad = \quad -\kappa^2|\alpha|^2\left[1-\eta\left(|\alpha|^2+2\mathrm{Re}(\alpha)|\alpha|\right)\right] . \tag{3.26}$$

For this, we can gain a lot of information about the future behaviour of the system. Firstly, we see that there exists a threshold where $\dot{I}(0)$ is either positive or negative. This is found by setting Eq. (3.26) equal to zero, which yields

$$\eta|\alpha|\left(|\alpha|+2\mathrm{Re}(\alpha)\right)-1 \quad = \quad 0 \quad \text{or} \quad |\alpha|=0 \tag{3.27}$$

Choosing feasible values for the parameters in Eq. (3.27) we may identify if the intensity initially increases or decreases. Furthermore, we know that the intensity is proportional to $|\alpha|^2$. Hence, we know that if $\dot{I}(t) > 0$, $|\alpha|$ is also increasing initially. Therefore, it seems clear the ensemble average intensity will always increase. For the cases with an initially decreasing ensemble average, it is not as clear whether it will always decreases or whether in a long enough amount of time it will begin to increase again.

3.2.4 Persistent dependence of ensemble averages on initial states

Perhaps even more surprising than the instability of the stationary state is the fact that the dynamics of the ensemble averages of expectation values depend strongly on the initial coherent state $|\alpha_S(0)\rangle$ of the cavity, even after long periods of time. In contrast to many other quantum optical systems, information about the initial state of the quantum system is never lost. This behaviour is illustrated

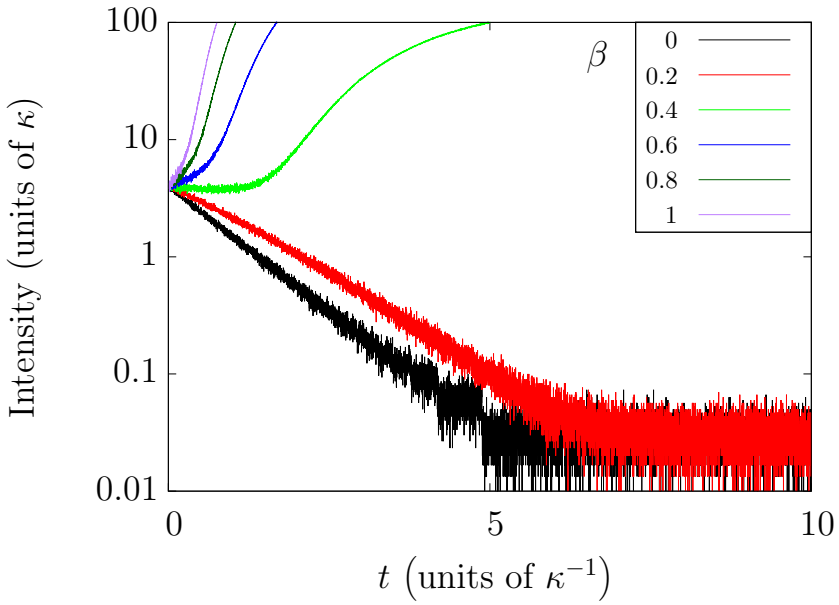

Figure 3.6: Time dependence of the photon emission rate $I(t)$ for different feedback parameters β. As in previous figures, we assume $\alpha_{\mathrm{I}}(0) = 2$ and $\eta = 0.5$. The figure is again the result of a quantum jump simulation, which averages over 10^6 individual quantum trajectories. For relatively small values of β, $I(t)$ tends to zero. However, as β increases, the dynamics of the cavity change and the mean number of photons inside the resonator continues to grow in time.

in Fig. 3.7, which shows the time-dependence of the photon emission rate $I(t)$ of the resonator for different initial states $|\alpha_{\mathrm{S}}(0)\rangle$ with $\alpha_{\mathrm{S}}(0) = |\alpha_{\mathrm{S}}(0)|\,\mathrm{e}^{\mathrm{i}\varphi}$. The amplitude of $|\alpha_{\mathrm{S}}(0)|$ and the feedback parameter β are the same in each case, but the considered phases φ differ for different curves. The figure clearly illustrates that information about φ is not lost. The emission rate $I(t)$ does not converge to a single value. On the contrary, the distance between curves that correspond to different values of φ even increases in time.

This interesting and highly unusual feature of open quantum systems opens the way to novel applications. For example, we recently showed that an optical cavity inside an instantaneous quantum feedback loop can be used to measure the phase shift between two pathways of light with an accuracy that exceeds the standard quantum limit [7].

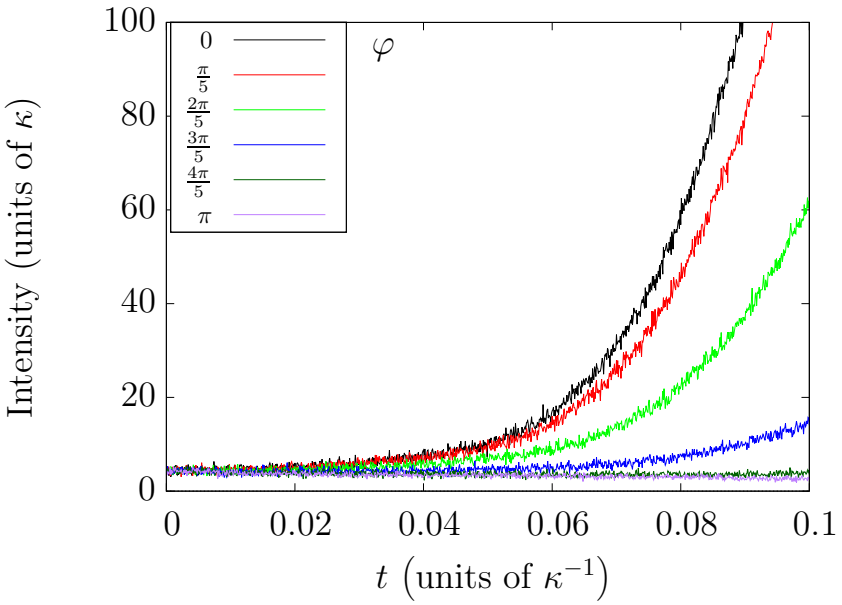

Figure 3.7: Time dependence of the photon emission rate $I(t)$ for different initial states $|\alpha_{\rm S}(0)\rangle$ with varying phase φ. Here $|\alpha_{\rm S}(0)| = 2$, $\beta = 2$ and $\eta = 0.5$. The figure is again the result of a quantum jump simulation which averages over 10^6 possible trajectories. The figure illustrates that there is a strong dependence of the dynamics of ensemble averages on the initial state of the resonator.

3.2.5 Individual quantum trajectories

As in Section 3.1, we may also have a closer look at the individual quantum trajectories of the resonator. As before, we model the time evolution between photon emissions by a non-Hermitian conditional Hamiltonian. Without laser driving, $\Omega = 0$ and $H_{\rm cond}$ is now of the form as in Eq. (2.66), where there is only a damping term. From Eq. (3.8) we see that the cavity evolves in the interaction picture into the state $|\alpha_{\rm I}(t)\rangle$ with

$$\alpha_{\rm I}(t) \;=\; {\rm e}^{-\frac{1}{2}\kappa t}\,\alpha_{\rm I}(0)\,, \tag{3.28}$$

in this case, if it is initially prepared in the coherent state $|\alpha_{\rm I}(0)\rangle$. The probability $P_0(\Delta t)$ for no photon emission in a time interval $(t, t+\Delta t)$ is still given by Eq. (3.10), which is later taken into account when we simulate quantum trajectories.

Next we have a closer look at the effect of a spontaneous photon emission. Again the state of the cavity remains unchanged, if the emission of a photon goes unnoticed. However, if the emission of a photon is detected and successfully triggers a feedback pulse, the state of the cavity changes from $|\alpha_{\mathrm{I}}(t)\rangle$ into $|\alpha_{\mathrm{I}}(t+\Delta t)\rangle = R_{\mathrm{I}}\,|\alpha_{\mathrm{I}}(t)\rangle$, with R_{I} being the displacement operator given in given in Eq. (A.4). Using the properties of displacement operators (see App. A for more details), we find

$$|\alpha_{\mathrm{I}}(t+\Delta t)\rangle \quad = \quad |\alpha_{\mathrm{I}}(t)+\beta\rangle\,, \tag{3.29}$$

under photon emission given that a feedback pulse is applied at a time t. The state of the resonator is no longer invariant under photon emission. Furthermore, even when all parameters are kept the same, every realisation of the described process now results in a different quantum trajectory. This leads to quantum jumps in the dynamics.

3.2.6 Non-ergodicity

The phase space diagrams in Fig. 3.8 show random samples of individual quantum trajectories in the Schrödinger picture. Figs. 3.8(a)–(c) and Figs. 3.8(d)–(f), respectively, depict the same ten runs of an experimental simulation. In Fig. 3.8(a)–(c) we have $\alpha_{\mathrm{S}}(0) = 2$ and in Fig. 3.8(d)–(f) we have $\alpha_{\mathrm{S}}(0) = -2$, while the feedback pulse in both cases is given by $\beta = 2$. There is a gradual zoom from (a) to (c) and from (d) to (f) to clearly show the difference between the dynamics of the resonator field for relatively large and for relatively small mean photon numbers. Most importantly, there are now two different types of dynamics. Many of the shown quantum trajectories move further and further away from the vacuum state. Once the amount of excitation inside the cavity reaches a certain threshold, the mean number of photons inside the resonator is likely to keep increasing. For other trajectories, the mean number of photons inside the resonator remains relatively small. Those trajectories are extremely likely to eventually reach the vacuum state, where the cavity cannot emit another photon and the dynamics of the system comes to a hold.

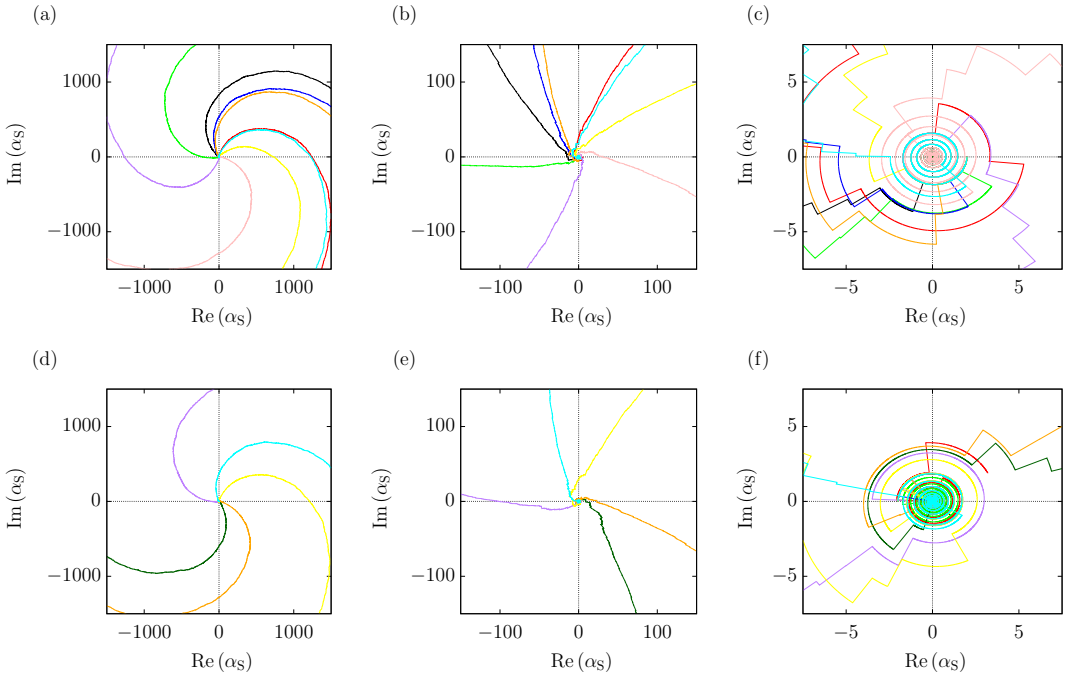

Figure 3.8: Phase space diagrams illustrating the dynamics of a random sample of ten possible quantum trajectories of an optical cavity inside an instantaneous quantum feedback loop with $\beta = 2$ and $\eta = 0.5$. All trajectories are the result of a quantum jump simulation of length $t = 10\kappa^{-1}$. In (a)–(c), we consider an initial state $|\alpha_{\mathrm{S}}(0)\rangle$ with $\alpha_{\mathrm{S}}(0) = 2$. One trajectory eventually reaches the vacuum state, while all others move further and further away from the origin. In (d)–(f), we have $\alpha_{\mathrm{S}}(0) = -2$. Now we see that only five of the ten trajectories diverge, while the other five appear to be converging. The diagrams in every row only differ by the size of the phase space volume, which is shown.

Moreover, Fig. 3.9 shows the time-dependence of the amplitude of $\alpha_{\mathrm{S}}(t)$ for the same runs of the experiment as in Fig. 3.8. Now the existence of two different types of dynamics becomes even more evident. We see that either the amount of excitation inside the resonator grows very rapidly in time or the cavity field approaches its vacuum state with $|\alpha_{\mathrm{S}}| \to 0$. This should not be surprising when considering the effect of the feedback on the two parameter regimes. On one hand, photon emissions at a relatively high rate attract more feedback pulses, thereby further increasing the amount of excitation inside the resonator. On the

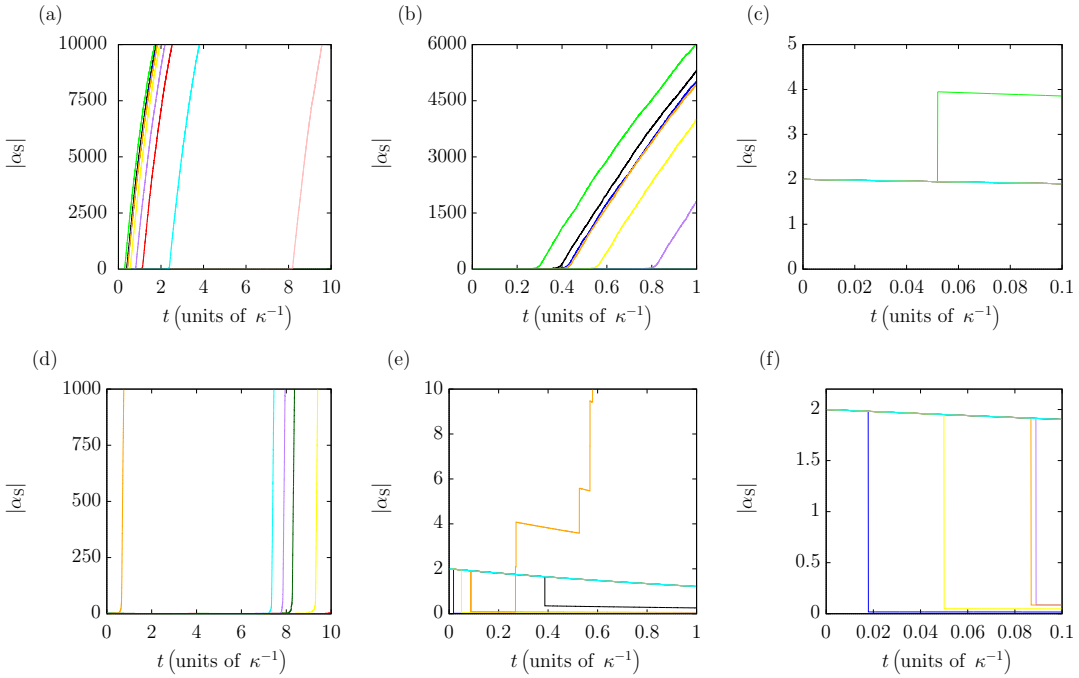

Figure 3.9: Explicit time dependence of the amplitude $|\alpha_S(t)|$ of the states $|\alpha_S(t)\rangle$ of the individual quantum trajectories shown in Fig. 3.8. These diagrams illustrate even more clearly than Fig. 3.8 that there are two types of dynamics. Either the mean number of photons inside the cavity increases in time and keeps on growing or the electric field amplitudes $|\alpha_S(t)|$ eventually becomes relatively small.

other hand, in the absence of any photon emissions the no-photon time evolution with the conditional Hamiltonian H_{cond} continuously reduces the field amplitude $|\alpha_S(t)|$ (c.f. Eq. (3.28)). This is due to the fact that not emitting a photon gradually reveals information about the quantum state of the resonator, which then needs to be updated accordingly [20]. Because of the fact that the cavity randomly exhibits two different types of dynamics, the statistical properties of the resonator field can no longer be deduced from a single, sufficiently long run of a single experiment. Consequently, the dynamics of an optical cavity inside an instantaneous quantum feedback loop are non-ergodic. The system now does not have a unique stationary state.

How likely it is for a single quantum trajectory to exhibit a certain type of

behaviour depends strongly on the initial state of the resonator. This is illustrated in Fig. 3.5, which shows the probability for an individual quantum trajectory to eventually reach the vacuum state as a function of the initial state $|\alpha_S(0)\rangle$. For example, if the cavity is initially in $|0\rangle$, Fig. 3.5 shows that it remains there with unit probability. However, when moving the initial state of the cavity field away from the vacuum, it becomes more and more likely that the resonator keeps on accumulating photon excitations. For sufficiently large values of $\alpha_S(0)$, effectively all the possible trajectories of the cavity field diverge. As we shall see below, the vacuum can become a repulsive fixed point of the system dynamics, even when averaged over a large number of repetitions of the same experiment.

3.3 Conclusions

This chapter addresses the question of how the often relatively complex dynamics of classical systems might arise in open quantum systems. For example, individual trajectories of open quantum systems with Markovian dynamics are usually ergodic and rapidly lose their dependence on their respective initial state [33]. In contrast to this, classical systems often evolve according to a set of non-linear differential equations. Classical stochastic processes are often non-ergodic and even chaotic, whereas classical systems usually maintain a dependence on initial conditions [24, 31, 32]. Nevertheless, it is widely believed that classical dynamics emerges from the behaviour of microscopic quantum systems. Quantum physics is believed to underly all other less complex physical theories. However, less is known about the mechanisms which induce classicality. The search for such mechanisms is an active area of research [19, 29, 30, 37, 38, 39].

This chapter identifies quantum feedback as a tool that dramatically alters the dynamics of open quantum systems. As an example, we study the stochastic dynamics of the electromagnetic field of an optical cavity inside an instantaneous quantum feedback loop. It is shown that the dynamics of ensemble averages, like the mean number of photons inside the resonator, can become non-linear even in the absence of non-linear interactions. In the presence of sufficiently strong feedback, the only fixed point of the dynamics of the cavity, i.e. its unique stationary state, can become repulsive. Moreover, it is no longer possible to deduce the the

dynamics of ensemble averages from individual quantum trajectories, which implies non-ergodicity. The dynamics of ensemble averages can depend strongly on the initial state of the cavity field. This feature can be employed, for example, in quantum-enhanced metrology [7], which we will later see in Chapter 5. In summary, the dynamics of even relatively simple quantum systems can become much more complex in the presence of back actions from the surrounding environment. We have thus provided a counter example to the idea that a Markovian quantum optical system with a single decay channel is ergodic in general.

Part III

Applications

Chapter 4

Comparing hidden Markov Models and hidden quantum Markov models

Hidden Markov Models are widely used in classical computer science to model stochastic processes with a wide range of applications. This chapter concerns the quantum analogues of these machines – so-called Hidden Quantum Markov Models (HQMMs) [10, 11]. Using the properties of Quantum Physics, HQMMs are able to generate more complex random output sequences than their classical counterparts, even when using the same number of internal states. They are therefore expected to find applications as quantum simulators of stochastic processes. Here, we emphasise that open quantum systems with instantaneous feedback are examples of HQMMs, thereby identifying a novel application of quantum feedback control.

In classical computer science, a Markov chain is a memoryless stochastic machine, which progresses from one state to another on a discrete time scale. Since their introduction in 1906 by Andrey Markov, the properties of Markov chains have been studied in great detail by mathematicians, computer scientists and physicists alike [43]. In the meantime, more complex versions of stochastic machines, like *Hidden Markov Models* (HMMs) [44], have been introduced. These progress randomly from one internal state to another, which remains unobserved (hidden), while producing a stochastic output sequence. HMMs are widely used

for the simulation of stochastic processes [44, 45, 46]. Applications include speech recognition, image analysis and the modelling of biological systems.

Over recent years, several attempts have been made to extend the definition of HMMs into the quantum world and to utilise the properties of quantum systems to generate more complex stochastic output sequences [10, 47, 48, 49, 50]. For example, in 2011, Monras *et al.* [10] introduced HQMMs. These are machines that progress from one quantum state to another, while generating classical output symbols. To produce an output symbol, a so-called generalised measurement or Kraus operation [23] is performed on the internal state of the machine. One way of implementing a Kraus operation is to use an auxiliary quantum system. In every time step, the internal state of the HQMM interacts with its ancilla, which is then read out by a projective measurement. After every measurement, the ancilla is reset into its initial state, while the internal state of the HQMM remains hidden.

A Kraus operation is the most general operation that a quantum system can experience, which is why Kraus operations are a vital part of the definition of a HQMM given by Monras *et al.* [10]. In a previous attempt to introduce quantum analogues of HMMs, Wiesner and Crutchfield [47] defined so-called quantum finite-state generators, which only involved unitary operations and projective measurements. In this way, they only obtained a subset of HQMMs, which are less powerful than their classical analogues. In contrast to this, HQMMs are able to produce more complex output sequences than HMMs of the same dimensional size.

Several ways of implementing HQMMs have already been identified. Firstly, as pointed out in Ref. [10], one way of implementing HQMMs is the successive, non-adaptive read-out of entangled many-body states. Another example of a HQMM is the time evolution of an open quantum system on a coarse grained time scale Δt, which produces a random sequence of classical output symbols. Already in Ref. [50], Sweke, Sinayskiy, and Petruccione use the language of HMMs to model open quantum systems. The purpose of this chapter is to highlight the connection between HQMMs and open quantum systems with instantaneous quantum feedback [14]. In this way, we identify a way of implementing an even wider set of HQMMs.

Like HQMMs, open quantum systems evolve randomly in time. Taking this perspective, the open quantum system itself provides the internal states of a HQMM, while its surrounding bath plays the role of the ancilla, which is constantly reset into an environmentally preferred state [19]. The continuous interaction between the internal states and the bath moves the bath away from its preferred (einselected) state, thereby producing a measurable response that manifests itself as a random classical symbol. The effective dynamics of such a machine when averaged over all possible trajectories can be described by a Markovian master equation [20, 21, 22]. When describing an open quantum system in this way, its accompanying output sequence is ignored. Here we suggest not to do so and to use the output sequences of open quantum systems to simulate stochastic processes. Like HMMs, we expect HQMMs to find a wide range of applications [10, 51, 52].

Quantum feedback is a process in which the classical output symbols produced by an open quantum system are used to change its internal dynamics. current applications of quantum feedback control can be found, for example, in Quantum Information Processing [14], where it is especially used to control state preparation [53] and quantum transport [17], as well as the applications presented in this thesis. In these applications, the feedback is used to guide the internal dynamics of a quantum system. In contrast to this, this chapter proposes to use quantum feedback to manipulate the classical output sequences of open quantum systems. We have already seen in the previous chapter that quantum feedback can significantly enhance the dynamics of an optical cavity. Hence, it is reasonable to assume that the same can be done for the purpose of a HQMM, as an optical cavity with quantum feedback can be used to model a HQMM.

There are four sections in this chapter. Section 4.1 discusses the mathematical treatment of HMMs and defines HQMMs. Afterwards, using the theoretical background of open quantum systems described in Section 2.1.4, we show how open quantum systems with instantaneous quantum feedback are examples of HQMMs in Section 4.2. In Section 4.3 we consider a numerical example to compare HMMs and HQMMs. Finally, we summarise our findings in Section 4.4.

4.1 Hidden Quantum Markov Models

In this section, we discuss Hidden Markov Models and provide some examples of their behaviour and dynamics. We will then introduce quantum versions of these machines.

4.1.1 Hidden Markov Models

The simplest Markovian machine is the Markov chain (MC). These are machines that stochastically evolve in time, where the evolution to a certain state depends only on its current state. More complex versions of these machines are HMMs. These are machines that evolve randomly from one internal state to another too. Now though, in every time step, an output symbol is produced. Only the output symbol is detected externally, while the internal state of the machine remains hidden (hence the hidden part of the name). We define the set of all possible internal states as $\mathcal{S} = \{X_s\}_0^{2^n-1}$, where n is the number of bits the internal state of the machine consists of. Similarly, we also define a set of all possible outputs for the machine as $\mathcal{A} = \{i_s\}_0^{2^m-1}$, where m is the number of bits the output contains.

In order to describe the evolution of these machines on a coarse-grained timescale, we introduce the transition matrix T. A transition matrix is an evolutionary map of the form

$$T : \mathcal{S} \to \mathcal{S}\,. \tag{4.1}$$

Transition matrices linearly transform one state or probability distribution of states to another. The transition matrix is normalised so as to preserve the normalisation of a probability distribution of states. The key difference between the MC and the HMM is that the internal state of the HMM remains hidden; we never actually know what state it is in. Hence, the information obtained comes only from the output states. This may reveal some information about the internal state depending on the specific properties of the system. Consequently, the time evolution of a HMM is characterised through a set of transition matrices T_x, where x denotes the output symbol generated during the respective time step.

In the case of an n-bit machine with m different output symbols, the system is characterised by m transition matrices of size $2^n \times 2^n$. An individual transition matrix T_x is not normalised like T and hence does not preserve normalisation. The magnitude of the state after the application of T_x is the probability of obtaining the symbol x after the respective evolutionary map. Consequentially, the individual transition matrices relate to the total transition matrix by

$$T \;=\; \sum_{x=0}^{m} T_x \,, \tag{4.2}$$

which describes the evolution of the internal state averaged over all possible output symbols or when the output is unknown. As such, this is in fact the transition matrix for a MC.

The probability of a specific output sequence can be calculated now using the transition matrices. For example, if the initial probability distribution of the internal states of the HMM is given by a column-vector $\vec{p}_0$, then the probability to obtain the outputs $abc\ldots def$, where a is the first symbol produced and f is the last, is given by (see eg. Ref. [10])

$$p(abc\ldots def) \;=\; \vec{\eta}\, T_f T_e T_d \ldots T_c T_b T_a\, \vec{p}_0 \,. \tag{4.3}$$

Here, $\vec{\eta}$ is a row-vector with all of its components equal to 1, the purpose of which is solely to provide a scalar probability. In this study, we shall just consider 1-bit machines where $m = n = 1$. By this, we mean the internal state can be one of two states (A and B). Furthermore, the output can also be one of two states (0 and 1). This is shown pictorially in Fig. 4.1, where all possible transitions are shown for the 1-bit machine.

The conditional probabilities are now defined as $p(i_{s+1}, X_{s+1}|X_s)$, where X_s is the internal state at time s, X_{s+1} is the internal state at time $s+1$ (the state immediately after X_s) and i_{s+1} is the output made during the evolution $X_s \to X_{s+1}$. We may define the transition matrices for a specific measurement (output), T_0 and T_1. These are given by

$$T_0 = \begin{pmatrix} p(0,A|A) & p(0,A|B) \\ p(0,B|A) & p(0,B|B) \end{pmatrix} \quad \text{and} \quad T_1 = \begin{pmatrix} p(1,A|A) & p(1,A|B) \\ p(1,B|A) & p(1,B|B) \end{pmatrix} . \tag{4.4}$$

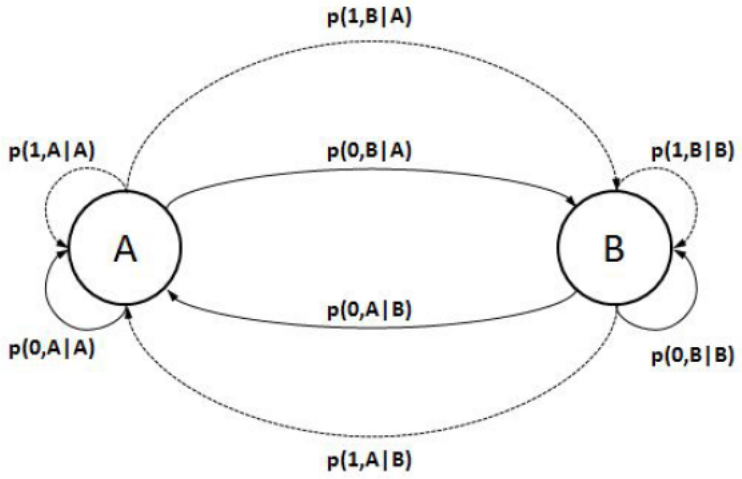

Figure 4.1: Diagram showing all possible transitions a 1-bit state ($\{A, B\}$) and 1-bit output ($\{0, 1\}$) a Hidden Markov Model may make. A solid line represents an output of '0' and a dashed line an output of '1' and the associated probabilites with each transition are shown.

From Eq. (4.2), we know that the total transition matrix is therefore

$$T \;=\; T_0 + T_1\,. \tag{4.5}$$

Hence,

$$T \;=\; \begin{pmatrix} p(A|A) & p(A|B) \\ p(B|A) & p(B|B) \end{pmatrix}, \tag{4.6}$$

where we have used that $p(0, A|A) + p(1, A|A) = p(A|A)$. Imposing that the conditional probabilities are normalised in the correct way, we can now impose two constraints on the system. These are simply

$$\begin{aligned} p(0,A|A) + p(1,A|A) + p(0,B|A) + p(1,B|A) &= p(A|A) + p(B|A) = 1 \\ p(0,A|B) + p(1,A|B) + p(0,B|B) + p(1,B|B) &= p(A|B) + p(B|B) = 1\,. \end{aligned} \tag{4.7}$$

Hence, we have eight variables and two constraints, meaning we have six free

parameters. We define our six free parameters as

$$\begin{aligned} p &= p(A|A) = p(0,A|A) + p(1,A|A)\,, \\ q &= p(B|B) = p(0,B|B) + p(1,B|B)\,, \\ p_1 &= p(1,A|A)\,, \\ p_1' &= p(1,B|A)\,, \\ q_1 &= p(1,B|B)\,, \\ q_1' &= p(1,A|B)\,. \end{aligned} \tag{4.8}$$

In order to make sure all probabilities are properly normalised, we must also impose that

$$\begin{aligned} 0 &\leq p_1 \leq p \\ 0 &\leq q_1 \leq q \\ 0 &\leq p_1' \leq 1-p \\ 0 &\leq q_1' \leq 1-q\,. \end{aligned} \tag{4.9}$$

Hence, we may now express the transition matrices as

$$\begin{aligned} T_0 &= \begin{pmatrix} p-p_1 & 1-q-q_1' \\ 1-p-p_1' & q-q_1 \end{pmatrix}, \\ T_1 &= \begin{pmatrix} p_1 & q_1' \\ p_1' & q_1 \end{pmatrix}, \\ T &= T_0 + T_1 = \begin{pmatrix} p & 1-q \\ 1-p & q \end{pmatrix}. \end{aligned} \tag{4.10}$$

These matrices can be used to find the probability of a certain sequence. For example, the sequence 1010 can be found by evaluating

$$p(1010) = \vec{\eta} T_0 T_1 T_0 T_1 \vec{p}_0\,. \tag{4.11}$$

If we only care about the output at certain points, we can use the total transition matrix to evaluate in-between points. So, if we wanted the probability to get a '1' at the first and fourth points say, we could find this by evaluating

$$p(1_{t=1}, 1_{t=4}) = \vec{\eta} T_1 T^2 T_1 \vec{p}_0\,, \tag{4.12}$$

where $1_{t=T}$ indicates the probability of obtaining a '1' at time step T.

In general, a HMM will also have a well-defined stationary state. If we apply the total transition matrix to generate a probability distribution and it is unchanged, we must be in the stationary state. In doing so, it can be shown that this stationary state, $\vec{p}_{\text{ss}}$ is given by

$$\vec{p}_{\text{ss}} = \frac{1}{2-p-q}\begin{pmatrix} 1-q \\ 1-p \end{pmatrix}. \tag{4.13}$$

It can be checked straightforwardly that indeed $T\vec{p}_{\text{ss}} = \vec{p}_{\text{ss}}$. This property is in part what makes these machines ergodic. In the same way that we considered ergodicity in Chapter 3, we require that a time average of the systems dynamics is equivalent to an ensemble average after a long enough time. In this case, we specifically require that a time average of the output sequence of a machine is equivalent to an ensemble average. As the machine has a well-defined unique stationary state in general, it will be ergodic. There are extreme cases that do not provide ergodicity however, such as $p = q = 1$. In this case, the stationary state is not defined and the output sequence depends entirely on how it is initially prepared and so does not satisfy the requirements for ergodicity.

4.1.2 Hidden Quantum Markov Models

Analogously, a HQMM with a certain probability distribution of its internal state populations can be described by a density matrix, ρ_{S}. This system can be thought of as being composed of some number of qubits, N. In order to produce an output, we may couple these internal qubits with some ancilla qubits. The Stinespring theorem [54] tells us that for a general evolution we require as many ancilla qubits as there are internal ones. We may of course have extra ancilla qubits, but this should not necessarily create any increase in complexity. In every time step, the system evolves and produces an output symbol. Again, only the output symbol is detected externally, while the internal state of the machine remains hidden. In contrast to HMMs, the time evolution of a HQMM is governed by a set of Kraus operators K_m, where the subscripts m coincide again with the output symbols of the machine. Using the same example as above, the probability of the output

$abc\ldots def$ occurring is now given by

$$p(abc\ldots def) \;=\; \mathrm{Tr}\left(K_f K_e K_d \ldots K_c K_b K_a\, \rho_{\mathrm{S}}\, K_a^\dagger K_b^\dagger K_c^\dagger \ldots K_d^\dagger K_e^\dagger K_f^\dagger\right) . \tag{4.14}$$

The Kraus operators evolve the system in time, but are different from the transition matrices for HMMs. This is due to the quantum system's evolution being able to produce quantum coherences, which do not have a classical analogue, rather than just producing a statistical mixture. Ultimately, this is what differentiates the two machines.

If the output symbol is ignored, then the density matrix $\rho_{\mathrm{S}}(t)$ of a HQMM evolves within a time step $(t, t+\Delta t)$ such that

$$\rho_{\mathrm{S}}(t+\Delta t) \;=\; \sum_{m=0}^{\infty} K_m\, \rho_{\mathrm{S}}(t)\, K_m^\dagger . \tag{4.15}$$

The above Kraus operators K_m should form a complete set to allow for simultaneous measurements. This means they need to obey the condition in Eq. (2.27) for the density matrix $\rho_{\mathrm{S}}(t+\Delta t)$ to be normalised. More details can be found in Ref. [10].

Kraus operators are more complex than the transition matrices described for HMMs, as briefly mentioned above. This also results in the Kraus operators being complex in general. As such, their parametrisation is less straightforward than that of transition matrices. Therefore, rather than consider a general analysis of HQMMs, we shall consider a specific implementation. Specifically, we shall consider an open quantum system with feedback and show how it can be used to implement a HQMM. For completeness the full parametrisation through real parameters of a HQMM can be found in Appendix B, though it will not be used for the numerical comparison of HMMs and HQMMs in Section 4.3.

4.2 Open quantum systems as HQMMs

Comparing the description of open quantum systems in Section 2.1.4 with the definition of the HQMM in Section 4.1, it is relatively straightforward to see that open quantum systems with instantaneous quantum feedback are concrete

examples of HQMMs. For example, the system studied in Chapter 3 could be used as an implementation of a HQMM. Though they are examples of HQMMs, they are not necessarily the most general examples. To show that they are indeed examples of HQMMs, we will now distinguish two cases of their dynamics.

4.2.1 Subensemble with energy transfer into the environment

We now recall the work from Section 2.1 to describe the two subensembles of the dynamics of the system. The first case is the one where the bath has been reset into its pointer state, $|0\rangle_{\mathrm{B}}$, within $(t, t+\Delta t)$ after having evolved into $|m\rangle_{\mathrm{B}}$. As shown in Section 2.1.4, $\rho_{\mathrm{S}}(t+\Delta t)$ is a statistical mixture of subensembles. The equations in that section and their given interpretation also tell us how $\rho_{\mathrm{S}}(t)$ evolved in Δt in case the state of the m-th bath mode changed due to the system-bath interaction Hamiltonian, which is followed by a feedback operation R_m by a Kraus decomposition. More precisely, we find that the density matrix of the corresponding subensemble equals

$$\rho_{\mathrm{S}}(t+\Delta t|m\geq 1) \quad = \quad K_m\,\rho_{\mathrm{S}}(t)\,K_m^{\dagger} \tag{4.16}$$

in this case, with the operator K_m given by

$$K_m \quad = \quad \sum_{n,n'=1}^{N} \xi_{nn',m}\,L_{nn'm}\sqrt{\Delta t} \tag{4.17}$$

for $m \geq 1$, as suggested by Eq. (2.26). As we shall see below, K_m is a Kraus operator which acts on the internal state of the open quantum system.

4.2.2 Subensemble without energy transfer into the environment

The remaining terms in the above master equation describe the time evolution of the open quantum system under the condition that the surrounding bath remains in its preferred state $|0\rangle_{\mathrm{B}}$. In this case, $\rho_{\mathrm{S}}(t)$ evolves within Δt into

$$\rho_{\mathrm{S}}(t+\Delta t|m=0) \quad = \quad K_0\,\rho_{\mathrm{S}}(t)\,K_0^{\dagger}\,. \tag{4.18}$$

Up to first order in Δt and using Eq. (2.26), the corresponding operator K_0 can be written as

$$K_0 \;=\; \exp\left(-\frac{\mathrm{i}}{\hbar}H_{\mathrm{cond}}\Delta t\right) \tag{4.19}$$

with the non-Hermitian Hamiltonian H_{cond} given by

$$H_{\mathrm{cond}} \;=\; H_{\mathrm{int\,I}} - \frac{\mathrm{i}}{2}\hbar\sum_{m=1}^{\infty}\sum_{n,n',n'',n'''=1}^{N}\xi_{nn',m}\xi^{*}_{n''n''',m}\,L^{\dagger}_{n''n''',m}L_{nn',m}\,. \tag{4.20}$$

The last term in this equation is crucial for the density matrix $\rho_{\mathrm{S}}(t+\Delta t)$ in Eq. (2.33) to remain normalised.

4.2.3 Comparison of Kraus operators

To show that open quantum systems with instantaneous feedback are examples of HQMMs, we now only need to identify the operators K_m in Eqs. (4.17) and (4.19) with the Kraus operators in Eq. (4.15). Summing over all of the above described subensembles with their respective output symbols given by $m = 0, 1, \ldots$, we immediately see that Eq. (4.15) applies. Since a density matrix $\rho_{\mathrm{S}}(t)$, which evolves according to the master equation of an open quantum system in Lindblad form remains normalised, we moreover have

$$\mathrm{Tr}\left(\sum_{m=0}^{\infty}K_m\,\rho_{\mathrm{S}}\,K_m^{\dagger}\right) \;=\; \mathrm{Tr}\left(\sum_{m=0}^{\infty}K_m^{\dagger}K_m\,\rho_{\mathrm{S}}\right) = 1\,. \tag{4.21}$$

This means Eq. (2.27) too is satisfied. Open quantum systems with instantaneous feedback are indeed examples of HQMMs.

4.3 Numerical Comparison

We now present a more quantitative comparison of HMMs and HQMMs. Our aim is to demonstrate that HQMMs can produce more complex dynamics than those of HMMs. There are many different statistical tests that can be conducted to determine the performance of these machines with respect to their output symbol sequences. In both cases, this is classical data, which can be analysed by classical

statistical measures. In this particular case, we shall use a two-point correlation function and the overall probability of detecting a '1'. The two-point correlation function will be defined as

$$\mathrm{Corr}(1_{t+1}, 1_t) = \frac{p\left(1_{t+1}|1_t\right)}{p\left(1_{t+1}\right)}. \tag{4.22}$$

This function describes the likelihood of a '1' at a time $t+1$ given there was a '1' at time t. It is also renormalised by the overall probability of obtaining a '1' at the time $t+1$. Here, we shall choose t to be sufficiently large such that it is the stationary state. Hence, we may redefine the correlation as

$$\mathrm{Corr}(1_{t+1}, 1_t) = \frac{p\left(1_{t+1}|1_t\right)}{p\left(1_{\mathrm{ss}}\right)}. \tag{4.23}$$

As the system is assumed to be in its stationary state, the term $p(1_{t+1})$ becomes $p(1_{\mathrm{ss}}$ as in the stationary state all single point probabilities are independent of the past. In order to obtain values for this function, we numerically evaluate it for a large number of combinations of the free parameters. For the HMM, we randomly choose sets of parameters for the transition matrices that satisfy the requirements upon them. For the HQMMs, we randomly choose parameters that satisfy the requirements of being a Kraus operator for the specific system that we have analysed, which is an open quantum system with instantaneous quantum feedback. In doing so, we may run numerical simulations of these machines for long time periods such that we may assume that they reach their stationary state. We then calculate the value of $p(1_{\mathrm{ss}})$ and the correlation. The results of this are shown in Fig. 4.2.

Comparing the two graphs, we see that the HQMM covers a larger area than that of the HMM. This tells us that for machines with comparable resources, the quantum machine may be capable of more complex statistics than its classical counterpart. Despite this, the difference between the two is not large. This is to be expected though, as any significant quantum advantage would come from allowing quantum correlations to be generated between the qubits, which cannot exist classically. Therefore, we expect this difference to grow drastically for a larger number of resources.

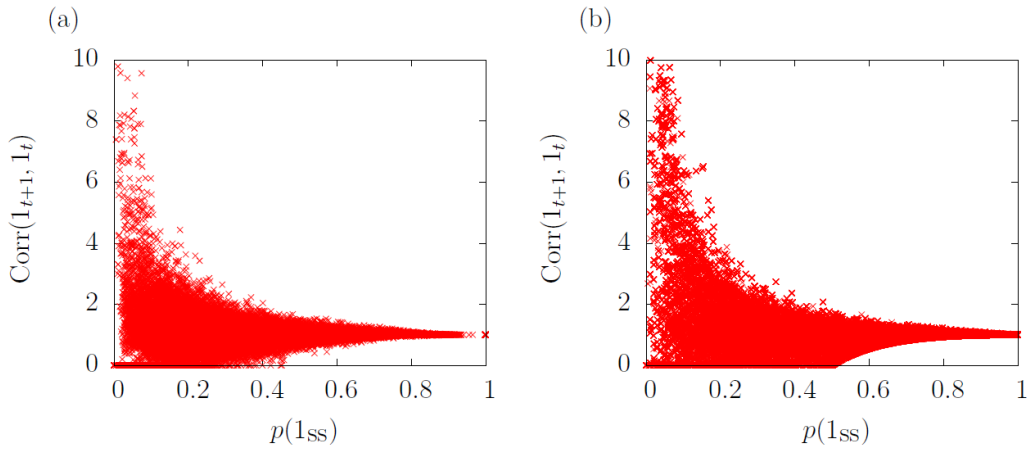

Figure 4.2: A statistical representation of the output of (a) a HMM and (b) a HQMM. We see both graphs appear to have the same funcitonal shape, but (b) seems to cover a larger area than (a), indicating that the HQMM is capable of more complex behaviour with a comparable amount of resources. In each figure 10^6 points are shown.

4.4 Conclusions

Motivated by the popularity of Hidden Markov Models (HMMs) in classical computer science, this chapter has a closer look at the quantum analogues of these machines – Hidden Quantum Markov Models [10]. Section 4.1 defines HQMMs in terms of Kraus operators. When comparing Section 4.1 and 2.1.4 in Section 4.2, it becomes obvious that open quantum systems with random classical output sequences are examples of HQMMs. As an example to show the superiority of HQMMs over HMMs, a numerical comparison was conducted in Section 4.3. Indeed, we found that the HQMMs do exhibit more complex behaviour than their classical counterparts. This chapter has proposed not to ignore the random classical output sequences of open quantum systems, since they could find interesting applications as quantum simulators of stochastic processes.

We have seen that HQMMs are capable of greater statistical power than of HMMs. However, the results presented here do not show a significant difference, as the region occupied in Fig. 4.2 is only slightly larger for the HQMMs compared with the HMMs. As highlighted, this is to be expected due to only using one

(qu)bit. When using more resources, we expect to see a more significant difference. A difficulty in doing this is the computational time required to simulate such a system. Particularly in the quantum case, the number of free parameters will vastly grow in moving up to a larger number of (qu)bits. Despite this, it would be possible to obtain results by using more sophisticated computing systems. This would be an interesting extension to this work. One way of achieving superior complexity may be to use the optical cavity scheme described in the previous two chapters, which occupies a larger state space than that of a single qubit. This would provide a continuous set of internal states rather than a discrete system like that of a qubit, which may offer significantly enriched dynamics in possible output sequences.

Finally, it might be worth noting that the above analysis of open quantum systems with instantaneous quantum feedback only allows for an environmental back action when the system-bath interaction changes the bath into a state that is different from its environmentally preferred state, $|0\rangle_{\mathrm{B}}$. This need not be the case. Physically, it is possible to design open quantum systems that experience feedback also or only when no exchange of energy occurs between system and bath. In this case, the open quantum system can no longer be modelled by a master equation. However, the effective system dynamics would remain Markovian and could be described using the language of HQMMs.

A further extension to this study may be to look for a true quantum-classical boundary. The Clauser-Horne-Shimony-H olt (CHSH) Bell inequality is often used to determine whether a process is quantum or classical [55, 56]. In Fig. 4.2, by comparing the areas occupied by the classical and quantum machines, it may be possible to identify a boundary between the two regimes. However in order to do so, a much more thorough analysis would need to be performed. Also, as already commented upon, the difference between the two cases appears to be minimal for the single (qu)bit case. However, when using a larger number of resources, this distinction is expected to grow. At this point, knowing the location of the boundary would be useful as it would allow us to determine whether a process is likely quantum or classical solely by analysing its output statistics.

Chapter 5

Quantum jump metrology

We have already seen one example of how the dynamics of an open quantum system can be used to enhance the dynamics of a quantum system with quantum feedback, namely the Hidden Quantum Markov Model described in Chapter 4. We now consider another. This example is a quantum metrology scheme, based in part on the work published in Ref. [7]. We begin in Section 5.1 by providing a brief overview of (quantum) metrology. We then proceed in Section 5.2 to introduce parameter estimation theory and the Fisher information, which are important tools in assessing how well a physical system can perform measuring a parameter. Afterwards in Section 5.3, we use these techniques to analyse a new approach, which we call *quantum jump metrology*. Finally in Section 5.4, we analyse a practical setup that could be implemented in a lab setting, based on the techniques introduced in Section 5.3. We then conclude in Section 5.6, where we discuss the implications of this work and potential further advancements based upon the results in this chapter.

5.1 Quantum metrology

The ability to measure a quantity is fundamentally important for many applications, not just in physics. Therefore, developing novel methods of conducting measurements with enhanced precision is of significant interest. One way of doing this is by exploiting the properties of quantum physics. Quantum metrology has been extensively studied in the literature [1]. Nevertheless, new schemes are

still being developed. In particular, these schemes typically involve measuring the phase difference between two pathways of light. Later, in Section 5.4, we will consider a novel example of such a setup.

In general, there are two main strategies for reducing the uncertainty in an experimentally measured quantity. One method is to repeat the experiment many times. Another is to use more of an appropriate resource N, in every run of the experiment. However, increasing N is not always possible. Suppose we want to measure the phase shift φ caused by a delicate material with the help of a standard light interference experiment. Increasing the number of photons passing through can increase the accuracy of every phase measurement but also limits the lifetime of the sample [57, 58, 59]. In this case, it is important that every run of the experiment is as accurate as possible. To allow for a fair comparison of different measurement schemes, the error propagation formula

$$\Delta\varphi \quad = \quad \frac{\Delta M(\varphi)}{\left|\frac{\partial M(\varphi)}{\partial \varphi}\right|} \tag{5.1}$$

can be used to calculate the accuracy $\Delta\varphi$ of a given signal $M(\varphi)$ [1]. Here $\Delta M(\varphi)$ is the standard deviation of a signal $M(\varphi)$ and denotes the uncertainty (or resolution) of $M(\varphi)$, while the visibility, $|\partial M(\varphi)/\partial\varphi|$, tells us how sensitive $M(\varphi)$ is to changes in φ. We see here that it is not enough to find a signal that is highly sensitive, as it must also have a low uncertainty itself to deduce information about the parameter to be measured.

Using N independent photons, the scaling of the lower bound of the uncertainty of the phase measurement between two pathways of light, $\Delta\varphi_{\text{class}}$, is given by the standard quantum limit (SQL),

$$\Delta\varphi_{\text{class}} \quad \propto \quad N^{-0.5}\,. \tag{5.2}$$

There are different ways in which this scaling can be improved. One way is to expose the incoming photons to a non-linear or interacting Hamiltonian [60]. In this case, the uncertainty of a single phase measurement, $\Delta\varphi_{\text{non-lin}}$, scales as

$$\Delta\varphi_{\text{non-lin}} \quad \propto \quad N^{-0.5\,k}\,, \tag{5.3}$$

where k denotes the order of the present non-linearity or interaction. However, highly-efficient optical non-linearities are hard to implement in general. Another way to obtain an enhancement is to replace the incoming independent photons by entangled or correlated ones [61, 62, 63, 64]. Using entangled states as probes, the measurement uncertainty $\Delta\varphi_{\text{quant}}$ can be as low as the Heisenberg limit, which is

$$\Delta\varphi_{\text{quant}} \propto N^{-1}. \tag{5.4}$$

To extract information from highly non-classical photon states [65, 66, 67, 68, 69, 70, 71, 72, 73, 74], quantum metrology schemes may use techniques such as quantum feedback, photon parity measurements, probes with fluctuating number states and photon subtraction [75, 76, 77, 78, 79]. Although it is possible to realise multi-photon entanglement in the laboratory [80], quantum metrology has not yet become readily-available for a wide range of applications. This is largely due to the experimental difficulty associated with producing large-scale entangled states, which are usually generated probabilistically.

In the next section, we review parameter estimation theory and establish where bounds such as the SQL and Heisenberg limit come from. This analysis is important as it allows us to calculate the ultimate precision bound for a system and hence tells us if it is possible to achieve a quantum enhancement.

5.2 Parameter estimation theory and the Fisher information

In order to see the need for quantum metrology, we shall consider a brief mathematical analysis of parameter estimation theory and give an overview of the Fisher information and Cramér-Rao bound. The classical Fisher information is useful in determining the precision of an estimator $\hat{\varphi}(\mathbf{x})$ of some parameter φ. The estimator $\hat{\varphi}(\mathbf{x})$ is assumed to depend on the value $\mathbf{x} \in \mathbb{R}^N$ for some $N \in \mathbb{N}$, of a real random vector $\mathbf{X}$ defined over a Kolmogorov probability space. The vector $\mathbf{x}$ is the data to be used to determine φ. The Fisher information associated with the probability density ρ_φ is defined by

$$F(\rho_\varphi) = \int d^N x \rho_\varphi(\mathbf{x})[\partial_\varphi \ln \rho_\varphi(\mathbf{x})]^2 = \int d^N x \frac{[\partial_\varphi \rho_\varphi(\mathbf{x})]^2}{\rho_\varphi(\mathbf{x})}, \tag{5.5}$$

where the second equality follows from carrying out the differentiation using the chain rule. The Fisher information is additive for independent sources of knowledge; $F(\rho) = F(\rho_1) + F(\rho_2)$ whenever $\rho(x_1, x_2) = \rho^1(x_1)\rho^2(x_2)$. This in part justifies its identification as an information.

The Cramér-Rao bound gives a lower bound on the precision of an estimate $\hat{\varphi}$ using the Fisher information. The bound is

$$\langle \Delta\hat{\varphi}^2 \rangle_{\rho_\varphi} \geq \frac{1}{F(\rho_\varphi)} + \langle \Delta\hat{\varphi} \rangle^2_{\rho_\varphi} \geq \frac{1}{F(\rho_\varphi)}\,, \tag{5.6}$$

where for an unbiased estimate $\langle \Delta\hat{\varphi} \rangle^2_{\rho_\varphi} = 0$. The proof of Eq. (5.6) involves a straightforward application of the Cauchy-Schwarz inequality $\|x\|\|y\| \geq |\langle x, y \rangle|^2$ applied to the inner-product defined over the function space [81, 82].

In practice one gathers information about a physical system in the form of a list of numbers obtained by querying the system. The values x_N can be viewed as the result of querying a physical system N times, which would be equivalent to having an ensemble of N identically prepared independent systems that have the same state $\tilde{\rho}_\varphi = \rho_\varphi(x_i)$, $\forall i = 1, ..., N$. More generally, systems that are independent but not necessarily identically prepared, are described by a *product* distribution $\rho_\varphi(\mathbf{x}) = \prod_{i=1}^N \rho^i_\varphi(x_i)$. For such a distribution the Cramér-Rao bound and the additvity of the Fisher information yield the bound

$$\langle \Delta\hat{\varphi}^2 \rangle_{\rho_\varphi} \geq \frac{1}{NF^{\max}}\,, \tag{5.7}$$

where $F^{\max} = \max_{x_i} F(\rho^i_\varphi(x_i))$. The number N is called the *resource* and is what was discussed in the previous section in terms of the limits. It is the number of times one has queried the system to gather information in the form of a list of numbers $\mathbf{x}$. The bound from Eq. (5.6) yields the so-called standard quantum limit (SQL) scaling of $1/\sqrt{N}$ for the lower bound of $\sqrt{\langle \Delta\hat{\varphi}^2 \rangle_{\rho_\varphi}}$.

In quantum metrology one considers a quantum system whose density matrix ρ_φ depends on an unknown parameter φ. According to quantum theory, a measurement of the physical system yields an outcome $\mathbf{x}$ with probability $\rho_\varphi(\mathbf{x}) = \mathrm{tr}(E_\mathbf{x}\rho_\varphi)$, where $E_\mathbf{x}$ is a positive operator-valued measure (POVM) describing the measurement process. The quantum Fisher information can be

defined as

$$F_Q(\rho_\varphi) = \max_{E_{\mathbf{x}}} F(\rho_\varphi(\mathbf{x}))\,. \tag{5.8}$$

The quantum Cramér-Rao bound

$$\langle \Delta\hat{\varphi}^2 \rangle_{\rho_\varphi} \geq \frac{1}{F_Q(\rho_\varphi)} \tag{5.9}$$

then follows from the Cramér-Rao bound (5.6). The Quantum Fisher information is additive in that $F_Q(\rho_\varphi^1 \otimes \rho_\varphi^2) = F_Q(\rho_\varphi^1) + F_Q(\rho_\varphi^2)$ whenever the composite state $\rho_\varphi = \rho_\varphi^1 \otimes \rho_\varphi^2$ varies with φ according to $\partial_\varphi \rho_\varphi = i[\rho_\varphi, h_\varphi^1 \otimes I^2 + I^1 \otimes h_\varphi^2]$ with $h_\varphi^{1,2}$ being a Hermitian operator. In this case, for an uncorrelated N-part state $\rho_\varphi = \bigotimes_{i=1}^N \rho_\varphi^i$ the quantum Cramér-Rao bound yields

$$\langle \Delta\hat{\varphi}^2 \rangle_{\rho_\varphi} \geq \frac{1}{N F_Q^{\max}}\,, \tag{5.10}$$

where $F_Q^{\max} = \max_i F_Q(\rho_\varphi^i)$. The above bound gives the standard quantum limit scaling for the precision. Since each system making up the N-part composite system is queried once in a measurement, the number N coincides with the number of queries made.

One way to obtain an enhancement over the SQL-scaling of $1/N$ given in Eq. (5.10) is to consider an N-part system which is prepared in an entangled state. This is since for an entangled state the Fisher information is not additive the bound in Eq. (5.10) does not follow from the Cramér-Rao bound. It is then possible to improve upon the SQL-scaling to obtain the Heisenberg scaling $\langle \Delta\hat{\varphi}^2 \rangle_{\rho_\varphi} \sim 1/N^2$ [81, 82]. The crucial ingredient in obtaining this enhancement is the breakdown of additivity of the quantum Fisher information due to the presence of correlations within the N-part system. Then, although not always, it is possible that the Fisher information will scale greater than linearly.

5.3 Quantum jump metrology

We will now introduce a method of creating non-additive Fisher information that can produce a non-linear scaling with the resource without the need for preparing

an entangled state. There exist already some alternative schemes that do not require entanglement [5, 6]. Here, we present a theoretical analysis of one such approach, by calculating the Fisher information for a simple toy model in the form of a two-level atom. The scheme can easily be extended to a larger system size and therefore has scalability. Unlike schemes that require entanglement, this scheme could easily be scaled up in an experiment. We demonstrate here that in order to obtain an enhancement in the uncertainty scaling, all that is required are correlations. Entanglement is one special example of such a correlation, but in general it is not unique. In this chapter, we show that the temporal correlation generated by the photon emission statistics of an open quantum system may also provide an enhanced scaling in precision. As such, we introduce a novel method of quantum metrology that could enrich the field and find use in many technological applications.

Although quantum metrology schemes without entanglement have already been proposed in the literature [5, 6, 7], it is not necessarily clear exactly where the enhancement comes from. In this section, we present a thorough analysis of the Fisher information to study where the necessary correlations are introduced. In particular, we shall study open quantum systems with instantaneous quantum feedback. As we saw already in Chapter 3, these systems may have highly complex and non-linear behaviour. These systems may therefore be able to facilitate quantum-enhanced measurements. Furthermore, we then see when these correlations are sufficient to generate an enhancement and therefore identify the type of process that may be useful for quantum metrology. The ideology presented here can potentially be implemented in real schemes in order to develop novel schemes for practical applications.

5.3.1 Correlated distributions yield non-additivite Fisher information

Temporal quantum correlations [83, 84] and sequential measurements [85, 86, 87] in open quantum systems are known to constitute an interesting resource for technological applications. To illustrate this, we show in the following that subsequent measurements on a single quantum system are in general equivalent to

single-shot measurements on an entangled state of several systems. Suppose a two-dimensional quantum system is in an initial state $|\psi\rangle$ and subsequent generalised measurements are performed, which can be described by two Kraus operators K_0 and K_1 of the form

$$K_i \;=\; |\tilde{\xi}_i\rangle\langle\xi_i|\,. \tag{5.11}$$

Here $|\xi_0\rangle$ and $|\xi_1\rangle$ are two orthogonal states with $\langle\xi_0|\xi_1\rangle = 0$. However no such constraint is imposed on the tilde-states $|\tilde{\xi}_0\rangle$ and $|\tilde{\xi}_1\rangle$ [23]. In case of two measurements, the initial state of the system changes according to

$$|\psi\rangle \;\rightarrow\; \begin{cases} K_0\,|\psi\rangle \rightarrow \begin{cases} K_0K_0\,|\psi\rangle \\ K_1K_0\,|\psi\rangle \end{cases} \\ K_1\,|\psi\rangle \rightarrow \begin{cases} K_0K_1\,|\psi\rangle \\ K_1K_1\,|\psi\rangle \end{cases} \end{cases}, \tag{5.12}$$

up to normalisation factors, which we neglect here for simplicity. Moreover suppose we perform a single-shot measurement of K_0 and K_1 on two quantum systems prepared in an effective state $|\psi_{\text{eff}}\rangle$,

$$\begin{aligned} |\psi_{\text{eff}}\rangle \;=\; & \sqrt{p_{00}}\,|\xi_0\rangle\otimes|\xi_0\rangle + \sqrt{p_{01}}\,|\xi_0\rangle\otimes|\xi_1\rangle \\ & + \sqrt{p_{10}}\,|\xi_1\rangle\otimes|\xi_0\rangle + \sqrt{p_{11}}\,|\xi_1\rangle\otimes|\xi_1\rangle\,, \end{aligned} \tag{5.13}$$

with the coefficients p_{ij} equal to

$$p_{ij} \;=\; \|K_jK_i\,|\psi\rangle\|^2\,. \tag{5.14}$$

It is easy to see that both measurements yield the outcome "ij" with exactly the same probability. This means the states $|\psi\rangle$ and $|\psi_{\text{eff}}\rangle$ effectively describe the same process. However, $|\psi_{\text{eff}}\rangle$ is in general an entangled state. For example, if $K_0 = |\xi_1\rangle\langle\xi_0|$ and $K_1 = |\xi_0\rangle\langle\xi_1|$, then $|\psi_{\text{eff}}\rangle = \sqrt{p_{01}}\,|\xi_0\rangle\otimes|\xi_1\rangle + \sqrt{p_{10}}\,|\xi_1\rangle\otimes|\xi_0\rangle$, which can be maximally entangled. Taking this into account, one can show that N successive measurements on a single system are in general equivalent to a single-shot measurement of N entangled quantum systems. This fact can be exploited for quantum metrology when using Kraus operators that depend on the unknown parameter.

The analysis of the previous section shows that enhancement over the SQL-scaling can be obtained when additivity of the quantum Fisher information fails to hold. The quantum Fisher information is simply a specific type of classical Fisher information having the form of Eq. (5.8). Of course one can consider the precision of parameter estimates without restricting one's attention to the quantum Fisher information. The SQL-scaling seen in Eq. (5.7) follows from the Cramér-Rao bound in Eq. (5.6) when the Fisher information is additive, i.e., when the probability density $\rho_\varphi(\mathbf{x})$ is uncorrelated; $\rho_\varphi(\mathbf{x}) = \prod_{i=1}^{N} \rho_\varphi(x^i)$. When there are correlations present within $\rho_\varphi(\mathbf{x})$ the SQL-scaling does not follow from the Cramér-Rao bound, which allows for the possibility of obtaining enhanced precision. One way to achieve such enhancement is to consider a distribution of the form $\rho_\varphi(\mathbf{x}; E_\mathbf{x}) = \mathrm{tr}(E_\mathbf{x}\rho_\varphi)$ in which ρ_φ is an entangled quantum state and $E_\mathbf{x}$ is a POVM. However, this is by no means the only way to obtain a correlated distribution $\rho_\varphi(\mathbf{x})$. The use of entanglement is not the only means by which to obtain enhanced precision [60].

5.3.2 Producing temporal correlations

In the context of non-linear optics it is well-known that $1/N^k$ scalings can be achieved when there are k-body interactions within the N quantum systems [60]. Indeed, super-Heisenberg enhancements can be obtained even with an initial product state. Therefore Ref. [60] provides an example of an enhancement that does not rely on entanglement. Another example can be seen in considering the time evolution of open quantum systems. In a variety of examples [5, 6, 7], an enhancement can be obtained without having to utilise an entangled state.

In this section we consider a different approach. Our aim is to determine precision bounds on parameter estimates when the queries of a system are represented by parameter-dependent POVMs. For example, on short timescales a photon number measurement of the radiation field surrounding an atom yields outcome 0 corresponding to no photons or 1 corresponding to one photon. If the measurement's back-action on the atom is parameter dependent their effect on the atom can be described by parameter-dependent Kraus operators $K_{0,1}(\varphi)$. These operators describe quantum jumps of the atom based on the outcomes of

measurements made on the environment and they must satisfy the completeness relation given in Eq. (2.27). The operator K_0 describes the effect on the atom if there are no photons detected, whereas K_1 describes the resetting of the atomic state after a photon is detected. A sequence of such jumps specifies a quantum trajectory within the atomic Hilbert space. See Chapter 2 for a more details.

Such parameter-dependent queries could be realised physically by connecting the photodetectors that monitor the radiation field around the atom to a laser directed toward the atom. The laser applies a pulse with unknown phase φ whenever a photon is detected by the photodetectors. In this case only the Kraus operator K_1 would be φ-dependent. Of course, this is merely one example, and there may be many other ways to implement sequential POVM queries that depend on an unknown parameter of interest. We could also consider a qubit that interacts with an ancilla, which is measured and reset after every discrete time step of the evolution of the system. The evolution of the internal system and the measurements of the ancilla may also be described by Kraus operators. Our goal is to find a scheme that is capable of quantum-enhanced measurements without the need for entanglement.

Firstly, we shall demonstrate that the output of an open quantum system does indeed possess correlations in general. To illustrate this, we shall consider a system for which there are two possible queries with corresponding Kraus operators K_0 and K_1 as an example. The distribution of outcomes after N sequential queries is given by

$$\rho_\varphi(\mathbf{x}) = \mathrm{tr}(K_{x_N} K_{x_{N-1}} ... K_{x_1} \rho K_{x_1}^\dagger ... K_{x_{N-1}}^\dagger K_{x_N}^\dagger)\,, \tag{5.15}$$

where ρ is the initial state of the system and $x_i = 0, 1$ is the outcome of the i'th measurement. In general the distribution $\rho_\varphi(\mathbf{x})$ is correlated, i.e., is not of the product form $\prod_{i=1}^N \tilde{\rho}_\varphi(x^i)$. Even when the reduced dynamics of the system are Markovian, the distribution $\rho_\varphi(\mathbf{x})$ does not result from a Markov chain of outcome events. To see this note that at each step $i = 1, ..., N$ the operators $K_{0,1}$ respectively select subensembles of systems for which outcomes $0, 1$ were obtained. The complete ensemble at step i is therefore represented by a density

matrix

$$\begin{aligned}\rho_\varphi(i) &= \mathcal{T}(\rho_\varphi(i-1)) \\ &:= K_0\rho_\varphi(i-1)K_0^\dagger + K_1\rho_\varphi(i-1)K_1^\dagger\,,\end{aligned} \tag{5.16}$$

where $\mathcal{T}$ denotes the Markovian evolution map that propagates the system's state to the next step. Consider the example $N = 3$. We have

$$\rho_\varphi(x_3|x_2,x_1) = \frac{\mathrm{tr}(K_{x_3}K_{x_2}K_{x_1}\rho K_{x_1}^\dagger K_{x_2}^\dagger K_{x_3}^\dagger)}{\mathrm{tr}(K_{x_2}K_{x_1}\rho K_{x_1}^\dagger K_{x_2}^\dagger)}\,, \tag{5.17}$$

whereas

$$\rho_\varphi(x_3|x_2) := \frac{\mathrm{tr}(K_{x_3}K_{x_2}\mathcal{T}(\rho)K_{x_2}^\dagger K_{x_3}^\dagger)}{\mathrm{tr}(K_{x_2}\mathcal{T}(\rho)K_{x_2}^\dagger)}\,. \tag{5.18}$$

In general the right-hand-side of Eq. (5.18) is not equal to the right-hand-side of Eq. (5.17), therefore the random variable sequence $X_1 \to X_2 \to X_3$ is not a Markov chain. Since the state of the system after each measurement depends on the outcome obtained, the probability density $\rho_\varphi(\mathbf{x})$ can become highly correlated throughout the course of the N-measurements. The presence of correlations in the distribution in Eq. (5.15) means that the SQL-scaling does not necessarily follow from the Cramér-Rao bound for the associated Fisher information.

5.3.3 Implementations

To illustrate the idea of determining precision bounds within the context described above we consider some simple examples involving just a single qubit. All of the examples considered could be constructed using a qubit and ancilla setup and applying simple operations to these. In the first cases, we shall examine a system that does not produce an enhancement, even when the Fisher information is constructed to be non-additive. After this, we shall consider a single atom allowed to decay freely, but is subject to parameter-dependent back-action upon photon emission.

Simple examples without enhanced precision

Our first example turns out to produce the usual SQL scaling and allows us to identify sufficient conditions for obtaining the SQL scaling. In this example we assume a qubit system with two Kraus operators chosen as

$$K_0 = \begin{pmatrix} \cos(\varphi) & 0 \\ 0 & \cos(\varphi) \end{pmatrix}, \qquad K_1 = \begin{pmatrix} 0 & \sin(\varphi) \\ \sin(\varphi) & 0 \end{pmatrix}. \tag{5.19}$$

This evolution could be generated by taking an ancilla initially prepared in $|0\rangle$ and performing a Pauli operation $\sigma_x = |1\rangle\langle 0| + |0\rangle\langle 1|$ on the system qubit and ancilla with probability $\sin^2(\varphi)$. By then measuring the ancilla in either state $|0\rangle$ or $|1\rangle$, we obtain the above Kraus operators, which satisfy

$$K_{0,1} = K_{0,1}^\dagger, \qquad K_0^2 + K_1^2 = \mathbb{1}, \qquad [K_0, K_1] = 0\,. \tag{5.20}$$

The second property together with the first ensures that the K_x are indeed Kraus operators. Since $K_0 = \cos(\varphi)\mathbb{1}$, the K_x commute, which makes them amenable to analytic calculations. Moreover $K_1 = \sin(\varphi)\,\sigma_x$ so that $K_0^2 = \cos^2(\varphi)\mathbb{1}$ and $K_1^2 = \sin^2(\varphi)\,\mathbb{1}$. For this choice of Kraus operators and for fixed φ the number of different values of $\rho_\varphi(\mathbf{x})$ is only $N+1$, because if $\mathbf{x}$ and $\mathbf{x}'$ contain the same number of zeros and ones then $\rho_\varphi(\mathbf{x}) = \rho_\varphi(\mathbf{x}')$. Since $\mathrm{tr}(\rho) = 1$ for any initial state ρ, if $\mathbf{x}$ contains k_x zeros we get

$$\begin{aligned} \rho_\varphi(\mathbf{x}) &= \mathrm{tr}(K_0^{2k_x} K_1^{2(N-k_x)} \rho) \\ &= \cos^{2k_x}(\varphi)\, \sin^{2(N-k_x)}(\varphi)\,, \end{aligned} \tag{5.21}$$

where we have used the cyclicity of the trace and the first and third properties in Eq. (5.20). The $\mathbf{x}$ are binomially distributed in that the number of $\mathbf{x}$'s with k_x zeros and $N-k_x$ ones is $\binom{N}{k_x}$. We can calculate the Fisher information (Eq. (5.5)) associated with ρ_φ as

$$\begin{aligned} F &= \sum_{\mathbf{x}} \frac{[\partial_\varphi \rho_\varphi(\mathbf{x})]^2}{\rho_\varphi(\mathbf{x})} \\ &= \sum_{k_x=0}^{N} \binom{N}{k_x} (N - 2k_x + N\cos(2\varphi))^2 \cos^{2(k_x-1)}(\varphi) \sin^{2(N-k_x-1)}(\varphi) \\ &= 4N\,. \end{aligned} \tag{5.22}$$

Thus, for the choices in Eq. (5.19) we get the standard quantum limit scaling from the Cramér-Rao bound in Eq. (5.6);

$$\langle(\Delta\varphi)^2\rangle \geq \frac{1}{4N}\,. \tag{5.23}$$

This result is due to the nature of the distribution $\rho_\varphi(\mathbf{x})$, which can in fact be written as a product distribution $\prod_{i=1}^N \rho_\varphi(x_i)$. To see this, note that in this particular example $\rho_\varphi^i(x_i) = \rho_\varphi^j(x_j)$ whenever $x_i = x_j$, so ρ_φ^i is actually independent of i. Over all steps $i = 1, \ldots, N$ there are only two possible probabilities;

$$\begin{aligned}\rho_\varphi^i(0) &= \rho_\varphi(0) = \mathrm{tr}(K_0^2\rho) = \cos^2(\varphi)\,,\\ \rho_\varphi^i(1) &= \rho_\varphi(1) = \mathrm{tr}(K_1^2\rho) = \sin^2(\varphi)\,.\end{aligned} \tag{5.24}$$

We therefore have

$$\begin{aligned}\rho_\varphi(\mathbf{x}) &= \cos^{2k_x}(\varphi)\sin^{2(N-k_x)}(\varphi) = \rho_\varphi(0)^{k_x}\rho_\varphi(1)^{N-k_x}\\ &= \prod_{i=1}^N \rho_\varphi(x_i)\,.\end{aligned} \tag{5.25}$$

We can define the single-shot distribution ρ_φ^s as the pair $\rho_\varphi^s = (\rho_\varphi(0), \rho_\varphi(1))$. The associated single-shot Fisher information is

$$\begin{aligned}F_s := F(\rho_\varphi^s) &= \sum_{x=0,1}\frac{[\partial_\varphi\rho_\varphi(x)]^2}{\rho_\varphi(x)}\\ &= \frac{4\cos^2(\varphi)\sin^2(\varphi)}{\cos^2(\varphi)} + \frac{4\cos^2(\varphi)\sin^2(\varphi)}{\sin^2(\varphi)}\\ &= 4\end{aligned} \tag{5.26}$$

and since the Fisher information is additive for a product distribution we obtain

$$F(\rho_\varphi) = \sum_{i=1}^N F(\rho_\varphi^s) = 4\sum_{i=1}^N = 4N\,, \tag{5.27}$$

as expected.

This SQL scaling follows from the use of the product distribution described in Eq. (5.25). Sufficient conditions for obtaining a product distribution appear to be that the K_x are Hermitian and share an orthonormal eigenbasis $\{|b_{1,2}\rangle\}$,

and that the initial state ρ is one of the corresponding spectral projections, i.e., $\rho = |b_1\rangle\langle b_1|$ or $\rho = |b_2\rangle\langle b_2|$. In the example above the first and third conditions in Eq. (5.20) imply that the K_x are Hermitian and share a common orthonormal eigenbasis that may or may not depend on φ. We have in this case that

$$K_x(\varphi) = \sum_{n=1,2} \lambda_x^n(\varphi)\, |b_n\rangle\langle b_n| \,, \tag{5.28}$$

where in general the eigenvalues depend on φ. If $\rho = |b_1\rangle\langle b_1|$ say, then for $x = 0, 1$

$$\begin{aligned} \rho_\varphi(x) &= \mathrm{tr}(K_x(\varphi)^2\rho) = \lambda_x^1(\varphi)^2, \\ \rho_\varphi(\mathbf{x}) &= \rho_\varphi(0)^{k_x}\rho_\varphi(1)^{N-k_x} = \prod_{i=1}^{N} \rho_\varphi(x_i)\,, \end{aligned} \tag{5.29}$$

where k_x is the number of $x_i = 0$, and $N - k_x$ is the number of $x_i = 1$, in the string $\mathbf{x}$. In order to get a φ-dependent result the eigenvalues λ_x^n must depend on φ. Alternatively if the $(\lambda_x^n)^2$ are independent of n as in the example from Eq. (5.19) above, then ρ can be a completely arbitrary density matrix and the same result will follow. In this case both $K_{0,1}^2$ are proportional to the identity $K_x^2 = \lambda_x^2\,\mathbb{1}$, so that $\rho_\varphi(x) = \mathrm{tr}(K_x^2\rho) = \lambda_x^2$ for any normalised ρ.

The most straightforward way to obtain a correlated distribution $\rho_\varphi(\mathbf{x})$ analytically is to consider an initially correlated state, i.e., a mixture $\rho = p\,|b_1\rangle\langle b_1| + (1-p)\,|b_2\rangle\langle b_2|$ (the off-diagonal elements can be arbitrary). We then obtain

$$\begin{aligned} \rho_\varphi(\mathbf{x}) =& (\lambda_0^1)^{2k_x}(1-(\lambda_0^1)^2)^{N-k_x}p \\ &+ (\lambda_0^2)^{2k_x}(1-(\lambda_0^2)^2)^{N-k_x}(1-p)\,, \end{aligned} \tag{5.30}$$

where we have used the completeness of the Kraus operators $(\lambda_0^n)^2 + (\lambda_1^n)^2 = 1,\ n = 1, 2$. If $p = 0, 1$ in Eq. (5.30) then ρ is one of the eigenprojectors of the K_x and only one component of the sum survives. Similarly if

$$(\lambda_x^1)^2 = (\lambda_x^2)^2 =: (\lambda_x)^2\,, \tag{5.31}$$

with $x = 0, 1$, then the p-dependent components in Eq. (5.30) cancel and one obtains a product distribution $\rho_\varphi(\mathbf{x}) = (\lambda_0)^{2k_x}(1-(\lambda_0)^2)^{N-k_x}$, as in the example from Eq. (5.19). Another example of a set of Hermitian commuting Kraus

operators is

$$K_0 = \begin{pmatrix} \cos(\varphi) & 0 \\ 0 & \sin(\varphi) \end{pmatrix}, \qquad K_1 = \begin{pmatrix} \sin(\varphi) & 0 \\ 0 & \cos(\varphi) \end{pmatrix}, \tag{5.32}$$

which are such that $\lambda_0^1 = \cos(\varphi) = \lambda_1^2$ and $\lambda_0^2 = \sin(\varphi) = \lambda_1^1$. Note however that $(\lambda_0^1)^2 = 1 - (\lambda_0^2)^2 \neq (\lambda_0^2)^2$ and $(\lambda_1^1)^2 = 1 - (\lambda_1^2)^2 \neq (\lambda_1^2)^2$, so that Eq. (5.31) does not hold. We therefore obtain from Eq. (5.32) the distribution

$$\begin{aligned} \rho_\varphi(\mathbf{x}) =& p \cos^{2k_x}(\varphi)\, \sin^{2(N-k_x)}(\varphi) \\ &+ (1-p) \sin^{2k_x}(\varphi)\, \cos^{2(N-k_x)}(\varphi)\,. \end{aligned} \tag{5.33}$$

This is not generally a product distribution. However, the associated Fisher information is extremely close (oscillates around) to $4N$ for all values of p and φ. This result indicates that having a correlated distribution is necessary but not generally sufficient to improve upon the SQL scaling. It remains to identify a correlated distribution that achieves the latter and hence provides an enhancement.

An alternative approach to those above would be to take inspiration from the dynamics of open quantum systems. Specifically, when an open quantum system interacts and creates an excitation within its environment, the system is reset. We shall call such an event an emission. Typically, such systems are reset to the ground state. However, they may be reset to any state in general. An example of such a system could be described by the Kraus operators K_0 and K_1 given by

$$K_0 = |0\rangle\langle 0| + \mathrm{e}^{-\frac{1}{2}\Gamma\Delta t}\,|1\rangle\langle 1|\,, \qquad K_1 = \sqrt{\Gamma\Delta t}\,|1\rangle\langle 1|\,. \tag{5.34}$$

Here, Δt is the time iteration between measurements and Γ is the decay rate of the system. Now, we reset the system to the excited state, $|1\rangle$, in the case of emission. This can be related to the two-level atom system studied in Section 2.3. We may now calculate the Fisher information once again, where we take Γ to be the parameter to be probed. Calculating the Fisher information, we find

$$F(N) \sim \begin{cases} N & \text{for} \quad \Gamma > 0 \\ N^2 & \text{for} \quad \Gamma = 0 \end{cases}. \tag{5.35}$$

Again therefore, we find that we obtain no improvement beyond linear scaling for all $\Gamma > 0$. Hence, we find that even having non-additive Fisher information,

we are not necessarily able to surpass linear scaling. This is in agreement with previous work showing that there cannot be an enhancement in measuring the decay rate of a system [88].

Example giving enhanced precision: A two-level system with parameter dependent resetting

Let us now finally consider a different scheme, with Kraus operators given by

$$\begin{aligned} K_0 &= |0\rangle\langle 0| + \mathrm{e}^{-\frac{1}{2}\gamma\Delta t}|1\rangle\langle 1| \\ K_1 &= \sin(\varphi)\sqrt{\gamma\Delta t}\,|0\rangle\langle 1| + \cos(\varphi)\sqrt{\gamma\Delta t}\,|1\rangle\langle 1| \,. \end{aligned} \tag{5.36}$$

Here, we reset into a state that is a function of a parameter φ. This is the system introduced in Section 2.3. Such feedback could be made by two short laser pulses applied t oeither side of a two-level atom, where completely in phase ($\varphi = 0$) the state would be reset to $|1\rangle$. These Kraus operators satisfy the completeness relation from Eq. (2.27) so long as Δt is sufficiently small. In this scheme, we calculate the Fisher information with respect to φ and in doing so we find

$$F(N) \sim \left(N^2 - N + c\right), \tag{5.37}$$

where c is a small constant.

For large N, this function should scale according to N^2. Hence, we find that we may achieve scaling in line with the Heisenberg limit using this system. We find again that the Fisher information of this system varies with φ as well. A good fit for this variation is given by

$$F(N,\varphi) = \sin^2(\varphi)\left(N^2 - N + c\right), \tag{5.38}$$

where c is a small correction made for the fit. This is shown in Fig. 5.1, where a fixed value of φ has been chosen and the Fisher information has been plotted. Furthermore, in Fig. 5.2, we see a plot of the Fisher information over a range of values of φ. We see clearly a non-linear growth. There are also points where the Fisher information appears to diverge. We find such cases at $\varphi = \frac{(2n-1)\pi}{2}$. These singularities have been neglected to allow for a smooth plot in Fig. 5.2, as

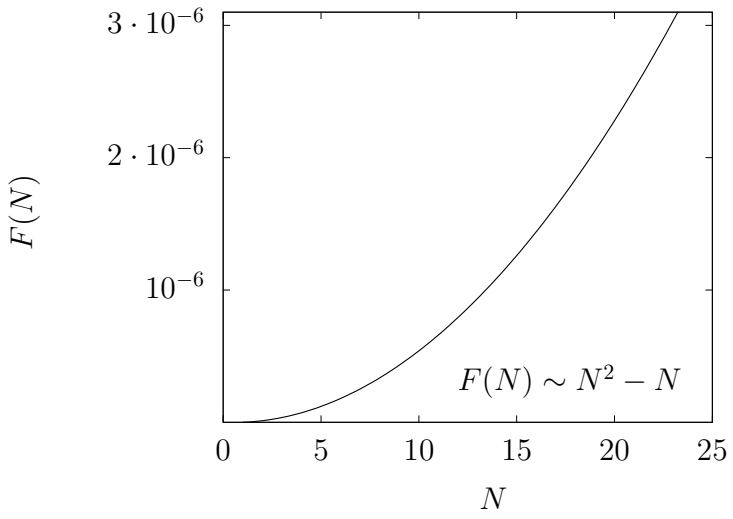

Figure 5.1: Fitted plot of the Fisher information for the Kraus operators given in Eq. (5.36) for $\varphi = \frac{499\pi}{500}$ and with $\Delta t = 10^{-4}\Gamma^{-1}$. The trend is clearly not linear and is therefore beyond the standard linear scaling of classical systems.

they are artefacts of the simulation process where probabilites of events become vanishingly small.

As well as varying the Fisher information with the phase, we may also vary other parameters. The above constructed example is highly physically motivated. However, the Kraus operators may be constructed in a more artificial way that doesn't necessarily reflect a physically motivated system, but still models an allowed implementation. Suppose in general our Kraus operators are of the form

$$K_0 = \begin{pmatrix} 1 & 0 \\ 0 & A \end{pmatrix}, \quad K_1 = \begin{pmatrix} 0 & \sin(\varphi)\sqrt{1-A^2} \\ 0 & \cos(\varphi)\sqrt{1-A^2} \end{pmatrix}, \tag{5.39}$$

where $0 \leq A \leq 1$. Furthermore, we may choose an initial state given by the density matrix

$$\rho = b\,|0\rangle\langle 0| + (1-b)\,|1\rangle\langle 1|\,, \tag{5.40}$$

where $0 \leq b \leq 1$.

For most cases, the Fisher information is highly non-linear initially, but becomes linear very quickly. For the cases where the Fisher information is non-linear

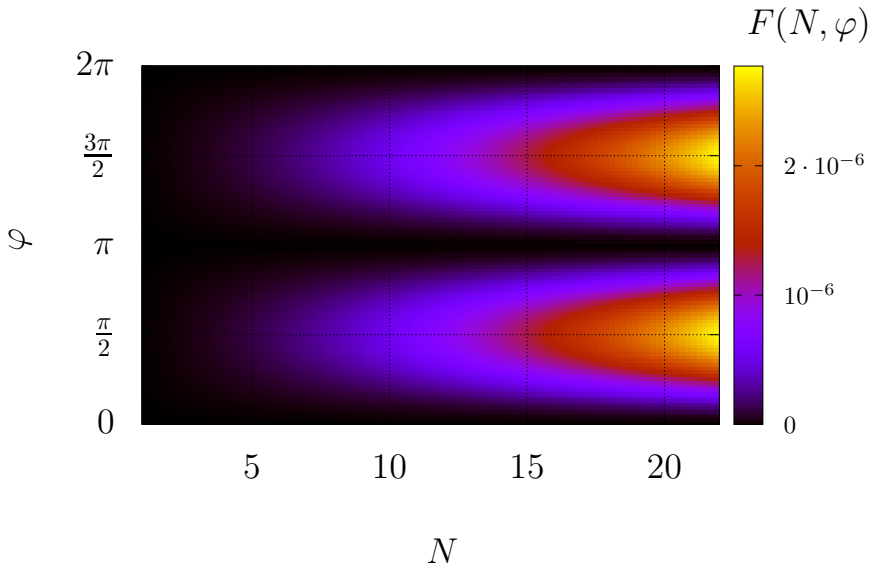

Figure 5.2: Fitted function of the Fisher information for the scheme described by the Kraus operators in Eq. (5.36), again taking $\Delta t = 10^{-4}\Gamma^{-1}$. We see that the Fisher information is maximised around $\frac{\pi}{2}/\frac{3\pi}{2}$ and also appears to grow non-linearly at these points.

for longer, its absolute size is significantly smaller. This parameter regime corresponds to the physically motivated scheme above (i.e. $A \simeq 1$). However, these results show a proof-of-principle that enhanced scaling can be generated in an open quantum system with no entanglement. It is highly possible that a system occupying a larger Hilbert space would persist with enhanced scaling for longer. It is also not clear how long the systems with enhanced scaling would continue as such at this point. As an example, we consider $A = 0.9$ and $b = 0.1$. The results of such parameters are shown in Fig. 5.3. Here, we see that the behaviour is very complex and does not follow a simple trend and could be investiagted further as an extenstion. However, for the purpsoe of this study we are only interested in a proof-of-principle that enhanced scaling can be obtained in this scenario.

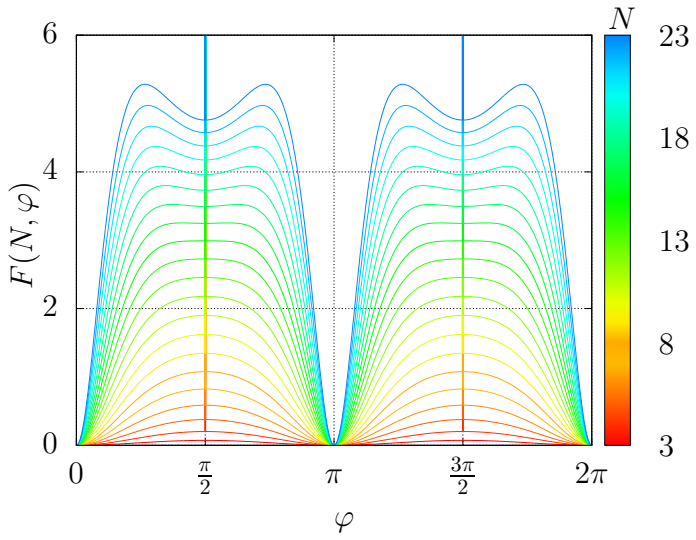

Figure 5.3: Fisher information as a function of the parameter φ. Each curve shows a different number of time steps N, as illustrated by the key. Here the free parameters are chosen to be $A = 0.9$ and $b = 0.1$. We see a steady increase in the Fisher information for all values of φ. However, the peak value seems to (neglecting the singularities) moves further from $\frac{\pi}{2}/\frac{3\pi}{2}$ as N increases.

5.3.4 Application to a two-level atom with controlled resetting

To give an example of a concrete system where this advantage in scaling can be found, we again consider a two-level atom with parameter dependent resetting. Following the dynamics described in Eq. (5.36), this corresponds to resetting the system into the state

$$|\psi^{\mathrm{ph}}\rangle \quad = \quad \cos(\varphi)\,|0\rangle - \mathrm{i}\sin(\varphi)\,|1\rangle\ , \tag{5.41}$$

after photon emission. For these dynamics, the probability of the system prepared in the state $|\psi^{\mathrm{ph}}\rangle$ not emitting a photon in a time T, $P_0(T)$, is given by

$$P_0(T) \quad = \quad \cos^2(\varphi) + \mathrm{e}^{-\Gamma T}\sin^2(\varphi)\,. \tag{5.42}$$

In such a case, the probability of the system emitting a photon in that time period can be written in general as

$$P_1(T) = \int_0^T \mathrm{d}t\, w(t) \tag{5.43}$$

with

$$w(t) = -\frac{\mathrm{d}}{\mathrm{d}t}P_0(t) = \Gamma \sin^2(\varphi)\mathrm{e}^{-\Gamma t}\,. \tag{5.44}$$

The measurement that we are interested in making for this scheme will be the average number of photons emitted in a time T, $\bar{N}(T)$. For simplicity, we will assume the state at time $t = 0$ has the form of $|\psi^{\mathrm{ph}}\rangle$. Hence, $\bar{N}(T)$ can be calculated by expressing it as a sum of the form

$$\bar{N}(T) = \sum_{n=1}^{\infty} np(n,T)\,, \tag{5.45}$$

where $p(n,T)$ is the probability of the system emitting n photons in a time T. This probability can be expressed as

$$p(n,T) = \left(\prod_{i=1}^{n}\int_{t_{i-1}}^{T} \mathrm{d}t_i w(t_i)\right) P_0(T-t_n)\,, \tag{5.46}$$

where we take $t_0 = 0$. If we consider the case where we wait for a large amount of time such that we may take $T \to \infty$, we find these integrals factorise nicely, meaning

$$\begin{aligned}\lim_{T\to\infty}\int_{t_{n-1}}^{T} \mathrm{d}t_n\, w(t_n - t_{n-1}) &= \sin^2(\varphi)\,,\\ \lim_{T\to\infty} P_0(T-t_n) &= \cos^2(\varphi)\,.\end{aligned} \tag{5.47}$$

Hence, we find that the probability for n photons is given by

$$p(n) = \sin^{2n}(\varphi)\cos^2(\varphi) \tag{5.48}$$

The average number of photons emitted for $T \to \infty$ can now be calculated by substituting Eq. (5.48) into Eq. (5.45), giving

$$\bar{N}(\infty) = \sum_{n=1}^{\infty} n \sin^{2n}(\varphi) \cos^2(\varphi) \,. \tag{5.49}$$

This is nearly a geometric series. After appropriately modifying it, it can be shown that

$$\sum_{n=1}^{\infty} n r^n = \frac{r}{(1-r)^2} \,. \tag{5.50}$$

Taking $r = \sin^2(\varphi)$, we hence find

$$\bar{N}(\infty) = \tan^2(\varphi) \,. \tag{5.51}$$

This function matches expectations, as we see that for the case where the system is reset to the excited state, we see an infinite number of photons, whereas when it is reset to the ground state we see no photons. This is shown in Fig. 5.4.

For the purposes of metrology, we want a signal we can scale with time. As such, we can calculate how this signal scales for finite T. By not imposing $T \to \infty$, the integrals no longer factorise nicely. Nevertheless, a solution can still be found for $p(n, T)$, which is given by

$$\begin{aligned} p(n,T) &= \sin^{2n}(\varphi)\cos^2(\varphi) + \frac{\mathrm{e}^{-\Gamma T}\sin^{2n}(\varphi)}{n!} \\ &\quad \times \left((\Gamma T)^n - \cos^2(\varphi) \sum_{m=0}^{n} \frac{n!}{m!} (\Gamma T)^m \right) . \end{aligned} \tag{5.52}$$

Summing up to the limit where $n \to \infty$ is now more difficult to resolve. Although the limit is well defined, it is not straightforward to explicitly calculate analytically. Hence, for simplicity, all results involving this term will be approximated by choosing a large finite value for n. In doing so, $\bar{N}(T)$ can be calculated to a very good approximation. In Fig. 5.5, we see how this function behaves as a function of φ at a variety of times T.

This signal clearly displays dependence on the parameter φ that grows in time. Hence it should be possible to use this signal to extract information about

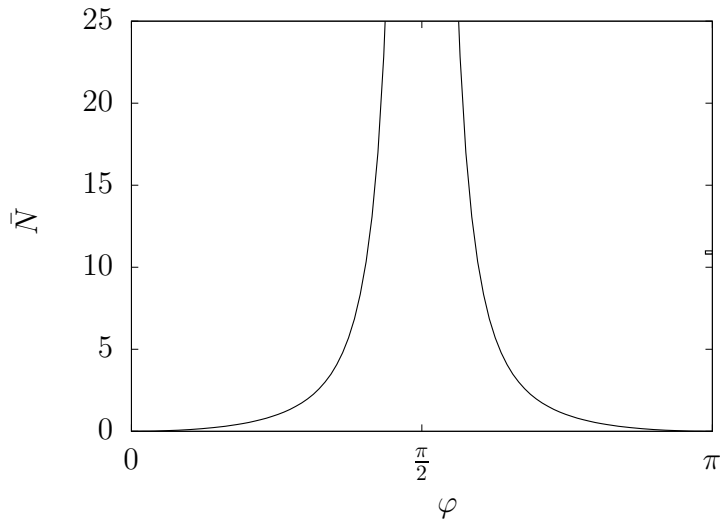

Figure 5.4: Plot of $\bar{N}$ for $T \to \infty$ for the two-level atom as a function of the feedback rotation parameter φ. As expected, if the atom is reset exactly into the excited state after emission there will be an infinite number of photon emissions for $T \to \infty$.

φ. In order to calculate the uncertainty in φ, we use the error propagation formula in Eq. (5.1). Specifically for this example, we shall use the variance for a more direct comparison with the Fisher information, where we take the square of Eq. (5.1). Plotting as a function of φ for a variety of times T, we see in Fig. 5.6 how the uncertainty in φ changes in time. In particular, the error decreases in time. However, the uncertainty appears to reach a fixed point that depends on the value of φ being considered for large T, which is reached faster the further φ is from $\frac{\pi}{2}$ in the range $\varphi \in [0, \pi]$. Also, the error is able to reach a lower value for a large amount of time the closer it is to $\frac{\pi}{2}$. Hence, to maximise the scaling it appears that we should choose a value of φ is close to $\frac{\pi}{2}$. Taking $\varphi = 1.5$, we now plot $(\Delta\varphi)^2$ as a function of time T. This is shown in Fig. 5.7. Here, we see the scaling is surpassing that of the standard quantum limit. In fact, the scaling of the error is better than the Heisenberg limit at its steepest point. However, this doesn't necessarily mean that the error has gone beyond the overall Heisenberg limit.

Crucially, we see that there is an enhanced scaling present for this measure-

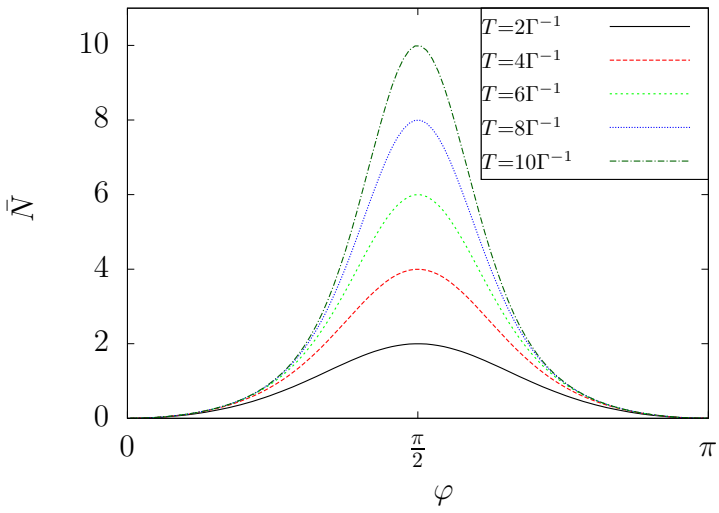

Figure 5.5: The plot of $\bar{N}$ now does not go to infinity, as a finite amount of time is considered. The curve has a similar functional shape to the case of infinite time and hence demonstrates the validity of the calculations. Here, the sum is taken up to $n = 1000$.

ment scheme. Although this measurement is not necessarily an optimum measurement, it serves as a proof-of-principle that an enhanced time-dependent scaling can be found for a relatively simple system with quantum feedback. Indeed, there are many ways in which this system can be developed further, including going to a larger system size or performing a more complex measurement, such as using photon correlations. In Fig. 5.7, we see that the uncertainty in φ seems to be levelling off to a fixed value. This is also suggested in Fig. 5.6 for other values of φ. If we move to a larger system size, the overall uncertainty should be reduced further. This is because in a larger system size two initially close together points in the relevant space can move further away from each other and hence become more distinguishable. In the next section, we consider another more complex system that cannot be solved analytically that also produces enhanced scaling without requiring exotic quantum states and hence offers relative experimental simplicity. In particular, this system occupies a large state space that allows for more persistent scaling.

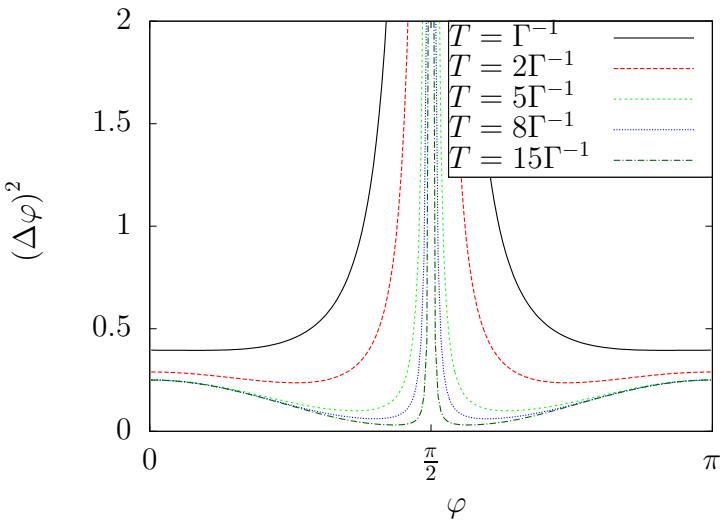

Figure 5.6: Uncertainty $(\Delta\varphi)^2$ plotted as a function of φ. Initially, the uncertainty is minimised at multiples of π. However, these uncertainties do not decrease in time. As T increases, the optimum value of φ for measurement moves closer to $\frac{\pi}{2}$. This result is again produced with a sum up to $n = 1000$.

5.3.5 The estimator

In order to use the results presented here for a metrological application, the estimator $\hat{\varphi}$ needs to be found. This can be done by interverting the measurement signal in order to make φ the subject, givng an equation of the form

$$\varphi \;=\; \ldots . \tag{5.53}$$

For a simple interferometric setup, this is straight forward. For example, if N photons are inserted into one arm of an interferometer with a phase shift of φ in one arm (like that in Fig. 1.1), the number detected in the two output arms (A and B) will be

$$N_{\mathrm{A}} \;=\; \frac{1}{2}\left(1+\cos(\varphi)\right)N\,, \quad N_{\mathrm{B}} = \frac{1}{2}\left(1-\cos(\varphi)\right)N\,, \tag{5.54}$$

with $N_{\mathrm{A}} + N_{\mathrm{B}} = N$ as required. Hence, rearranging we may write

$$\varphi = \cos^{-1}\left(\frac{2N_{\mathrm{A}}}{N_{\mathrm{A}}+N_{\mathrm{B}}} - 1\right). \tag{5.55}$$

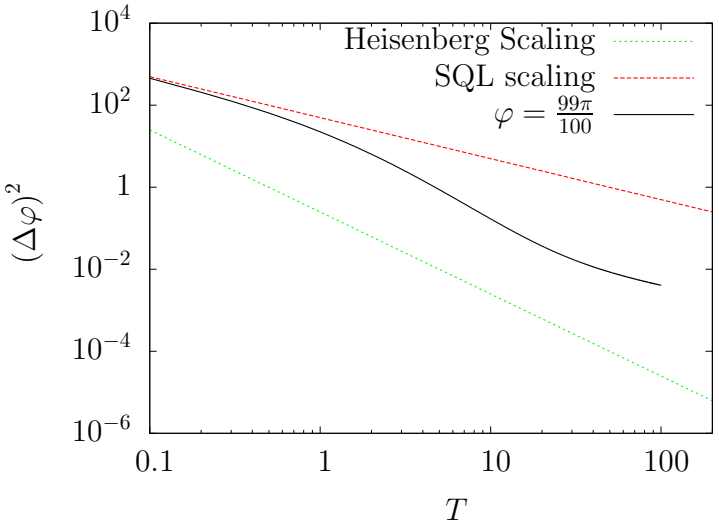

Figure 5.7: Considering the uncertainty $(\Delta\varphi)^2$ as a function of T for fixed value of φ ($\varphi = \frac{99\pi}{100}$). For illustrative purposes, scaling according to the SQL ($\sim \frac{1}{T}$) and the Heisenberg limit ($\sim \frac{1}{T^2}$) are shown. We see that the scaling of our system lies between these two. At its steepest point, the scaling of the two level atom goes beyond that of the Heisenberg limit. However, this does not mean the uncertainty is beyond the absolute value of the Heisenberg limit. The results are produced with a sum up to $n = 1000$ again.

This provides the estimator for the system in terms of the experimentally measured quantities N_A and N_B.

For the system we describe here, inverting our measurement signal to give φ in the form of Eq. (5.53) is not straightforward. In general, this is something that may be obtained (at the least by some numerical method) but is not determined here explicitly. Here, we shall accept the enhanced scaling calculated by the error propogation formula given in Eq. (5.1) and accept that the estimator could be determined for use in a real experiment.

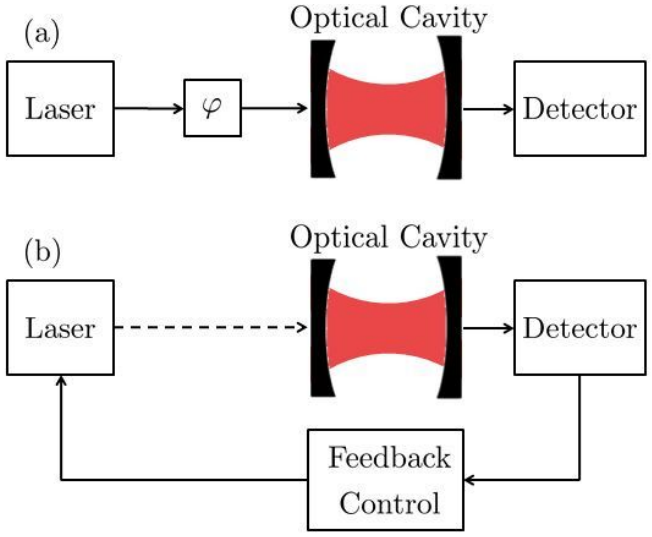

Figure 5.8: The proposed quantum-enhanced metrology scheme involves two main stages. (a) During the preparation stage, a laser experiences an unknown phase φ before entering the resonator, thereby preparing the cavity in a coherent state $|\alpha\rangle$ with α as in Eq. (5.56). (b) During the measurement stage, the continuous laser driving is replaced by an instantaneous feedback loop. Whenever a photon is detected, with a finite detector efficiency η, the feedback laser displaces the resonator field with a fixed phase that can be set to zero without loss of generality. Whether or not the feedback pulse increases the energy inside the cavity and how often it is triggered depends strongly on φ.

5.4 A quantum-enhanced metrology scheme with the single mode coherent states of an optical cavity inside a quantum feedback loop

As a concrete example of a scheme that achieves quantum-enhanced metrology without entanglement, we now present analysis of the scheme proposed in Ref. [7]. This scheme involves the use of a laser-driven optical cavity inside a quantum feedback loop, as described previously in Sections 2.2. As we have seen already, quantum feedback can perturb the system in a way that generates non-linear behaviour and complex correlations.

In this section, we propose to measure the unknown phase shift φ between two

pathways of light using a leaky optical resonator inside an instantaneous quantum feedback loop. As illustrated in Fig. 5.8, the quantum-enhanced metrology scheme that we propose here consists of two main stages. Firstly, the preparation stage prepares the cavity field in a coherent state $|\alpha\rangle$ with

$$\alpha \quad = \quad |\alpha| \, \mathrm{e}^{\mathrm{i}\varphi} \, . \tag{5.56}$$

Afterwards, during the measurement stage, the cavity is placed inside a quantum feedback loop. Whenever a photon is detected, a laser pulse is applied, which does not experience the unknown phase φ. The pulse displaces the field inside the resonator in a certain direction, thereby providing the reference frame for the proposed phase measurement. For the feedback pulse to be approximately instantaneous, it needs to be short compared to the average cavity photon life time $1/\kappa$. In the following we extract information about the unknown phase φ from the temporal quantum correlations in the spontaneous photon emissions of the optical resonator. The measurement of these correlations does not require highly-efficient single photon detectors. Hence realising the experimental setup in Fig. 5.8 is feasible with current technology [89, 90, 91].

As we shall see below, the only density matrix ρ of the cavity field with a vanishing time derivative $\dot{\rho} = 0$ is the vacuum state. When starting in this state, the system remains there and never experiences a feedback pulse. However, in general, the cavity field remains in a single-mode coherent state $|\alpha\rangle$ with $\alpha \neq 0$. In many cases, α increases rapidly in time. Unlike most quantum optical systems with spontaneous photon emission, the ensemble average of the resonator *never* reaches a stationary state [41, 92], as we saw in Chapter 3. The final state of the cavity depends very strongly on the phase φ, which has initially been imprinted onto the resonator (c.f. Eq. (5.56)). Moreover, the temporal quantum correlations of the single trajectories of the cavity field cannot be expressed as first-order expectation values and do not evolve according to a set of linear differential equations. Their *non-linear* dynamics is what allows us to perform better-than-classical phase estimation. Using the dissipative dynamics of open quantum systems [11, 13, 14, 18], Refs. [5, 6] already designed quantum metrology schemes that exceed the standard quantum limit. The main advantage of the scheme that we discuss here is that it is relatively easy to realise experimentally.

Our quantum-enhanced metrology scheme should be of practical interest until highly-entangled many-photon states become more readily available.

The quantum-enhanced metrology scheme that we propose here extracts information about the unknown phase φ of the initial state in Eq. (5.56) by performing N successive measurements on a single quantum system. This means, our scheme is equivalent to performing single-shot measurements on a combination of N entangled quantum systems. Instead of multi-partite entanglement, we use temporal quantum correlations [93, 94]. The main resource of our quantum metrology scheme, i.e. the number of queries posed during each run of the experiment, hence equals the number of successive measurements on the cavity field. In other words, it essentially equals the number of time steps in which the cavity either emits a photon or not, which is proportional to the duration of the proposed experiment. As long as the behaviour of the cavity field generates temporal quantum correlations with non-linear dynamics, actual physical entanglement does not need to be present [60]. We are therefore not in contradiction with previous work that claims entanglement is required to go beyond standard scaling, as in such cases only linear generators of change in the unknown parameter are considered [61, 62].

Before presenting the exact metrology scheme, we briefly review some of the physical behaviour of the optical cavity with quantum feedback. In particular, we highlight the key long term behaviour that allows an enhanced measurement to be performed.

5.4.1 Long term behaviour

Before presenting the metrology scheme, we briefly review the work done in Chapter 3. In particular, we remind ourselves of the long-term behaviour of an optical cavity inside a quantum feedback loop.

Convergence without feedback

Previously in Chapter 3, we have seen that the coherent state $|\alpha_{\text{ss}}\rangle$ in Eq. (3.12) is invariant under the no-photon time evolution of a laser-driven optical cavity. Furthermore, we know that this state is also invariant under the emission of a

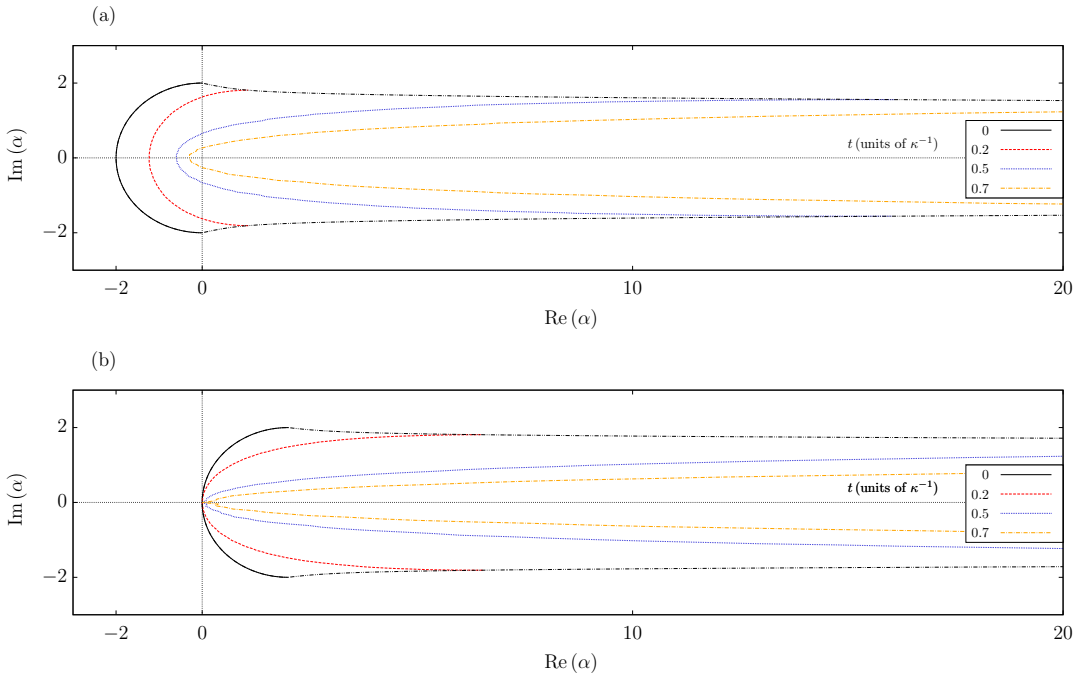

Figure 5.9: (a) Phase diagram illustrating the dynamics of the single-mode coherent states $|\alpha\rangle$ of the cavity field during the measurement stage. The initial states of the resonator form a circle centred about the origin. The lines show the occupied state space of the states corresponding to $\varphi \in [\frac{\pi}{2}, \frac{3\pi}{2}]$ at a later time t. As time elapses, the circle turns into an increasingly stretched ellipse. States that correspond to different phases φ move further and further away from each other. (b) Dynamics of the cavity field under the condition of a photon emission at $t = 0$, which triggered an instantaneous feedback pulse. Both graphs are the result of a quantum jump simulation based on the calculations in Section 2.2.3, where we assume a detector efficiency of $\eta = 0.5$ and consider 10^6 repetitions of the experiment. Here the feedback pulse is given by $\beta = |\alpha|$ with $\alpha = 2$. The dash-triple dot lines extended from the original semi-circle represent the trend of the evolution of the states corresponding to $\varphi = \frac{\pi}{2}$ and $\varphi = \frac{3\pi}{2}$.

photon due to it being a coherent state (see Appendix A). Consequently, $|\alpha_{\text{ss}}\rangle$ is the stationary state of a laser-driven optical cavity without feedback. Once the cavity reaches this state, it no longer evolves in time. Indeed, one can easily check that the corresponding density matrix $\rho_{\text{ss}} = |\alpha_{\text{ss}}\rangle\langle\alpha_{\text{ss}}|$ solves $\dot{\rho} = 0$.

Divergence with feedback

Combining the stationary state condition $\dot{\rho} = 0$ with the master equation in Eq. (2.67), we can calculate the stationary state of the laser-driven optical cavity inside an instantaneous feedback loop. From the discussion in Section 3.2.2, we know that the field inside the resonator in this case too remains always in a coherent state, if initially coherent. This implies that the stationary state, if it is ever reached, has to be of the form of Eq. (3.21), i.e. a statistical mixture of coherent states $|\alpha\rangle$ with weighting $P(\alpha)$. However, the master equation (2.67) does not possess a stationary state of this form except for $\alpha = 0$, where the dynamics become trivial. However, from what we have seen in Chapter 3, we know that this stationary state is a repulsive fixed point in the dynamics and many quantum trajectories diverge away from this point in general. From this we conclude that the laser-driven cavity with instantaneous quantum feedback that we consider in this chapter does not reach a stationary state in general [41, 92]. It exhibits a much richer dynamics than what was previously assumed [95, 96]. This even applies if the continuous laser driving is turned off, unless the cavity is initially empty.

Fig. 5.9 illustrates the non-linear dynamics of an optical cavity inside an instantaneous quantum feedback loop with the help of a so-called phase diagram. This diagram represents coherent states $|\alpha\rangle$ as points by using the real part and the imaginary part of α as coordinates. It is the result of a numerical simulation which averages $\alpha(t)$ over a large number of quantum trajectories. Different times t and a wide range of initial states $|\alpha\rangle$ with $\varphi \in [\frac{\pi}{2}, \frac{3\pi}{2}]$ and with α as in Eq. (5.56) are considered. As one can see, the half circle representing these initial states deforms rapidly into an increasingly stretched ellipse, thereby constantly increasing the phase space volume occupied by the cavity field. In Fig. 5.9(b), the cavity field is initially in the same state as in Fig. 5.9(a) but experiences a feedback

pulse at $t = 0$ with $\beta = |\alpha|$. In this case, the constant growth and stretching of the phase space volume of the cavity field is even more pronounced. For example, a cavity in an initial coherent state with $\varphi = \pi$ and a photon detection at $t = 0$ never emits another photon and never experiences another feedback pulse. On the contrary, a cavity with $\varphi \neq \pi$ is likely to emit many photons, thereby attracting an exponentially-increasing number of feedback pulses. As a result, the distance between two coherent states $|\alpha_1(t)\rangle$ and $|\alpha_2(t)\rangle$ corresponding to two different phases φ_1 and φ_2 increases rapidly in time.

5.4.2 Quantum-enhanced metrology scheme

Now we have all the tools needed to analyse the quantum metrology scheme illustrated in Fig. 5.8. It consists of two main stages:

1. **The preparation stage**. A continuous laser field experiences an unknown phase shift φ before entering an optical cavity, as illustrated in Fig. 5.8(a). The main purpose of this stage is to prepare the field inside the resonator in a coherent state, which depends on φ. For simplicity, we assume that the cavity is driven for a time which is relatively long compared to the time scale given by the laser Rabi frequency and the cavity decay rate. This approach prepares the resonator in its stationary coherent state $|\alpha_{\rm ss}\rangle$ in Eq. (3.12) with the phase φ encoded into the phase of $\alpha^{\rm ss}$.

2. **The measurement stage**. Here the continuous laser driving is turned off. Instead the optical cavity evolves freely, while experiencing instantaneous feedback pulses, as illustrated in Fig. 5.8(b). These are triggered by the observation of a spontaneously emitted photon with a finite detector efficiency η. We assume that every feedback pulse displaces the field inside the cavity by an amount β given by

$$\beta \;=\; |\alpha_{\rm ss}| \tag{5.57}$$

which is independent of φ. This means the feedback laser provides a reference frame. The measured phase is indeed the relative phase between the phase of the driving laser used during the preparation stage and the phase

of the feedback laser (with respect to the interaction picture). All photon detection times should be registered.

As we shall see below, temporal quantum correlations reveal information about φ with an accuracy above the standard quantum limit.

Resource counting

To identify the main resource, N, of our metrology scheme, we take inspiration from the approach by Zwierz *et al.* [63] and assume that N equals the query complexity of our scheme. Each time the phase φ is probed, a resource is used. In every time step, we perform a (conditional) phase dependent operation on the system. Continuously observing the leakage of photons through the cavity mirrors means a continuous probing of the unknown phase φ. As illustrated in Fig. 5.10, every time step can be seen as one query posed and hence provides one resource count. The amount of time T, which the system spends within the measurement stage during each repetition of the experiment, is therefore the most relevant resource of our quantum metrology scheme. To calculate $\Delta\varphi$ as a function of T, we now simulate a relatively large number of quantum trajectories of the experimental setup in Fig. 5.8 using the methodology which we introduced in the previous section and then use the error propagation formula in Eq. (5.1) to analyse the precision of the proposed experiment. For completeness and to allow for a comparison with other quantum metrology schemes, we also consider the mean number of photons passing through the unknown phase φ as a resource N. In our scheme, this number is essentially given by the mean number of photons $|\alpha_{\rm ss}|^2$ inside the resonator at the end of the preparation stage.

Accuracy of intensity measurements

Let us first have a closer look at the average photon emission rate $I(T)$ of the cavity at a time T after the preparation of the initial coherent state $|\alpha_{\rm ss}\rangle$ in Eq. (3.12), which depends on the unknown phase φ. To calculate $I(T)$ numerically, we divide the time interval $[0, T]$ into relatively short time intervals Δt. We then use the quantum jump approach [20, 21, 22] described in Section 2.2.3 to simulate a relatively large number of possible quantum trajectories of the cavity

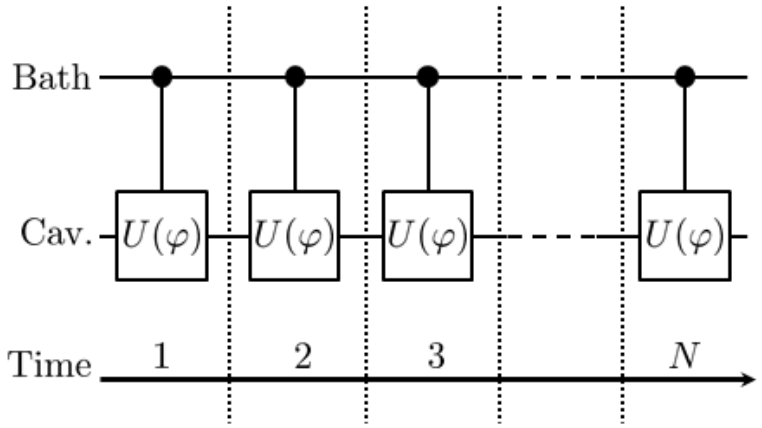

Figure 5.10: Circuit diagram of the time evolution of the experimental setup in Fig. 5.8 during the measurement stage. The black dots indicate that the bath is measured in every time step, $n = 1, \ldots, N$, and when a photon emission is detected triggers the operator $U(\varphi)$ to act on the cavity. This process provides information about the state of the cavity and the unknown phase, φ.

and average over the respective number of photon emissions in $(T, T + \Delta t)$. The result of this simulation is shown in Figs. 5.11 and 5.12. While Fig. 5.11 shows the average photon emission rate $I(T)$ as a function of T for different phases φ, Fig. 5.12 shows the $I(T)$ as a function φ for different times T. Both logarithmic plots illustrate that the dynamics of the mean number of photons inside the resonator depends indeed very strongly on the initial coherent state $|\alpha_{\text{ss}}\rangle$ of the cavity field.

Next we investigate the accuracy of a measurement, which uses the strong dependence of $I(T)$ on φ to deduce information about φ. Figs. 5.11 and 5.12 show that this dependence is maximised for φ around $0.3\,\pi$. We therefore consider in the following the signal $M = I(T)$ and $\varphi = 0.3\,\pi$ as an example and calculate the accuracy of the proposed quantum metrology scheme $\Delta\varphi$ using the error propagation formula in Eq. (5.1) as a function of T. The standard deviation in this equation is obtained through statistical analysis of the simulation data created by many quantum jump simulations described in Section 2.2.3, while the sensitivity is found by finding the gradient between two very close phases. Again we average over a large number of quantum trajectories. The result of this

numerical simulation is shown in Fig. 5.13. To a very good approximation, we find that

$$\Delta\varphi(T) \quad \propto \quad T^{-0.49} \quad \text{for} \quad \varphi = 0.3\,\pi\,. \tag{5.58}$$

This means, using only intensity measurements, the experimental setup in Fig. 5.8 does not allow us to beat the standard quantum limit in Eq. (5.2). In fact, we almost saturate this limit. This is to be expected as the dynamics of the mean number of photons inside the cavity obeys a master equation, which represents a set of *linear* differential equations. Moreover, intensity measurements are essentially classical measurements. Finally, it should be noted that the fit In Eq. (5.58) is an approximation, as the data appears to be showing a more complex dependence whose exact functional form will not be investiagted here. However, it seems safe to conclude that the scaling of $\Delta\varphi(T)$ does not exceed the standard quantum limit.

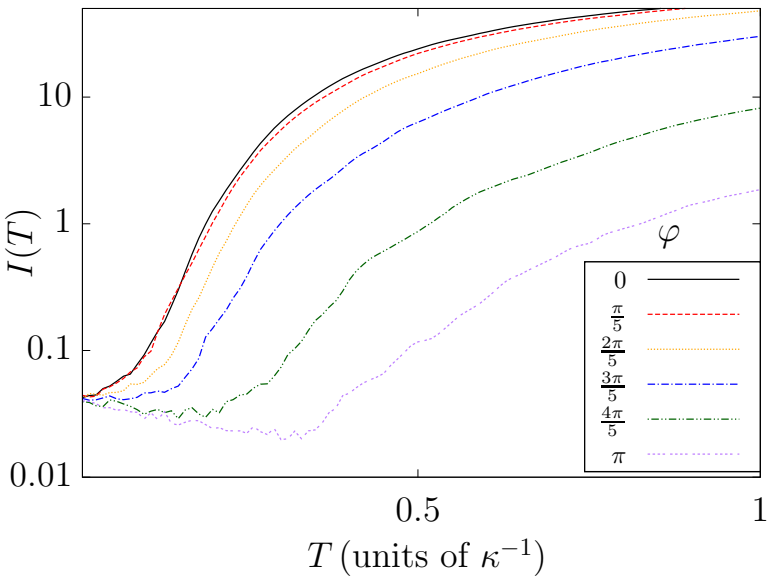

Figure 5.11: Average intensity $I(T)$ plotted on a Log_{10} scale, as a function of the time, T, after the preparation of the initial coherent state, $|\alpha_{\text{ss}}\rangle$, for various unknown phases, φ. This simulation assumes $|\alpha_{\text{ss}}|^2 = 4$, $\eta = 0.5$ and averages over 10^6 trajectories and is generated by the quantum jump method.

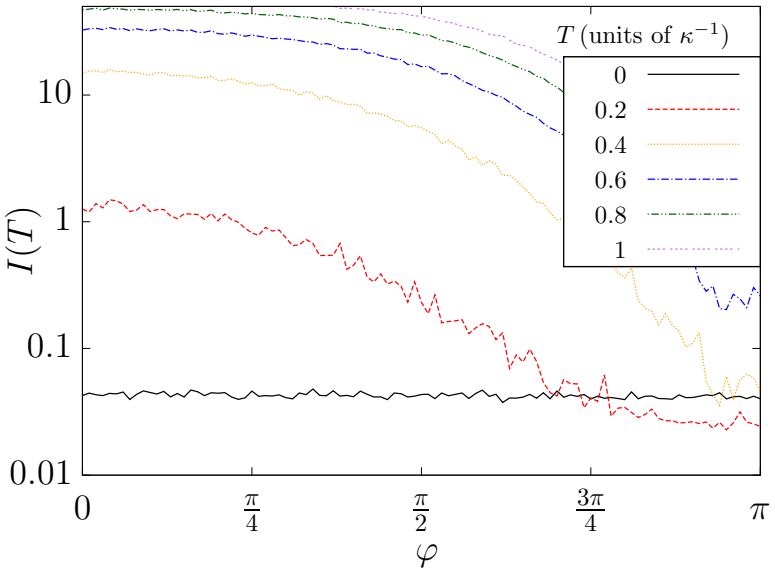

Figure 5.12: Average intensity $I(T)$ plotted on a Log_{10} scale, as a function of the unknown phase, φ, for different times, T. As in Fig. 5.11, we have $|\alpha_{\mathrm{ss}}|^2 = 4$, $\eta = 0.5$ and average over 10^6 trajectories and is generated by the quantum jump method.

Accuracy of second-order correlation function measurements

A comparison between Figs. 5.9(a) and (b) suggests that measurements of the joint probability to detect a photon at a time t *and* at a time t' should be able to reveal information about φ more efficiently than measurements of the average photon intensity $I(T)$. This joint probability is known to quantum opticians as the second-order photon correlation function $G^{(2)}(t, t')$. Hence, according to probability theory, $G^{(2)}(t, t')$ equals

$$G^{(2)}(t, t') \equiv I(t|t')I(t')\,, \tag{5.59}$$

where $I(t|t')$ denotes the probability for the detection of a photon at a time t conditional on the detection of a photon at t'. Second-order correlation functions are usually normalised by the product of the photon emission rate at t' and at t. Taking this into account and dividing Eq. (5.59) by $I(t')I(t)$, we define the

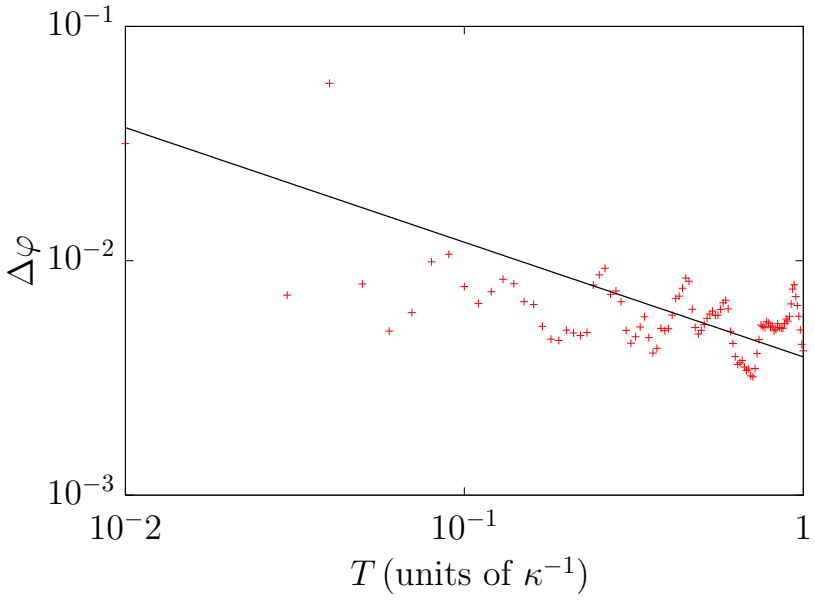

Figure 5.13: Dependence of the accuracy, $\Delta\varphi$, on the length of the measurements stage, T, in the case of intensity measurements. Here, $\varphi = 0.3\,\pi$, $|\alpha_{\rm ss}|^2 = 4$, $\eta = 0.5$ and we averaged over 10^6 trajectories. The black line illustrates the approximate fit given in Eq. (5.58).

renormalised second-order correlation function, $g^{(2)}(t, t')$, by

$$g^{(2)}(t, t') \equiv \frac{I(t|t')}{I(t)}\,. \tag{5.60}$$

This correlation function describes correlations between photon emission events without depending on the detector efficiency η with which these events are registered. It can therefore be measured accurately, even when using imperfect detectors with $\eta < 1$.

In the following, we assume that $M = g^{(2)}(T, 0)$ is the actual measurement signal used to obtain information about the unknown phase φ. As we shall see, this measurement signal also contains a dependence in the unknown parameter φ. Hence, using the same techniques as before, we may test how well we can determine φ from this signal. To determine the accuracy $\Delta\varphi$ of this approach as a function of the length T of the measurement stage, we again simulate a relatively large number of quantum trajectories and average over all of them. The

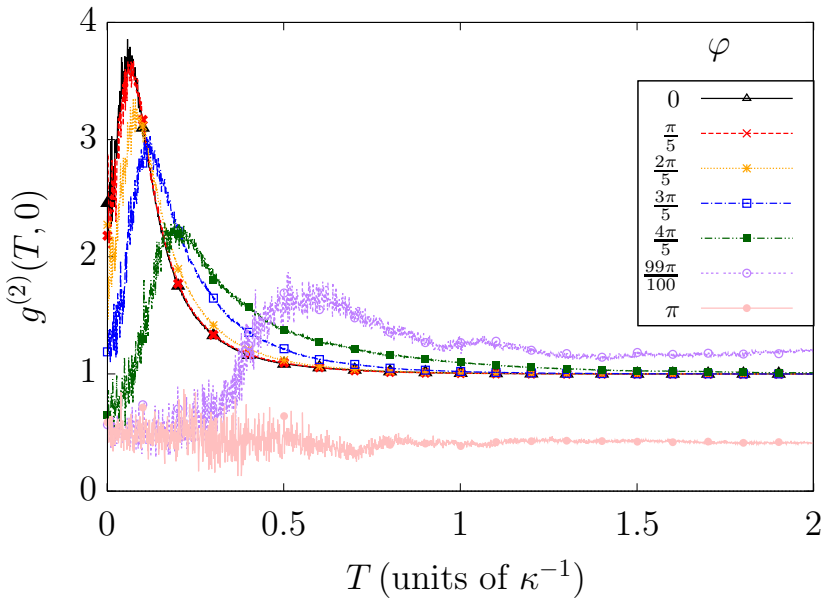

Figure 5.14: Second-order correlation function $g^{(2)}(T,0)$, as a function of the duration of the measurement stage, T, for various phases φ. Again we assume $|\alpha_{\rm ss}|^2 = 4$, $\eta = 0.5$ and averages over 10^6 trajectories and is generated by the quantum jump method.

results of this simulation are shown in Figs. 5.14 and 5.15, which are analogous to Figs. 5.11 and 5.12 in the previous subsection. As expected, the correlation function $g^{(2)}(T,0)$ too exhibits a very strong φ-dependence. This dependence is most pronounced when $\varphi = \pi$. As suggested by Fig. 5.9, we have $g^{(2)}(T,0) = 0$ for sufficiently large detector efficiencies η and $\varphi = \pi$, while $g^{(2)}(T,0)$ rapidly tends to unity for all other angles. Indeed Fig. 5.14 shows very large differences between neighbouring curves, when φ is close to π, even when φ is varied only by a relatively small amount. Moreover Fig. 5.15 shows a distinct spike at $\varphi = \pi$ as a function of φ. This spike in the second-order correlation function is what allows us to distinguish this phase with a very high accuracy $\Delta\varphi$ from other close-by values of φ due to a very high visibility $|\partial M/\partial\varphi|$.

This is confirmed by Fig. 5.16 which shows the dependence of $\Delta\varphi$ on the resource T for phase measurements based on the second-order correlation function for the optimal case of $\varphi = \pi$. To calculate this quantity we use again the error

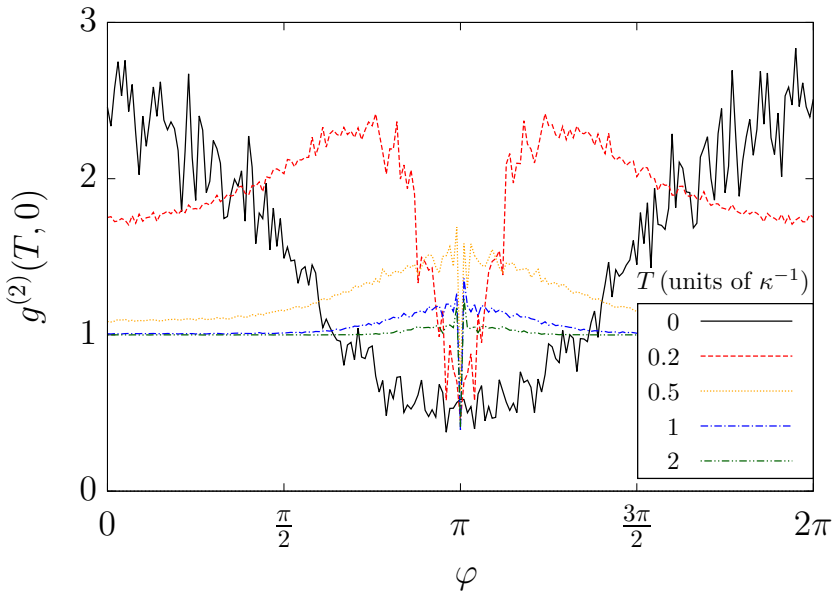

Figure 5.15: Second-order correlation function $g^{(2)}(T,0)$ as a function of the unknown phase, φ for various times, T, with $|\alpha_{\rm ss}|^2 = 4$ and $\eta = 0.5$ averaged over 10^6 trajectories and is generated by the quantum jump method.

propagation formula in Eq. (5.1) and average over a relatively large number of quantum trajectories. We now find that

$$\Delta\varphi(T) \quad \propto \quad T^{-0.71} \quad \text{for} \quad \varphi = \pi \tag{5.61}$$

to a very good approximation. This accuracy clearly beats the standard quantum limit. In other words, measurements of the second-order photon correlation function of the photon statistics of an optical cavity inside an instantaneous quantum feedback loop can be very sensitive to phase fluctuations.

This is not surprising, since measurements of the second-order photon correlation function $g^{(2)}(T,0)$ require the detection of single photons. This is different from intensity measurements which are essentially classic measurements. These can be done without high-resolution single-photon detection. Moreover, second-order photon correlations are an intrinsic property of the individual quantum trajectories of the cavity field. They cannot be calculated with the help of a linear master equations but require the quantum jump approach [20, 21, 22], which

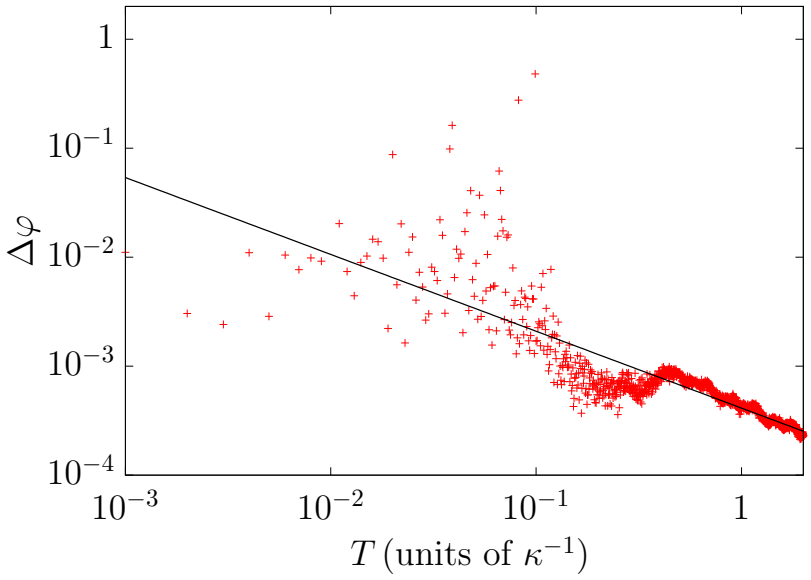

Figure 5.16: Accuracy $\Delta\varphi$ of the proposed metrology scheme as a function of the duration of the measurement stage, T, for measurements of the second-order correlation function $g^{(2)}(T,0)$ around $\varphi = \pi$ to maximise the sensitivity of the proposed scheme. As before, we assume $|\alpha_{\rm ss}|^2 = 4$, $\eta = 0.5$ and average over 10^6 trajectories. The black line shows the approximate solution in Eq. (5.61).

we introduced in Section 2.2.3. The conditional dynamics of the individual trajectories of the cavity field is in general non-linear. For example, between photon emission, the cavity field evolves in a non-linear fashion with the non-Hermitian conditional Hamiltonian $H_{\rm cond}$ in Eq. (2.59), which requires a constant renormalisation of the state vector of the quantum system. In summary, it is the measurement of the temporal quantum correlations in an open quantum system that allows us to exceed the standard quantum limit. This observation is consistent with analogous observations by other authors [5, 6, 83, 84, 85, 86, 87].

A more standard method of resource counting in quantum metrology is to consider the average number of photons that passed through the unknown phase φ as the resource N. This approach can also be applied to the quantum-enhanced metrology scheme which we propose here. Performing quantum jump simulations, averaging over many quantum trajectories and using again the error propagation

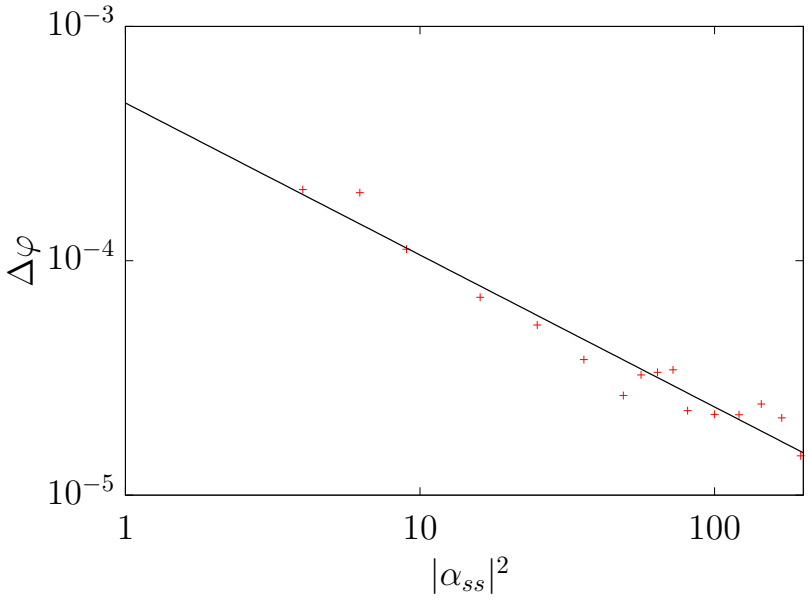

Figure 5.17: Accuracy, $\Delta\varphi$, of the proposed metrology scheme as a function of the initial mean photon number, $|\alpha_{\rm ss}|^2$, for measurements of the second-order correlation function $g^{(2)}(T,0)$ and $\varphi = \pi$. Here, $\eta = 0.5$ and we average over 10^6 trajectories generated by the quantum jump method. To remove noisy fluctuations in the signal in time, we take a sample of uncertainties over a fixed period of time, find the average uncertainty in that period and compare this average to the same time average for other initial states. The black line shows the approximate solution in Eq. (5.62).

formula in Eq. (5.1) with $M = g^{(2)}(T,0)$, we now calculate the dependence of $\Delta\varphi$ on the average population of the initial coherent state inside the cavity, which is given by $|\alpha_{\rm ss}|^2$. The result is shown in Fig. 5.17. For the parameters that we consider here, we find that

$$\Delta\varphi(|\alpha_{\rm ss}|^2) \;\propto\; \left(|\alpha_{\rm ss}|^2\right)^{-0.65} \quad \text{for} \quad \varphi = \pi \tag{5.62}$$

to a very good approximation. Eq. (5.62) too clearly beats the standard quantum limit. In practical applications, it might be best to consider both the duration of the measurement stage and the number of photons that passed through the sample as a resource. Numerical results for such an experiment are shown in

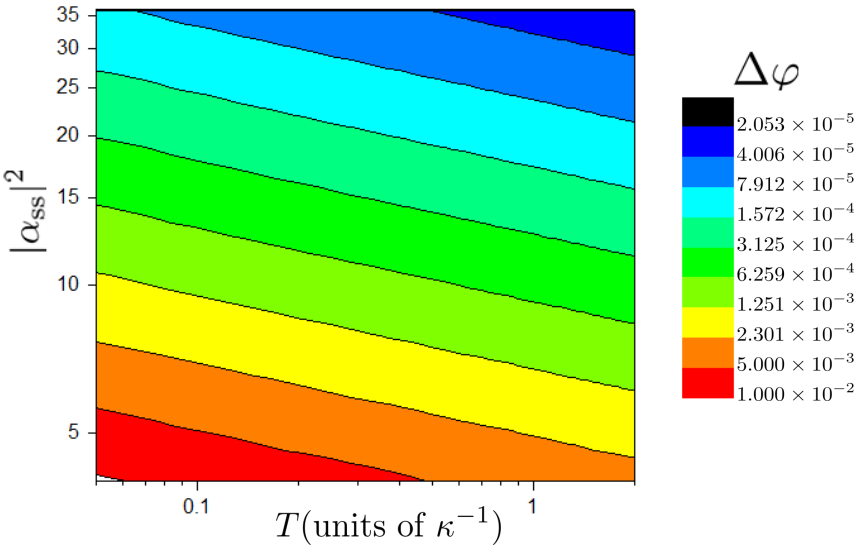

Figure 5.18: Accuracy $\Delta\varphi$ plotted on a Log_{10}-Log_{10} scale, when both the duration of the measurement stage, T, and the initial mean number of photons, $|\alpha_{ss}|^2$, is taken into account and the second-order correlation function $g^{(2)}(T, 0)$ is analysed. Here we have $\eta = 0.5$ and we consider 10^6 repetitions of the experiment.

Fig. 5.18. When we have two scalable resources, our scheme allows more freedom in gaining information about the phase φ with high accuracy, even when one of the resources is constrained. More precisely, if the number of photons that can be used is limited for example, a coherent state with a smaller average phton number $|\alpha|^2$ can be used and allowed to run for longer instead of running an experiment with a larger number of photons for a shorter amount of time to obtain the same precision.

Once again, in order to use this scheme for a real experimental application, the estimator should be obtained. As the results presented in this section are completely numerically generated, the estimator cannot be analytically obtained. However, the estimator could be approximated by fitting a curve to the measurement signal in Fig. 5.15 and inverting it as described in Section 5.3.5. This has not been done here as the goal was to demonstrate the scaling, but could be

obtained if required as described.

5.5 Comment on ultimate limits of scaling for metrological systems

While a lot of theoretical work predicts enhanced scalings in the uncertainty of an unknown parameter φ, it is often assumed that the system conducting the probing is completely noiseless. However, if noise is incorporated into the phase estimation calculations, the results can be extremely damaging to the resulting scaling. As described in some recent studies [97, 98], the introduction of nose into the measurement process can reduce the optimum scaling to that of the standard quantum limit, but enhanced with a constant factor. Depending on the magnitude of the noise or loss (whatever form it may take), the scaling gradually reduces towards this standard quantum limit scaling for increasing number N at a rate determined by this.

In the work presented here, no such random noise or loss is considered explicitly. Despite this, there are two points that should be noted. Firstly, in the scheme presented in Section 5.3, we have seen scalings in the Fisher information that grow at an enhanced rate. However, for certain parametric choices, the Fisher information eventually changes to growth at the standard linear rate. In this work this has not been investigated, as the goal was to present a proof-of-principle in generating enhanced scalings by beens of quantum feedback. Furthermore, in the case of a solid example where we considered the average number of photons emitted by an atom $\bar{N}$ in a time T, we also found the enhancement wore off after a large amount of time T (or resources N). Whether this is due to intrinisic noise in the system, perhaps due to the random nature in which the parameter is encoded into the system, or something else is not known.

Secondly, in the case of an optical cavity as discussed in this section, we did not see a decline in scaling for larger values of T. Whether this is due to not taking T to a large enough size to properly see this effect or whether it is simply because we have not inserted any noisey effects into the system is not known at this stage. However, because of the experimental setup presented here (i.e. the

use of coherent states), we would expect this system to be rather robust to most forms of noise. Hence, we should expect that any decline in scaling enhancements would be highly suppressed.

A final difference with this work from the general scaling results discussed in Refs. [97, 98] is that in our analysis and proposed schemes we only probe the output sequence generated by a quantum system. Essentially, the internal system is never directly measured. This differs from previous work where the focus is on either measuring a system (with or without its environment also measured) directly. Instead, we take advantage of the temporally correlated output signals produced by an open quantum system.

5.6 Conclusions

In this chapter, we have presented an analysis of a novel approach to quantum metrology, using the temporal correlations generated in open quantum systems. To do this, we have calculated the Fisher information of the dynamics of a quantum jump analysis of an open quantum system. This has led to an identification of how useful correlations may be induced that allow a better-than-classical parameter estimation scheme.

Our scheme highlights that by making the resetting of the system after emission into the environment dependant upon the unknown parameter, the Fisher information may scale non-linearly and hence offer an enhancement. However, this is not the case for all parameter regimes. In particular, when the scaling is non-linear, the absolute size of the Fisher information is small. However, we believe this may be combated in a more sophisticated scheme away from our toy model approach, either with a larger Hilbert space or allowed to run for a longer time. Because of this, our scheme should be of particular interest for technological applications, as it offers a feasible method of obtaining enhanced scaling in the laboratory without extreme experimental difficulty.

Furthermore, we then proposed a quantum metrology scheme to measure an unknown phase φ between two pathways of light with an accuracy above the standard quantum limit. Our scheme is based on a laser-driven optical cavity inside an instantaneous quantum feedback loop, as illustrated in Fig. 5.8. The

measurement process includes two main steps. Firstly, during the preparation stage, a continuous laser experiences the phase shift, φ, before entering the cavity field. Its purpose is to prepare the cavity in a coherent stationary state which depends strongly on this phase. Secondly, during the measurement phase, the cavity experiences only the quantum feedback loop. Whenever the spontaneous emission of a photon is detected, a laser pulse, which does not experience φ and provides the reference frame for the proposed phase measurement, is activated and displaces the resonator field in a controlled way.

In the scheme with an optical cavity inside a quantum feedback loop, we have assumed that the detector that monitors the cavity during the measurement stage determines its second-order photon correlation function $g^{(2)}(T, 0)$. This means, it essentially measures the joint probability for the detection of a photon at the very beginning (at $t = 0$) and at the end (at $t = T$) of the measurement stage. As shown in Section 5.4.2, this second-order correlation function can be used to determine φ with an accuracy $\Delta\varphi$ that scales better than what can be achieved classically according to the standard quantum limit in Eq. (5.2). For the parameters that we consider in this chapter, we find that $\Delta\varphi$ scales as $T^{-0.71}$ (c.f. Eq. (5.61)). If we consider instead the mean number of photons seen by the unknown phase φ during the preparation stage as the main resource of our quantum metrology scheme, we find that $\Delta\varphi$ scales as $(|\alpha_{\rm ss}|^2)^{-0.65}$ (c.f. Eq. (5.62)).

To achieve this quantum enhancement, our metrology scheme uses the temporal correlations of an individual quantum system instead of using multi-partite entanglement. It is worth noticing that subsequent measurements on a single quantum system are in general equivalent to single-shot measurements on multi-partite entangled states. Temporal quantum correlations, which cannot be predicted by a linear master equation, constitute an interesting approach for technological applications [83, 84, 85, 86, 87]. As shown in Chapter 3, the dynamics of the individual quantum trajectories of the cavity field inside an instantaneous feedback loop is indeed non-linear and depends very strongly on the initial state of the resonator, which encodes the unknown phase φ [41, 92]. As illustrated in Fig. 5.9, there is constant stretching and growths of the initially occupied phase space volume. The distance between two different states $|\alpha_1\rangle$ and $|\alpha_2\rangle$ which correspond to different φ_1 and φ_2 increases rapidly in time.

The main advantage of the quantum metrology scheme which we propose here is that its experimental realisation is relatively straightforward. As mentioned already above, we do not require highly-entangled many-photon states. Although the proposed scheme requires a relatively good optical cavity, it does not require highly efficient single photon detectors. This is due to the definition of the correlation function $g^{(2)}(t_1, t_2)$ being independent of a detectpor efficiency η. High-quality optical cavities and relatively fast photon detectors are already available in many laboratories worldwide (see for example Refs. [89, 90, 91]). We therefore believe that our quantum metrology scheme will be of significant practical interest until highly-entangled many-photon states become more readily available.

It should be possible to generalise the results described in this chapter to larger and more sophisticated systems. In particular, it is possible to generalise the scheme described in Section 5.4 by interfering the emitted light by multiple cavities in a linear optics network. In doing so, it is possible to create multiple fixed points in the dynamics. These fixed points should be able to take advantage of the enriched dynamics to gain a quantum-enhanced measurement scheme. This system should not only be more sensitive than the previous, but also capable of measuring multiple phases with persistent enhanced precision. This could find potential applications in quantum neural networks and quantum machine learning, as well as in quantum metrology. Also, a further method in which the phase estimation could be improved may be to use higher order correlation functions than the second-order ones considered in this work. Already in quantum imaging it has been shown that the use of higher order correlation functions can improve resolution [99]. It is reasonable to speculate that this may also be true for the system under consideration here, though it has not been explicitly investigated at this stage. In particular, it may be the case that the achievable scaling approaches the Heisenberg-limited value for higher order correlation measurments.

Chapter 6

Conclusions

This thesis has presented a novel approach to understanding open quantum systems with instantaneous quantum feedback. We began in Chapter 2 by presenting a theoretical model to analyse these types of quantum systems. This involved a general derivation of the quantum optical master equation before applying to two concrete systems: a laser-driven optical cavity and a laser-driven two level atom, both of which had quantum feedback incorporated. The former of these two systems is the main focus of all the proceeding work in the following chapters. In Chapter 3 we presented work that shows the behaviour of a relatively simple system like a laser-driven optical cavity can become significantly enriched by the presence of quantum feedback. In particular, we found that the dynamics are no longer ergodic and do not always reach a well-defined stationary state.

Building upon this knowledge, we then considered two applications. Firstly, in Chapter 4, we considered a computer science based application in Hidden Quantum Markov Models. In that study, we found that even in the most primitive of systems a quantum-enhancement is present. If this is scaled up to a larger and more general system, the enhancement should become even more pronounced, as in other quantum systems. The other application considered was a quantum metrology scheme. In Chapter 5 we demonstrated how a quantum enhancement can be achieved without the need to prepare highly complex states. This presents a significant advantage over standard methods, as the experimental difficulty is reduced. This is due to both the ability to control an open quantum system with quantum feedback requiring relatively simple techniques and also the appropriate

resource being time allows for measurements with the resource number being high with relative ease.

There are of course still some difficulties in implementing the ideas presented within this thesis. For instance, in implementing the proposed metrology schemes, the feedback is analysed as if it is exact. An imperfect implementation of this scheme could result in errors reducing the accuracy of the measurements being made, which could propagate errors through the measurements. The exact effect of this could be investigated further to determine how robust the system is to these errors. However, the potential advantages of this method should still outweigh the possible experimental imperfections in potential implementation. Furthermore, the systems considered are rather primitive. In the case of the two-level atom, a larger number of qubits could be used for example. This may lead to even better scaling in the uncertainty.

Furthermore, the investigation into Hidden Quantum Markov Models found only a minimal enhancement over the classical Hidden Markov Model so far. As already stated though, this should not be too surprising as the more exotic behaviour typical of quantum systems usually requires more than a single qubit. Advancing to larger systems should show further enhancements that are expected to be much more significant. As Hidden Markov Models have many applications in classical computer science (see Refs. [44, 45, 46] for some examples), Hidden Quantum Markov Models should be expected to also have many applications in the future as computer science begins investigating quantum speed-up. The potential implementation using open quantum systems and quantum feedback offers a feasible implementation that could be conducted with currently available technology.

Moreover, the architecture described in this thesis may also be able to be used as the building blocks for a quantum neural network or quantum machine learning. As we have shown, open quantum systems with quantum feedback offer a speed-up in determining a parameter. This is essentially the aim of neural networks: how quickly can we resolve if a given input is a specific symbol/value? By combining many of the systems considered here together (e.g. in the form of a network of cavities), it may be possible to develop a neural network architecture. Quantum neural networks and quantum machine learning are rapidly growing

fields with many exciting potential applications [8, 9]. As such, the work done here has scope to provide novel insights into this new field in the future, as well as extensions to the applications already considered.

Appendix A

Coherent states

Coherent states are often called the "most classical" quantum states. The reason for this is that they have a minimum uncertainty. Despite this though, they are still capable of exhibiting interesting quantum behaviour if treated in an appropriate way, as is shown throughout this thesis. Here, coherent states are formally introduced and their basic properties analysed.

A.1 Definition

The Glauber formalism is the most commonly used form used to describe a coherent state [100] and is what shall be used here. A coherent state $|\alpha\rangle$ is defined as the eigenstate of the photon annihilation operator a, meaning

$$a\,|\alpha\rangle \;=\; \alpha\,|\alpha\rangle\;, \tag{A.1}$$

where α is a complex number with $|\alpha|^2$ being the average number of photons in the coherent state $|\alpha\rangle$. This has an interesting physical corollary, as the emission/detection of a photon from a coherent state does not change its state. This is because of the statistical nature of coherent states. Specifically, the reason for this and that we must consider an average number of photons for a coherent state is that it is an infinite superposition over the Fock space that obeys Poissonian statistics. Specifically, in the Fock space it has the form

$$|\alpha\rangle \;=\; \mathrm{e}^{-\frac{|\alpha|^2}{2}} \sum_{n=0}^{\infty} \frac{\alpha^n}{\sqrt{n!}}\,|n\rangle\;. \tag{A.2}$$

Fairly straightforwardly, it can be shown that applying the annihilation operator to the definition in Eq. (A.2) does indeed reproduce Eq. (A.1). Interestingly, although coherent states are eigenstates of the annihilation operator, the creation operator acting upon them is non trivial. It creates so-called photon added coherent states, which now behave like displaced excited Fock states (i.e. non-zero Fock states). In fact, the creation operator does not have an eigenstate. These states are not used in this thesis and so shall not be analysed further.

A.2 The displacement operator

An important operator that is commonly used with coherent states and that is used as the form of the feedback discussed in this thesis is the displacement operator. This operator displaces a coherent state in phase space by a complex parameter. It is defined as

$$D(\beta) \;=\; \exp\left(\beta\, c^\dagger - \beta^*\, c\right) , \tag{A.3}$$

where β is the complex number parametrising the displacement. Applying this operator to a coherent state $|\alpha\rangle$ gives

$$D(\beta)\,|\alpha\rangle \;=\; |\alpha+\beta\rangle \ . \tag{A.4}$$

Hence, the displacement operator simply adds its parameter to that of the coherent state, giving another coherent state.

An interesting case of the coherent state is when α is set to zero. In this case, Eq. (A.2) gives exactly the vacuum state, i.e. $|\alpha=0\rangle = |0\rangle$. Hence, all coherent states may be considered as displaced vacuum states, as

$$|\alpha\rangle \;=\; D(\alpha)\,|0\rangle \ . \tag{A.5}$$

This is why coherent states have minimum uncertainty, as they are fundamentally ground states displaced in phase space rather than true quantum excitations created by a creation operator.

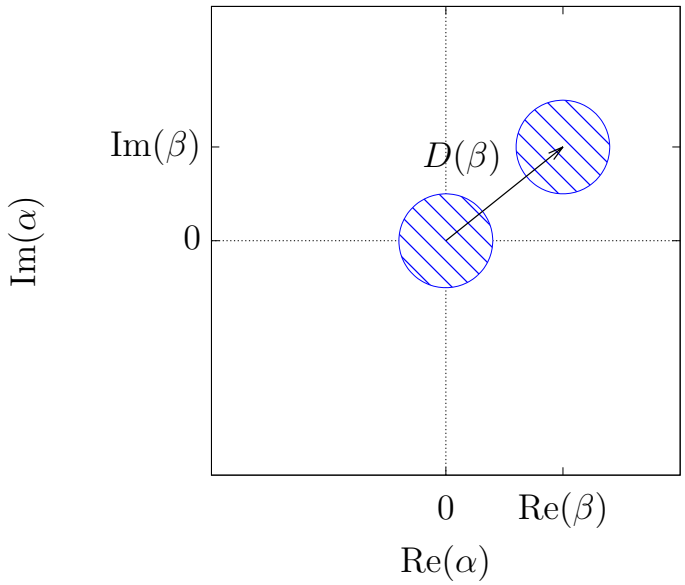

Figure A.1: Phase space diagram of a coherent state initially prepared in the vacuum. A displacement of β is made onto this coherent state, translating it in phase space to a new position without altering any of its other properties.

A.3 Displaced creation and annihilation operators

Rather than acting on a state, the displacement operator can also be acted upon operators. In particular, we shall consider the effect of applying it to the creation and annihilation operators. Let us consider $D^\dagger(\beta)cD(\beta)$ first. It can be shown that

$$\mathrm{e}^X Y \mathrm{e}^{-X} \;=\; Y + [X,Y] + \frac{1}{2!}[X,[X,Y]] + \ldots\,, \tag{A.6}$$

by an extension of the Baker-Campbell-Hausdorff forumula. Now, choosing $X = \beta^* c - \beta c^\dagger$ where $D(\beta) = \mathrm{e}^{-X}$ and $Y = c$, we may evaluate $D^\dagger(\beta)cD(\beta)$. Noticing that here $[X,Y] = \beta$ and all higher order commutators equal zero, we find that

$$D^\dagger(\beta)cD(\beta) \;=\; c + \beta\,. \tag{A.7}$$

Similarly, one can show that

$$D^\dagger(\beta)c^\dagger D(\beta) \;=\; c + \beta^*\,. \tag{A.8}$$

These relations become important when attempting to solve rate equations for quantum systems with feedback in the form of a displacement operator.

Appendix B

Parametrisation and stationary state of a HQMM

Using the properties of quantum systems, we can place some restrictions on the allowed values of the Kraus operators. This is much more complicated than that of the classical machines however, as would be expected. Hence for simplicity and to be able to efficiently study these machines, this study shall instead just consider numerical simulations of the above described implementation of a HQMM. For completeness, we shall present an overview of the parametrisation process, though this will not be used for the numerical comparison in the next section.

B.1 Matrix Elements of the Internal Density Matrix

It is important that we are able to calculate the elements of the density matrix representing our system, otherwise we have no way to simulate all possible machines numerically. Let ρ_{t+1} be the density matrix of the internal state at time $t+1$, and ρ_t be the density matrix at the iteration before, time t. Then the element ρ_{ab} can be picked out by

$$\langle a|\rho_{t+1}|b\rangle \quad = \quad \sum_{i,j,k=0}^{1} \langle a|R(\theta_k,\delta_k)\langle\mu_k|\xi_i\rangle\langle e_i|\left(|0_A\rangle\rho_t\langle 0_A|\right)|e_j\rangle\langle\xi_j|\mu_k\rangle R^\dagger(\theta_k\delta_k)|b\rangle$$

$$\Rightarrow \langle a|\rho_{t+1}|b\rangle \;=\; \sum_{i,j,k=0}^{1} \langle a|R(\theta_k,\delta_k)\langle\mu_k|\xi_i\rangle\langle\tilde{e}_i|\rho_t|\tilde{e}_j\rangle\langle\xi_j|\mu_k\rangle R^{\dagger}(\theta_k,\delta_k)|b\rangle, \tag{B.1}$$

where $|\tilde{e}_i\rangle = \langle 0_A|e_i\rangle = \{|0_I\rangle, |1_I\rangle\}$, with the subscripts A and I corresponding to ancilla and internal respectively. It now becomes useful to express the $|\xi_i\rangle$ terms of the measurement basis. We write

$$|\xi_0\rangle = \xi_{00}^{(0)}|0\mu_0\rangle + \xi_{01}^{(0)}|0\mu_1\rangle + \xi_{10}^{(0)}|1\mu_0\rangle + \xi_{11}^{(0)}|1\mu_1\rangle, \tag{B.2}$$

$$|\xi_1\rangle = \xi_{00}^{(1)}|0\mu_0\rangle + \xi_{01}^{(1)}|0\mu_1\rangle + \xi_{10}^{(1)}|1\mu_0\rangle + \xi_{11}^{(1)}|1\mu_1\rangle. \tag{B.3}$$

It is possible to write the components of the density matrix in vector form, namely

$$\vec{\rho^{t+1}} = \begin{pmatrix} \rho_{00}^{t+1} \\ \rho_{01}^{t+1} \\ \rho_{10}^{t+1} \\ \rho_{11}^{t+1} \end{pmatrix} = \begin{pmatrix} A_{11} & A_{12} & A_{13} & A_{14} \\ A_{21} & A_{22} & A_{23} & A_{24} \\ A_{31} & A_{32} & A_{33} & A_{34} \\ A_{41} & A_{42} & A_{43} & A_{44} \end{pmatrix} \begin{pmatrix} \rho_{00}^{t} \\ \rho_{01}^{t} \\ \rho_{10}^{t} \\ \rho_{11}^{t} \end{pmatrix} = A\vec{\rho^{t}}, \tag{B.4}$$

where

$$A_{ij} = \sum_{k=0}^{1} \langle x|R(\theta_k,\delta_k)\langle\mu_k|\xi_m\rangle\langle\xi_n|\mu_k\rangle R^{\dagger}(\theta_k,\delta_k)|y\rangle, \tag{B.5}$$

with

$$m = \begin{cases} 0 \text{ for } j = 1,2 \\ 1 \text{ for } j = 3,4 \end{cases}, \tag{B.6}$$

$$n = \begin{cases} 0 \text{ for } j = 1,3 \\ 1 \text{ for } j = 2,4 \end{cases}, \tag{B.7}$$

$$x = \begin{cases} 0 \text{ for } i = 1,2 \\ 1 \text{ for } i = 3,4 \end{cases}, \tag{B.8}$$

$$y = \begin{cases} 0 \text{ for } i = 1,3 \\ 1 \text{ for } i = 2,4 \end{cases}. \tag{B.9}$$

In order to look for conditions on the matrix A, we may write the $|\xi_i\rangle$ terms in the basis given above. The components of matrix A can then be expanded as below.

$$\begin{aligned} A_{11} \;=\; \sum_{k=0}^{1} \Big(& \xi_{0k}^{(0)}\xi_{0k}^{(0)*}\cos^2(\theta_k) + \xi_{0k}^{(0)}\xi_{1k}^{(0)*}e^{-i\delta_k}\cos(\theta_k)\sin(\theta_k) \\ & + \xi_{1k}^{(0)}\xi_{0k}^{(0)*}e^{i\delta_k}\cos(\theta_k)\sin(\theta_k) + \xi_{1k}^{(0)}\xi_{1k}^{(0)*}\sin^2(\theta_k) \Big), \end{aligned}$$

$$
\begin{aligned}
A_{12} &= \sum_{k=0}^{1} \Big(\xi_{0k}^{(0)} \xi_{0k}^{(1)*} \cos^2(\theta_k) + \xi_{0k}^{(0)} \xi_{1k}^{(1)*} e^{-i\delta_k} \cos(\theta_k) \sin(\theta_k) \\
&\quad + \xi_{1k}^{(0)} \xi_{0k}^{(1)*} e^{i\delta_k} \cos(\theta_k) \sin(\theta_k) + \xi_{1k}^{(0)} \xi_{1k}^{(1)*} \sin^2(\theta_k) \Big), \\
A_{13} &= \sum_{k=0}^{1} \Big(\xi_{0k}^{(1)} \xi_{0k}^{(0)*} \cos^2(\theta_k) + \xi_{0k}^{(1)} \xi_{1k}^{(0)*} e^{-i\delta_k} \cos(\theta_k) \sin(\theta_k) \\
&\quad + \xi_{1k}^{(1)} \xi_{0k}^{(0)*} e^{i\delta_k} \cos(\theta_k) \sin(\theta_k) + \xi_{1k}^{(1)} \xi_{1k}^{(0)*} \sin^2(\theta_k) \Big), \\
A_{14} &= \sum_{k=0}^{1} \Big(\xi_{0k}^{(1)} \xi_{0k}^{(1)*} \cos^2(\theta_k) + \xi_{0k}^{(1)} \xi_{1k}^{(1)*} e^{-i\delta_k} \cos(\theta_k) \sin(\theta_k) \\
&\quad + \xi_{1k}^{(1)} \xi_{0k}^{(1)*} e^{i\delta_k} \cos(\theta_k) \sin(\theta_k) + \xi_{1k}^{(1)} \xi_{1k}^{(1)*} \sin^2(\theta_k) \Big), \\
A_{21} &= \sum_{k=0}^{1} \Big(- \xi_{0k}^{(0)} \xi_{0k}^{(0)*} e^{i\delta_k} \cos(\theta_k) \sin(\theta_k) + \xi_{0k}^{(0)} \xi_{1k}^{(0)*} \cos^2(\theta_k) \\
&\quad - \xi_{1k}^{(0)} \xi_{0k}^{(0)*} e^{2i\delta_k} \sin^2(\theta_k) + \xi_{1k}^{(0)} \xi_{1k}^{(0)*} e^{i\delta_k} \cos(\theta_k) \sin(\theta_k) \Big), \\
A_{22} &= \sum_{k=0}^{1} \Big(- \xi_{0k}^{(0)} \xi_{0k}^{(1)*} e^{i\delta_k} \cos(\theta_k) \sin(\theta_k) + \xi_{0k}^{(0)} \xi_{1k}^{(1)*} \cos^2(\theta_k) \\
&\quad - \xi_{1k}^{(0)} \xi_{0k}^{(1)*} e^{2i\delta_k} \sin^2(\theta_k) + \xi_{1k}^{(0)} \xi_{1k}^{(1)*} e^{i\delta_k} \cos(\theta_k) \sin(\theta_k) \Big), \\
A_{23} &= \sum_{k=0}^{1} \Big(- \xi_{0k}^{(1)} \xi_{0k}^{(0)*} e^{i\delta_k} \cos(\theta_k) \sin(\theta_k) + \xi_{0k}^{(1)} \xi_{1k}^{(0)*} \cos^2(\theta_k) \\
&\quad - \xi_{1k}^{(1)} \xi_{0k}^{(0)*} e^{2i\delta_k} \sin^2(\theta_k) + \xi_{1k}^{(1)} \xi_{1k}^{(0)*} e^{i\delta_k} \cos(\theta_k) \sin(\theta_k) \Big), \\
A_{24} &= \sum_{k=0}^{1} \Big(- \xi_{0k}^{(1)} \xi_{0k}^{(1)*} e^{i\delta_k} \cos(\theta_k) \sin(\theta_k) + \xi_{0k}^{(1)} \xi_{1k}^{(1)*} \cos^2(\theta_k) \\
&\quad - \xi_{1k}^{(1)} \xi_{0k}^{(1)*} e^{2i\delta_k} \sin^2(\theta_k) + \xi_{1k}^{(1)} \xi_{1k}^{(1)*} e^{i\delta_k} \cos(\theta_k) \sin(\theta_k) \Big), \\
A_{31} &= \sum_{k=0}^{1} \Big(- \xi_{0k}^{(0)} \xi_{0k}^{(0)*} e^{-i\delta_k} \cos(\theta_k) \sin(\theta_k) - \xi_{0k}^{(0)} \xi_{1k}^{(0)*} e^{-2i\delta_k} \sin^2(\theta_k) \\
&\quad + \xi_{1k}^{(0)} \xi_{0k}^{(0)*} \cos^2(\theta_k) + \xi_{1k}^{(0)} \xi_{1k}^{(0)*} e^{-i\delta_k} \cos(\theta_k) \sin(\theta_k) \Big), \\
A_{32} &= \sum_{k=0}^{1} \Big(- \xi_{0k}^{(0)} \xi_{0k}^{(1)*} e^{-i\delta_k} \cos(\theta_k) \sin(\theta_k) - \xi_{0k}^{(0)} \xi_{1k}^{(1)*} e^{-2i\delta_k} \sin^2(\theta_k) \\
&\quad + \xi_{1k}^{(0)} \xi_{0k}^{(1)*} \cos^2(\theta_k) + \xi_{1k}^{(0)} \xi_{1k}^{(1)*} e^{-i\delta_k} \cos(\theta_k) \sin(\theta_k) \Big),
\end{aligned}
$$

$$
\begin{aligned}
A_{33} &= \sum_{k=0}^{1}\Big(-\xi_{0k}^{(1)}\xi_{0k}^{(0)*}e^{-i\delta_k}\cos(\theta_k)\sin(\theta_k) - \xi_{0k}^{(1)}\xi_{1k}^{(0)*}e^{-2i\delta_k}\sin^2(\theta_k) \\
&\quad + \xi_{1k}^{(1)}\xi_{0k}^{(0)*}\cos^2(\theta_k) + \xi_{1k}^{(1)}\xi_{1k}^{(0)*}e^{-i\delta_k}\cos(\theta_k)\sin(\theta_k)\Big), \\
A_{34} &= \sum_{k=0}^{1}\Big(-\xi_{0k}^{(1)}\xi_{0k}^{(1)*}e^{-i\delta_k}\cos(\theta_k)\sin(\theta_k) - \xi_{0k}^{(1)}\xi_{1k}^{(1)*}e^{-2i\delta_k}\sin^2(\theta_k) \\
&\quad + \xi_{1k}^{(1)}\xi_{0k}^{(1)*}\cos^2(\theta_k) + \xi_{1k}^{(1)}\xi_{1k}^{(1)*}e^{-i\delta_k}\cos(\theta_k)\sin(\theta_k)\Big), \\
A_{41} &= \sum_{k=0}^{1}\Big(\xi_{0k}^{(0)}\xi_{0k}^{(0)*}\sin^2(\theta_k) - \xi_{0k}^{(0)}\xi_{1k}^{(0)*}e^{-i\delta_k}\cos(\theta_k)\sin(\theta_k) \\
&\quad - \xi_{1k}^{(0)}\xi_{0k}^{(0)*}e^{i\delta_k}\cos(\theta_k)\sin(\theta_k) + \xi_{1k}^{(0)}\xi_{1k}^{(0)*}\cos^2(\theta_k)\Big), \\
A_{42} &= \sum_{k=0}^{1}\Big(\xi_{0k}^{(0)}\xi_{0k}^{(1)*}\sin^2(\theta_k) - \xi_{0k}^{(0)}\xi_{1k}^{(1)*}e^{-i\delta_k}\cos(\theta_k)\sin(\theta_k) \\
&\quad - \xi_{1k}^{(0)}\xi_{0k}^{(1)*}e^{i\delta_k}\cos(\theta_k)\sin(\theta_k) + \xi_{1k}^{(0)}\xi_{1k}^{(1)*}\cos^2(\theta_k)\Big), \\
A_{43} &= \sum_{k=0}^{1}\Big(\xi_{0k}^{(1)}\xi_{0k}^{(0)*}\sin^2(\theta_k) - \xi_{0k}^{(1)}\xi_{1k}^{(0)*}e^{-i\delta_k}\cos(\theta_k)\sin(\theta_k) \\
&\quad - \xi_{1k}^{(1)}\xi_{0k}^{(0)*}e^{i\delta_k}\cos(\theta_k)\sin(\theta_k) + \xi_{1k}^{(1)}\xi_{1k}^{(0)*}\cos^2(\theta_k)\Big), \\
A_{44} &= \sum_{k=0}^{1}\Big(\xi_{0k}^{(1)}\xi_{0k}^{(1)*}\sin^2(\theta_k) - \xi_{0k}^{(1)}\xi_{1k}^{(1)*}e^{-i\delta_k}\cos(\theta_k)\sin(\theta_k) \\
&\quad - \xi_{1k}^{(1)}\xi_{0k}^{(1)*}e^{i\delta_k}\cos(\theta_k)\sin(\theta_k) + \xi_{1k}^{(1)}\xi_{1k}^{(1)*}\cos^2(\theta_k)\Big). \qquad \text{(B.10)}
\end{aligned}
$$

It is now clearer to see where some of these conditions occur. Namely, these are $A_{12} = A_{13}^*$, $A_{42} = A_{43}^*$, $A_{21} = A_{31}^*$, $A_{24} = A_{34}^*$, $A_{22} = A_{33}^*$ and $A_{23} = A_{32}^*$. Furthermore, it must be true that

$$
\begin{aligned}
\left|\alpha_{11}^{(0)}\right|^2 &= 1 - \left|\alpha_{00}^{(0)}\right|^2 - \left|\alpha_{01}^{(0)}\right|^2 - \left|\alpha_{10}^{(0)}\right|^2 \quad \text{and} \qquad \text{(B.11)} \\
\left|\alpha_{11}^{(1)}\right|^2 &= 1 - \left|\alpha_{00}^{(1)}\right|^2 - \left|\alpha_{01}^{(1)}\right|^2 - \left|\alpha_{10}^{(1)}\right|^2, \qquad \text{(B.12)}
\end{aligned}
$$

meaning we also have that $A_{41} = 1 - A_{11}$ and $A_{44} = 1 - A_{14}$. Hence, we may write A as

$$A = \begin{pmatrix} A_{11} & A_{12} & A_{12}^* & A_{14} \\ A_{21} & A_{22} & A_{23} & A_{24} \\ A_{21}^* & A_{23}^* & A_{22}^* & A_{24}^* \\ 1 - A_{11} & A_{42} & A_{42}^* & 1 - A_{14} \end{pmatrix}. \tag{B.13}$$

B.2 Stationary State

As with all the machines we consider, it is vital that they form a stationary state for our analysis of them. Using the notation defined in eq. (B.4), for a stationary state ρ^{SS}, we must have

$$\vec{\rho^{\text{SS}}} = \begin{pmatrix} \rho_{00}^{\text{SS}} \\ \rho_{01}^{\text{SS}} \\ \rho_{10}^{\text{SS}} \\ \rho_{11}^{\text{SS}} \end{pmatrix} = \begin{pmatrix} A_{11} & A_{12} & A_{12}^* & A_{14} \\ A_{21} & A_{22} & A_{23} & A_{24} \\ A_{21}^* & A_{23}^* & A_{22}^* & A_{24}^* \\ 1 - A_{11} & A_{42} & A_{42}^* & 1 - A_{14} \end{pmatrix} \begin{pmatrix} \rho_{00}^{\text{SS}} \\ \rho_{01}^{\text{SS}} \\ \rho_{10}^{\text{SS}} \\ \rho_{11}^{\text{SS}} \end{pmatrix} = A\vec{\rho^{\text{SS}}}, \tag{B.14}$$

This is an eigenvalue problem, where the stationary state is the eigenvector corresponding to the eigenvalue 1, i.e. $A\vec{\rho^{\text{SS}}} = (1)\rho^{\text{SS}}$. Using eq. (B.14), with the fact that for a density matrix we must have $\rho_{00} + \rho_{11} = 1$ and $\rho_{01} = \rho_{10}^*$, the components of the stationary state density matrix can be found from the equations below.

$$\rho_{00} = A_{11}\rho_{00} + A_{12}\rho_{01} + (A_{12}\rho_{01})^* + A_{14}(1 - \rho_{00}) \tag{B.15}$$

$$\rho_{01} = A_{21}\rho_{00} + A_{22}\rho_{01} + A_{23}\rho_{01}^* + A_{24}(1 - \rho_{00}) \tag{B.16}$$

$$\rho_{10} = A_{21}^*\rho_{00} + A_{23}^*\rho_{01} + (A_{22}\rho_{01})^* + A_{24}^*(1 - \rho_{00}) \tag{B.17}$$

$$\rho_{11} = (1 - A_{11})\rho_{00} + A_{42}\rho_{01} + (A_{42}\rho_{01})^* + (1 - A_{14})(1 - \rho_{00}) \tag{B.18}$$

where the "ss" notation for stationary state has been dropped for convenience. It is clear to see from the above equations that $\rho_{01} = \rho_{10}^*$ as required. To satisfy $\rho_{00} + \rho_{11} = 1$, we must have $\text{Re}(A_{12}\rho_{01}) = -\text{Re}(A_{42}\rho_{01})$. This is true automatically due to the orthogonality constraint of the states. The simultaneous equations above can be solved to give the density matrix components in terms of the A_{ij} terms or the $\xi_{jk}^{(i)}$ terms.

B.3 Specific Outputs and Probabilities

In a similar way to what was done for the HMM, we can create sub-transition operators for the HQMM, namely $A = A^{(0)} + A^{(1)}$. This can be done quite simply for the HQMM from the way we have defined it, specifically the $A^{(0)}$ terms come from the $|\mu_0\rangle$ measurements and the $A^{(1)}$ terms come from the $|\mu_1\rangle$ measurements. The matrices $A^{(0)}$ and $A^{(1)}$ are analogous to the matrices T_0 and T_1 that were used for the HMM. Then, we can write

$$\begin{aligned} A &= A^{(0)} + A^{(1)} \\ &= \begin{pmatrix} A^{(0)}_{11} & A^{(0)}_{12} & A^{(0)}_{13} & A^{(0)}_{14} \\ A^{(0)}_{21} & A^{(0)}_{22} & A^{(0)}_{23} & A^{(0)}_{24} \\ A^{(0)}_{31} & A^{(0)}_{32} & A^{(0)}_{33} & A^{(0)}_{34} \\ A^{(0)}_{41} & A^{(0)}_{42} & A^{(0)}_{43} & A^{(0)}_{44} \end{pmatrix} + \begin{pmatrix} A^{(1)}_{11} & A^{(1)}_{12} & A^{(1)}_{13} & A^{(1)}_{14} \\ A^{(1)}_{21} & A^{(1)}_{22} & A^{(1)}_{23} & A^{(1)}_{24} \\ A^{(1)}_{31} & A^{(1)}_{32} & A^{(1)}_{33} & A^{(1)}_{34} \\ A^{(1)}_{41} & A^{(1)}_{42} & A^{(1)}_{43} & A^{(1)}_{44} \end{pmatrix}, \end{aligned} \tag{B.19}$$

with,

$$\begin{aligned} A^{(k)}_{11} &= \Big(\xi^{(0)}_{0k}\xi^{(0)*}_{0k}\cos^2(\theta_k) + \xi^{(0)}_{0k}\xi^{(0)*}_{1k}e^{-i\delta_k}\cos(\theta_k)\sin(\theta_k) \\ &\quad + \xi^{(0)}_{1k}\xi^{(0)*}_{0k}e^{i\delta_k}\cos(\theta_k)\sin(\theta_k) + \xi^{(0)}_{1k}\xi^{(0)*}_{1k}\sin^2(\theta_k)\Big), \\ A^{(k)}_{12} &= \Big(\xi^{(0)}_{0k}\xi^{(1)*}_{0k}\cos^2(\theta_k) + \xi^{(0)}_{0k}\xi^{(1)*}_{1k}e^{-i\delta_k}\cos(\theta_k)\sin(\theta_k) \\ &\quad + \xi^{(0)}_{1k}\xi^{(1)*}_{0k}e^{i\delta_k}\cos(\theta_k)\sin(\theta_k) + \xi^{(0)}_{1k}\xi^{(1)*}_{1k}\sin^2(\theta_k)\Big), \\ A^{(k)}_{13} &= \Big(\xi^{(1)}_{0k}\xi^{(0)*}_{0k}\cos^2(\theta_k) + \xi^{(1)}_{0k}\xi^{(0)*}_{1k}e^{-i\delta_k}\cos(\theta_k)\sin(\theta_k) \\ &\quad + \xi^{(1)}_{1k}\xi^{(0)*}_{0k}e^{i\delta_k}\cos(\theta_k)\sin(\theta_k) + \xi^{(1)}_{1k}\xi^{(0)*}_{1k}\sin^2(\theta_k)\Big), \\ A^{(k)}_{14} &= \Big(\xi^{(1)}_{0k}\xi^{(1)*}_{0k}\cos^2(\theta_k) + \xi^{(1)}_{0k}\xi^{(1)*}_{1k}e^{-i\delta_k}\cos(\theta_k)\sin(\theta_k) \\ &\quad + \xi^{(1)}_{1k}\xi^{(1)*}_{0k}e^{i\delta_k}\cos(\theta_k)\sin(\theta_k) + \xi^{(1)}_{1k}\xi^{(1)*}_{1k}\sin^2(\theta_k)\Big), \\ A^{(k)}_{21} &= \Big(-\xi^{(0)}_{0k}\xi^{(0)*}_{0k}e^{i\delta_k}\cos(\theta_k)\sin(\theta_k) + \xi^{(0)}_{0k}\xi^{(0)*}_{1k}\cos^2(\theta_k) \\ &\quad - \xi^{(0)}_{1k}\xi^{(0)*}_{0k}e^{2i\delta_k}\sin^2(\theta_k) + \xi^{(0)}_{1k}\xi^{(0)*}_{1k}e^{i\delta_k}\cos(\theta_k)\sin(\theta_k)\Big), \\ A^{(k)}_{22} &= \Big(-\xi^{(0)}_{0k}\xi^{(1)*}_{0k}e^{i\delta_k}\cos(\theta_k)\sin(\theta_k) + \xi^{(0)}_{0k}\xi^{(1)*}_{1k}\cos^2(\theta_k) \\ &\quad - \xi^{(0)}_{1k}\xi^{(1)*}_{0k}e^{2i\delta_k}\sin^2(\theta_k) + \xi^{(0)}_{1k}\xi^{(1)*}_{1k}e^{i\delta_k}\cos(\theta_k)\sin(\theta_k)\Big), \end{aligned}$$

$$
\begin{aligned}
A_{23}^{(k)} &= \Big(-\xi_{0k}^{(1)}\xi_{0k}^{(0)*}e^{i\delta_k}\cos(\theta_k)\sin(\theta_k) + \xi_{0k}^{(1)}\xi_{1k}^{(0)*}\cos^2(\theta_k) \\
&\quad -\xi_{1k}^{(1)}\xi_{0k}^{(0)*}e^{2i\delta_k}\sin^2(\theta_k) + \xi_{1k}^{(1)}\xi_{1k}^{(0)*}e^{i\delta_k}\cos(\theta_k)\sin(\theta_k)\Big), \\
A_{24}^{(k)} &= \Big(-\xi_{0k}^{(1)}\xi_{0k}^{(1)*}e^{i\delta_k}\cos(\theta_k)\sin(\theta_k) + \xi_{0k}^{(1)}\xi_{1k}^{(1)*}\cos^2(\theta_k) \\
&\quad -\xi_{1k}^{(1)}\xi_{0k}^{(1)*}e^{2i\delta_k}\sin^2(\theta_k) + \xi_{1k}^{(1)}\xi_{1k}^{(1)*}e^{i\delta_k}\cos(\theta_k)\sin(\theta_k)\Big), \\
A_{31}^{(k)} &= \Big(-\xi_{0k}^{(0)}\xi_{0k}^{(0)*}e^{-i\delta_k}\cos(\theta_k)\sin(\theta_k) - \xi_{0k}^{(0)}\xi_{1k}^{(0)*}e^{-2i\delta_k}\sin^2(\theta_k) \\
&\quad +\xi_{1k}^{(0)}\xi_{0k}^{(0)*}\cos^2(\theta_k) + \xi_{1k}^{(0)}\xi_{1k}^{(0)*}e^{-i\delta_k}\cos(\theta_k)\sin(\theta_k)\Big), \\
A_{32}^{(k)} &= \Big(-\xi_{0k}^{(0)}\xi_{0k}^{(1)*}e^{-i\delta_k}\cos(\theta_k)\sin(\theta_k) - \xi_{0k}^{(0)}\xi_{1k}^{(1)*}e^{-2i\delta_k}\sin^2(\theta_k) \\
&\quad +\xi_{1k}^{(0)}\xi_{0k}^{(1)*}\cos^2(\theta_k) + \xi_{1k}^{(0)}\xi_{1k}^{(1)*}e^{-i\delta_k}\cos(\theta_k)\sin(\theta_k)\Big), \\
A_{33}^{(k)} &= \Big(-\xi_{0k}^{(1)}\xi_{0k}^{(0)*}e^{-i\delta_k}\cos(\theta_k)\sin(\theta_k) - \xi_{0k}^{(1)}\xi_{1k}^{(0)*}e^{-2i\delta_k}\sin^2(\theta_k) \\
&\quad +\xi_{1k}^{(1)}\xi_{0k}^{(0)*}\cos^2(\theta_k) + \xi_{1k}^{(1)}\xi_{1k}^{(0)*}e^{-i\delta_k}\cos(\theta_k)\sin(\theta_k)\Big), \\
A_{34}^{(k)} &= \Big(-\xi_{0k}^{(1)}\xi_{0k}^{(1)*}e^{-i\delta_k}\cos(\theta_k)\sin(\theta_k) - \xi_{0k}^{(1)}\xi_{1k}^{(1)*}e^{-2i\delta_k}\sin^2(\theta_k) \\
&\quad +\xi_{1k}^{(1)}\xi_{0k}^{(1)*}\cos^2(\theta_k) + \xi_{1k}^{(1)}\xi_{1k}^{(1)*}e^{-i\delta_k}\cos(\theta_k)\sin(\theta_k)\Big), \\
A_{41}^{(k)} &= \Big(\xi_{0k}^{(0)}\xi_{0k}^{(0)*}\sin^2(\theta_k) - \xi_{0k}^{(0)}\xi_{1k}^{(0)*}e^{-i\delta_k}\cos(\theta_k)\sin(\theta_k) \\
&\quad -\xi_{1k}^{(0)}\xi_{0k}^{(0)*}e^{i\delta_k}\cos(\theta_k)\sin(\theta_k) + \xi_{1k}^{(0)}\xi_{1k}^{(0)*}\cos^2(\theta_k)\Big), \\
A_{42}^{(k)} &= \Big(\xi_{0k}^{(0)}\xi_{0k}^{(1)*}\sin^2(\theta_k) - \xi_{0k}^{(0)}\xi_{1k}^{(1)*}e^{-i\delta_k}\cos(\theta_k)\sin(\theta_k) \\
&\quad -\xi_{1k}^{(0)}\xi_{0k}^{(1)*}e^{i\delta_k}\cos(\theta_k)\sin(\theta_k) + \xi_{1k}^{(0)}\xi_{1k}^{(1)*}\cos^2(\theta_k)\Big), \\
A_{43}^{(k)} &= \Big(\xi_{0k}^{(1)}\xi_{0k}^{(0)*}\sin^2(\theta_k) - \xi_{0k}^{(1)}\xi_{1k}^{(0)*}e^{-i\delta_k}\cos(\theta_k)\sin(\theta_k) \\
&\quad -\xi_{1k}^{(1)}\xi_{0k}^{(0)*}e^{i\delta_k}\cos(\theta_k)\sin(\theta_k) + \xi_{1k}^{(1)}\xi_{1k}^{(0)*}\cos^2(\theta_k)\Big), \\
A_{44}^{(k)} &= \Big(\xi_{0k}^{(1)}\xi_{0k}^{(1)*}\sin^2(\theta_k) - \xi_{0k}^{(1)}\xi_{1k}^{(1)*}e^{-i\delta_k}\cos(\theta_k)\sin(\theta_k) \\
&\quad -\xi_{1k}^{(1)}\xi_{0k}^{(1)*}e^{i\delta_k}\cos(\theta_k)\sin(\theta_k) + \xi_{1k}^{(1)}\xi_{1k}^{(1)*}\cos^2(\theta_k)\Big). \qquad \text{(B.20)}
\end{aligned}
$$

These parametrisations can be used to describe a general HQMM. However, they are clearly computationally difficult to implement. Hence, we shall use the specific example of an open quantum system with instantaneous quantum feedback as a concrete example to study the behaviour of a HQMM.

References

[1] J. P. Dowling and K. P. Seshadreesan. Quantum Optical Technologies for Metrology, Sensing, and Imaging. *J. Lightwave Technol.*, 33:2359, 2015. 1, 2, 4, 74, 75

[2] N. Gisin and R. Thew. Quantum communication. *Nature Photon.*, 1:165, 2007. 1

[3] M. A. Nielsen and I. L. Chuang. *Quantum Computation and Quantum Information*. Cambridge University Press, 2000. 1

[4] G. Lindblad. On the generators of quantum dynamical semigroups. *Comm. Math. Phys.*, 48:119, 1976. 4, 8, 9, 17, 39

[5] D. Braun and J. Martin. Heisenberg-limited sensitivity with decoherence-enhanced measurements. *Nat. Commun.*, 2:223, 2011. 4, 79, 81, 99, 111

[6] K. Macieszczak, M. Guta, I. Lesanovsky, and J. P. Garrahan. Dynamical phase transitions as a resource for quantum enhanced metrology. *Phys. Rev. A*, 93:022103, 2016. 4, 39, 79, 81, 99, 111

[7] L. A. Clark, A. Stokes, and A. Beige. Quantum-enhanced metrology through the single mode coherent states of optical cavities with quantum feedback. *Phys. Rev. A*, 94:023840, 2016. 4, 8, 19, 26, 27, 40, 49, 52, 58, 74, 79, 81, 98

[8] M. Schuld, I. Sinayskiy, and F. Petruccione. The quest for a quantum neural network. *Quantum Information Processing*, 13:2567, 2014. 4, 120

[9] M. Schuld, I. Sinayskiy, and F. Petruccione. An introduction to quantum machine learning. *Contemporary Physics*, 56:172, 2015. 4, 120

[10] A. Monras, A. Beige, , and K. Wiesner. Hidden Quantum Markov Models and non-adaptive read-out of many-body states. *App. Math. and Comp. Sciences*, 3:93, 2011. 5, 60, 61, 62, 64, 68, 72

[11] L. A. Clark, W. Huang, T. M. Barlow, and A. Beige. *Hidden Quantum Markov Models and Open Quantum Systems with Instantaneous Feedback*, volume 14, page 143. Springer International Publishing Switzerland, 2015. 5, 8, 13, 19, 40, 60, 99

[12] M. Cholewa, P. Gawron, P. Gomb, and D. Kurzyk. Quantum Hidden Markov Models based on Transition Operation Matrices. *Quantum Inf Process*, 16:101, 2017. 5

[13] H.-P. Breuer and F. Petruccione. *The Theory of Open Quantum Systems*. Oxford University Press, 2002. 5, 8, 19, 99

[14] H. M. Wiseman and G. J. Milburn. *Quantum Measurement and Control*. Cambridge University Press, 2010. 5, 8, 13, 16, 27, 34, 40, 61, 62, 99

[15] A. R. R. Carvalho and J. J. Hope. Stabilizing entanglement by quantum-jump based feedback. *Phys. Rev. A*, 76:010301, 2007. 5

[16] R. N. Stevenson, J. J. Hope, and A. R. R. Carvalho. Engineering steady states using jump-based feedback for multipartite entanglement generation. *Phys. Rev. A*, 84:022332, 2011. 5

[17] C. Emary. Delayed feedback control in quantum transport. *Phil. Trans. R. Soc. A*, 371:1999, 2013. 5, 62

[18] A. Stokes, A. Kurcz, T. P. Spiller, and A. Beige. Extending the validity range of quantum optical master equations. *Phys. Rev. A*, 85:053805, 2012. 8, 9, 11, 12, 14, 19, 39, 99

[19] W. H. Zurek. Decoherence, einselection, and the quantum origins of the classical. *Rev. Mod. Phys.*, 75:715, 2003. 8, 11, 12, 40, 57, 62

[20] G. C. Hegerfeldt. How to reset an atom after a photon detection. Applications to photon counting processes. *Phys. Rev. A*, 47:449, 1993. 8, 11, 12, 13, 14, 26, 39, 56, 62, 104, 110

[21] J. Dalibard, Y. Castin, and K. Mølmer. Wave-function approach to dissipative processes in quantum optics. *Phys. Rev. Lett.*, 68:580, 1992. 8, 11, 13, 26, 39, 62, 104, 110

[22] H. Carmicheal. *Lecture notes in physics*, volume 18. Springer, Berlin, 1993. 8, 11, 13, 26, 39, 62, 104, 110

[23] K. Kraus. *Lecture Notes in Physics*, volume 190. Springer-Verlag (Berlin, Heidelberg New York, Tokyo), 1983. 15, 61, 80

[24] N. G. Van Kampen. *Stochastic processes in Physics and Chemistry*. Elsevier Science B.V. Amsterdam, 1992. 38, 57

[25] A. Polkovnikov, K. Sengupta, A. Silva, and M. Vengalattore. Nonequilibrium dynamics of closed interacting quantum systems. *Rev. Mod. Phys.*, 83:863, 2011. 38

[26] G. D. Birkhoff. Proof of the ergodic theorem. *Proc. Natl. Acad. Sci. USA*, 17:656, 1931. 38

[27] J. von Neumann. Proof of the quasi-ergodic hypothesis. *Proc. Natl. Acad. Sci. USA*, 18:70, 1932. 38

[28] G. Gallavotti. *Non-equilibrium and Irreversibility*. Springer-Verlag Cham, 2014. 38

[29] A. Polkovnikov, K. Sengupta, A. Silva, and M. Vengalattore. Colloquium: Nonequilibrium dynamics of closed interacting quantum systems. *Rev. Mod. Phys.*, 83:863, 2011. 38, 40, 57

[30] L. D'Alessio, Y. Kafri, A. Polkovnikov, and M. Rigol. From quantum chaos and eigenstate thermalization to statistical mechanics and thermodynamics. *Adv. Phys.*, 65:239, 2016. 38, 40, 57

[31] M. C. Gutzwiller. *Chaos in Classical and Quantum Mechanics*, volume 1. Springer-Verlag New York, 1990. 38, 40, 57

[32] R. Kautz. *Chaos: The Science of Predictable Random Motion*. Oxford University Press, 2011. 38, 57

[33] J. D. Cresser. *Ergodicity of Quantum Trajectory Detection Records*. Springer-Verlag Berlin, 2001. 39, 45, 57

[34] L. Mandel and E. Wolf. *Optical coherence and quantum optics*. Cambridge University Press, 1995. 39

[35] J. C. Bergquist, R. G. Hulet, W. M. Itano, and D. J. Wineland. Observation of Quantum Jumps in a Single Atom. *Phys. Rev. Lett.*, 57:1699, 1986. 39

[36] A. Beige and G. C. Hegerfeldt. Quantum Zeno effect and light-dark periods for a single atom. *J. Phys. A*, 30:1323, 1997. 39

[37] W. H. Zurek. Decoherence and the transition from quantum to classical. *Phys. Today*, 44:36, 1991. 40, 57

[38] T. P. Spiller and J. F. Ralph. The emergence of chaos in an open quantum system. *Phys. Lett. A*, 194:235, 1994. 40, 57

[39] T. A. Brun, I. C. Percival, and R. Schack. Quantum chaos in open systems: A quantum state diffusion analysis. *J. Phys. A*, 29:2077, 1996. 40, 57

[40] M. Znidaric, T. Prosen, G. Benenti, G. Casati, and D. Rossini. Thermalization and ergodicity in many-body open quantum systems. *Phys. Rev. E*, 81:051135, 2010. 40

[41] A. V. Masalov, A. A. Putilin, and M. V. Vasilyev. Sub-poissonian Light and Photocurrent Shot-noise Suppression in Closed Optoelectronic Loop. *J. Mod. Opt.*, 41:1941, 1994. 40, 99, 102, 116

[42] J. E. Reinder, W. P. Smith, L. A. Orozco, H. M. Wiseman, and J. Gambetta. Quantum feedback in a weakly driven cavity QED system. *Phys. Rev. A*, 70:023819, 2004. 40

[43] J. R. Norris. *Markov chains*. Cambridge University Press, 1998. 60

[44] L. R. Rabiner. A tutorial on hidden Markov models and selected applications in speech recognition. *Proc. IEEE*, 77:257, 1989. 60, 61, 119

[45] H. Xue. Hidden Markov Models Combining Discrete Symbols and Continuous Attributes in Handwriting Recognition. *IEEE Transactions on Pattern Analysis and Machine Intelligence*, 28:458, 2006. 61, 119

[46] B. Vanluyten, J. C. Willems, and B. D. Moor. Equivalence of State Representations for Hidden Markov Models. *Systems and Control Letters*, 57: 410, 2008. 61, 119

[47] K. Wiesner and C. P. Crutchfield. Computation in finitary stochastic and quantum processes. *Physica D*, 237:1173, 2008. 61

[48] Equality conditions for internal entropies of certain classical and quantum models, *arXiv:1108.5303*, 2011. 61

[49] B. O'Neill, T. M. Barlow, D. Safranek, and A. Beige. Hidden Quantum Markov Models and non-adaptive read-out of many-body states. *AIP Conf. Proc.*, 1479:667, 2012. 61

[50] R. Sweke, I. Sinayskiy, and F. Petruccione. Simulation of Single-Qubit Open Quantum Systems. *Phys. Rev. A*, 90:022331, 2014. 61

[51] N. Goldenfeld and C. Woese. Life is Physics: evolution as a collective phenomenon far from equilibrium. *Ann. Rev. Cond. Matt. Phys.*, 2:375, 2011. 62

[52] M. Schuld, I. Sinayskiy, and F. Petruccione. Quantum walks on graphs representing the firing patterns of a quantum neural network. *Phys. Rev. A*, 89:032333, 2014. 62

[53] G. Kiesslich, C. Emary, G. Schaller, and T. Brandes. Reverse quantum state engineering using electronic feedback loops. *New. J. Phys.*, 14:123036, 2012. 62

[54] W. F. Stinespring. Positive Functions on C* algebras. *Proc. Amer. Math. Soc.*, 6:211, 1955. 67

[55] J. Bell. On the Einstein Podolsky Rosen Paradox. *Physics*, 1:195, 1964. 73

[56] J. Clauser, M. Horne, A. Shimony, and R. Holt. Thermalization and ergodicity in many-body open quantum systems. *Phys. Rev. Lett.*, 23:880, 1969. 73

[57] F. Wolfgramm, C. Vitelli, F. A. Beduini, N. Godbout, and M. W. Mitchell. Entanglement-enhanced probing of a delicate material system. *Nature Photon.*, 7:28–32, 2013. 75

[58] M. A. Taylor, J. Janousek, V. Daria, J. Knittel, B. Hage, H.-A. Bachor, and W. P. Bowen. Biological measurement beyond the quantum limit. *Nature Photon.*, 7:229–233, 2013. 75

[59] A. Crespi, M. Lobino, J. C. F. Matthews, A. Politi, C. R. Neal, R. Ramponi, R. Osellame, and J. L. O'Brien. Measuring protein concentration with entangled photons. *Appl. Phys. Lett.*, 100:233704, 2012. 75

[60] S. Boixo, A. Datta, S. T. Flammia, A. Shaji, E. Bagan, and C. M. Caves. Quantum-limited metrology with product states. *Phys. Rev. A*, 77:012317, 2008. 75, 81, 100

[61] V. Giovannetti, S. Lloyd, and L. Maccone. Quantum-enhanced measurements: beating the standard quantum limit. *Science*, 306:1330, 2004. 76, 100

[62] V. Giovannetti, S. Lloyd, and L. Maccone. Quantum metrology. *Phys. Rev. Lett.*, 96:010401, 2006. 76, 100

[63] M. Zwierz, C. A. Perez-Delgado, and P. Kok. Ultimate limits to quantum metrology and the meaning of the Heisenberg limit. *Phys. Rev. A*, 85: 042112, 2012. 76, 104

[64] B. L. Higgins, D. W. Berry, S. D. Bartlett, H. M. Wiseman, and G. J. Pryde. Entanglement-free Heisenberg-limited phase estimation. *Nature*, 450:393, 2007. 76

[65] C. M. Caves. Quantum-mechanical noise in an interferometer. *Phys. Rev. D*, 23:1693, 1981. 76

[66] R. S. Bondurant and J. H. Shapiro. Squeezed states in phase-sensing interferometers. *Phys. Rev. D*, 30:2548, 1984. 76

[67] P. Kok, H. Lee, and J. P. Dowling. The creation of large photon-number path entanglement conditioned on photodetection. *Phys. Rev. A*, 65:052104, 2002. 76

[68] R. A. Campos, C. C. Gerry, and A. Benmoussa. Optical interferometry at the Heisenberg limit with twin Fock states and parity measurements. *Phys. Rev. A*, 68:023810, 2003. 76

[69] C. C. Gerry, J. Mimih, and R. Birrittella. State-projective scheme for generating pair coherent states in traveling-wave optical fields. *Phys. Rev. A*, 84:023810, 2011. 76

[70] P. A. Knott, W. J. Munro, and J. A. Dunningham. Attaining subclassical metrology in lossy systems with entangled coherent states. *Phys. Rev. A*, 89:053812, 2014. 76

[71] J. Joo, W. J. Munro, and T. P. Spiller. Quantum metrology with entangled coherent states. *Phys. Rev. Lett.*, 107:083601, 2011. 76

[72] C. C. Gerry, A. Benmoussa, and R. A. Campos. Nonlinear interferometer as a resource for maximally entangled photonic states: Application to interferometry. *Phys. Rev. A*, 66:013804, 2002. 76

[73] S. D. Huver, C. F. Wildfeuer, and J. P. Dowling. Entangled Fock states for Robust Quantum Optical Metrology, Imaging, and Sensing. *Phys. Rev. A*, 78:063828, 2008. 76

[74] K. Jiang, C. J. Brignac, Y. Weng, M. B. Kim, H. Lee, and J. P. Dowling. Strategies for choosing path-entangled number states for optimal robust quantum-optical metrology in the presence of loss. *Phys. Rev. A*, 86:013826, 2012. 76

[75] D. W. Berry and H. M. Wiseman. Optimal states and almost optimal adaptive measurements for quantum interferometry. *Phys. Rev. Lett.*, 85: 5098, 2000. 76

[76] C. C. Gerry. Heisenberg-limit interferometry with four-wave mixers operating in a nonlinear regime. *Phys. Rev. A*, 61:043811, 2000. 76

[77] C. C. Gerry and J. Mimih. The parity operator in quantum optical metrology. *Contemp. Phys.*, 51:497, 2010. 76

[78] A. De Pasquale, P. Facchi, G. Florioand V. Giovannetti, K. Matsuoka, and K. Yuasa. Two-Mode Bosonic Quantum Metrology with Number Fluctuations. *Phys. Rev. A*, 92:042115, 2015. 76

[79] R. Carranza and C. C. Gerry. Photon-subtracted two-mode squeezed vacuum states and applications to quantum optical interferometry. *JOSA B*, 29:2581, 2012. 76

[80] B. P. Abbott *et al.* (LIGO Scientific Collaboration and Virgo Collaboration). Observation of Gravitational Waves from a Binary Black Hole Merger. *Phys. Rev. Lett.*, 116:061102, 2016. 76

[81] S. L. Braunstein and C. M. Caves. Statistical distance and the geometry of quantum states. *Phys. Rev. Lett.*, 72:3439, 1994. 77, 78

[82] P. Kok and B. Lovett. *Introduction to Optical Information Quantum Processing Quantum information processing.* Cambridge University Press, 2010. 77, 78

[83] S. Oppel, T. Büttner, P. Kok, , and J. von Zanthier. Super-resolving multiphoton interferences with independent light sources. *Phys. Rev. Lett.*, 109: 233603, 2012. 79, 111, 116

[84] M. E. Pearce, T. Mehringer, J. von Zanthier, and P. Kok. Precision Estimation of Source Dimensions from Higher-Order Intensity Correlations. *Phys. Rev. A*, 92:043831, 2015. 79, 111, 116

[85] M. Guta. Fisher information and asymptotic normality in system identification for quantum Markov chains. *Phys. Rev. A*, 83:062324, 2011. 79, 111, 116

[86] D. Burgarth, V. Giovannetti, A. N. Kato, and K. Yuasa. Quantum estimation via sequential measurements. *New J. Phys.*, 17:113055, 2015. 79, 111, 116

[87] A. H. Kiilerich and K. Mølmer. Bayesian parameter estimation by continuous homodyne detection. *Phys. Rev. A*, 94:032103, 2016. 79, 111, 116

[88] G. Adesso, F. DellAnno, S. De Siena, F. Illuminati, , and L. A. M. Souza. Optimal estimation of losses at the ultimate quantum limit with non-Gaussian states. *Phys. Rev. A*, 79:040305, 2009. 88

[89] A. Kuhn, M. Hennrich, and G. Rempe. Deterministic single-photon source for distributed quantum networking. *Phys. Rev. Lett.*, 89:067901, 2002. 99, 117

[90] J. McKeever, A. Boca, A. D. Boozer, R. Miller, J. R. Buck, A. Kuzmich, and H. J. Kimble. Deterministic Generation of Single Photons from One Atom Trapped in a Cavity. *Science*, 303:1992, 2004. 99, 117

[91] E. Pomarico, B. Sanguinetti, P. Sekatski, H. Zbinden, and N. Gisin. Experimental amplification of an entangled photon: what if the detection loophole is ignored? *New J. Phys.*, 13:063031, 2011. 99, 117

[92] L. A. Clark, B. Maybee, F. Torzewska, and A. Beige. Non-ergodiciity and non-classical correlations through quantum feedback. submitted, arXiv:1611.03716, 2017. 99, 102, 116

[93] A. J. Leggett and A. Garg. Quantum mechanics versus macroscopic realism: Is the flux there when nobody looks? *Phys. Rev. Lett.*, 54:857, 1985. 100

[94] C. Emary, N. Lambert, and F. Nori. LeggettGarg inequalities. *Rep. Prog. Phys.*, 77:016001, 2014. 100

[95] D. B. Khoroshko and S. A. Kilin. Suppression of photocurrent shot noise in a feedback loop. *J. Exp. Theor. Phys.*, 79:691, 1994. 102

[96] Y. M. Golubev, I. V. Sokolov, and M. I. Kolobov. Possibility of suppressing quantum light fluctuations when excess photon fluctuations occur inside a cavity. *J. Exp. Theor. Phys.*, 84:864, 1997. 102

[97] B. M. Escher, R. L. de Matos Filho, and L. Davidovich. General framework for estimating the ultimate precision limit in noisy quantum-enhanced metrology. *Nat. Phys*, 7:406, 2011. 114, 115

[98] R. Demkowicz-Dobrzanski, J. Kolodynski, and M. Guta. Precision Estimation of Source Dimensions from Higher-Order Intensity Correlations. *Nat. Commun.*, 3:1063, 2012. 114, 115

[99] M. E. Pearce, T. Mehringer, J. von Zanthier, and P. Kok. Precision Estimation of Source Dimensions from Higher-Order Intensity Correlations. *Phys. Rev. A*, 92:043831, 2015. 117

[100] R.J. Glauber. Coherent and incoherent states of radiation field. *Phys. Rev*, 131:2766, 1963. 121